석사 학위논문
Master's Thesis

수중폭발에 의한 구조물의 충격응답 실험과 시뮬레이션 및 상사법칙 적용에 관한 연구

Underwater explosion testing of catamaran-like structure vs. simulation and feasibility of using scaling law

박 종 완(朴 鍾 完, Park, Jong Wan)
기계항공시스템학부 해양시스템공학전공
School of Mechanical, Aerospace and Systems Engineering,
Division of Ocean Systems Engineering

KAIST

2012

수중폭발에 의한 구조물의 충격응답 실험과 시뮬레이션 및 상사법칙 적용에 관한 연구

Underwater explosion testing of catamaran-like structure vs. simulation and feasibility of using scaling law

심사위원장 신 영 식 _____

심사위원 한 순 흥 _____

심사위원 정 정 훈 _____

Underwater explosion testing of catamaran-like structure vs. simulation and feasibility of using scaling law

Advisor: Professor Shin, Young Sik

by

Park, Jong Wan

School of Mechanical, Aerospace and Systems Engineering

Division of Ocean Systems Engineering

KAIST

A thesis submitted to the faculty of KAIST in partial fulfillment of the requirements for the degree of Master of Science and Engineering in the School of Mechanical, Aerospace and Systems Engineering, Division of Ocean Systems Engineering. The study was conducted in accordance with Code of Research Ethics[1]

2012. 05. 25

Approved by

Professor Shin, Young Sik

[1] Declaration of Ethical Conduct in Research: I, as a graduate student of KAIST, hereby declare that I have not committed any acts that may damage the credibility of my research. These include, but are not limited to: falsification, thesis written by someone else, distortion of research findings or plagiarism. I affirm that my thesis contains honest conclusions based on my own careful research under the guidance of my thesis advisor.

수중폭발에 의한 구조물의 충격응답 실험과 시뮬레이션 및 상사법칙 적용에 관한 연구

박 종 완

위 논문은 한국과학기술원 석사학위논문으로
학위논문심사위원회에서 심사 통과하였음.

2012 년 05 년 25 일

MOSE

20104329

박 종 완. Park, Jong Wan. Underwater explosion testing of catamaran-like structure vs. simulation and feasibility of using scaling law. 수중폭발에 의한 구조물의 충격응답 실험과 시뮬레이션 및 상사법칙 적용에 관한 연구. School of Mechanical, Aerospace and Systems Engineering, Division of Ocean Systems Engineering. 2012. 112p. Advisor Prof. Shin, Young Sik.

ABSTRACT

The objective of this study is a comparison of test and simulation results. The simulation is conducted using the LS-DYNA code, and the actual explosion test is conducted at a reservoir. To study the impact of an underwater explosion on a structure, a 1 m × 2 m ship (catamaran)-like structure is constructed using aluminum. Velocity, acceleration, and blast pressure sensors are used to measure the dynamic response of the structure caused by the shock wave and bubble pulse pressure.

To investigate the dynamic response of the ship-like structure and underwater explosion phenomena, a numerical study is conducted by employing the ALE (arbitrary Lagrangian-Eulerian) method. A finite element model is created by using TrueGrid for the fluid model and VPG for the structure. The model analysis is performed with the FSI (fluid structure interaction) technique by using LS-DYNA.

In this study, small-scale underwater explosion experiments are carried out. Therefore, the experiment procedures of this study can be applied to scaled-down ship shock tests. Hence, the feasibility of using the scaled-down method is investigated by a simulation technique.

KEY WORDS: UNDEX (Underwater Explosion), UNDEX shock test, FSI, ALE, Shock Wave, Bubble Effect, Scaling law, Bubble pulse pressure.

Table of Contents

List of Tables

List of Figures

Chapter 1 Introduction

1.1 Background and object

Ocean structures such as ships, ocean plants and submarine as well as battle ships always could damage by the shock. There are many kinds of impact like as collision and underwater explosion etc. In this study, underwater explosion phenomena are considered. Especially, In World War II, the U.S. Navy experienced the highly destructive effects of near proximity underwater explosions (UNDEX) from mines and torpedoes. Many combatants with the latest in combat technology for the time were rendered helpless due to inadequate shock proofing of the ship systems. Since this time, extensive work has gone into the research and study of the effects of UNDEX. A major goal in the design of modern combatant ships has been to eliminate or at least reduce damage caused by underwater explosion.

In this study, the procedure of the underwater explosion shock test and simulation are presented. Next, the feasibility of the scaled down model is showed by the simulation by using the LS-DYNA.

Keith G. Webster(2007) suggested Investigation of close proximity underwater explosion effects on a ship-like structure using the multi-material arbitrary lagrangian eulerian (ALE) finite element method [1]. Jin Qiankun(2010) examined a finite element analysis of ship sections subjected to underwater exposion by using the abaqus [2]. J.H.Kim(2003) researched a study of survivability improvement method for naval ship design; damage assesment method by ALE technique. In that study, suggested the ways to modeling the air, water and explosive [3]. Kengi Murata(1999) suggested the precise measurements of underwater explosion phenomena by pressure sensor using fluoropolymer [4]. Sang-Gab Lee(2007) studied the intgrated structural dynamic response analysis considering the UNDEX shock wave and gas bubble pulse [5]. Lloyd Hammond(1997) examined the applicability of scaling laws to underwater shock tests [6].

Underwater explosion research is conducted actively in the world. However, in Korea, the

research is only conducted by computer simulation. Underwater explosion shock test for the ship is an important affair to survive the ships and crews. Underwater explosion tests have been conducted in some of the developed countries for enhancement of the ship's and mounted equipment's survivability. However, the results and test data are maintained as military classified materials.

As a result of this study, the row data which cannot obtain by using computer simulation is obtained in the real underwater explosion test. Next, the tested row data could be utilized to improve the simulation techniques.

Through this study, increase the understanding of underwater explosion shock. Moreover, applications for enhancing the ship's and mounted equipment’s survivability are available by improved simulation technique.

Chapter 2 Theoretical Background

2.1 Underwater explosion Phenomena

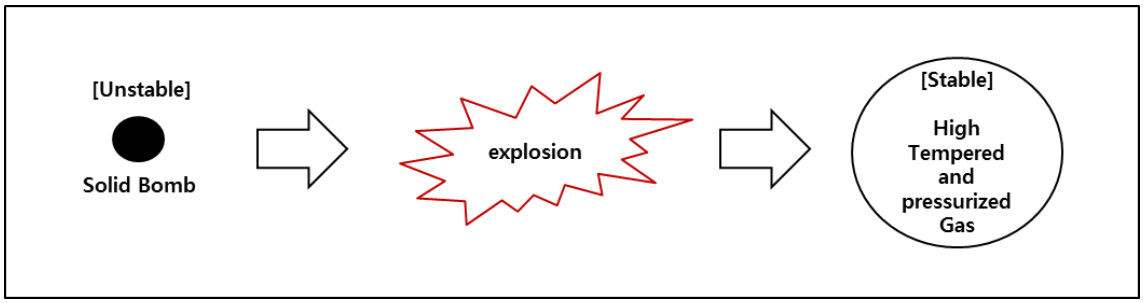

Figure 2.1 Explosion process

An explosion can occur in environment at air and water. In this thesis, the phenomena caused by an explosion in the water are studied. The phenomenon of the explosion is a chemical reaction in a substance and it changes the original material to a gas with a extremely high pressure and temperature.

Because of the dynamical properties of the water, the study of an underwater explosion can be considered a part of a field of physics known as hydrodynamics. As the first step in discussing the phenomena according to hydro dynamical relations, it is necessary to present the basic laws of mechanics into a mathematical form. The first assumption is that fluid is ideal. This assumption implies that viscous stresses and effects of heat transfer can be neglected. Next, the second assumption is that there are no discontinuities in pressure, fluid velocity and internal energy. The followings are the basic approach to the mathematical forms of the explosion.

A. Conservation of mass

$$\frac{\partial \rho}{\partial t} + \rho \mathbf{Div}\left(\tilde{\mathbf{V}}\right) = 0 \tag{2.1}$$

B. Conservation of Momentum

$$\rho \frac{d\tilde{\mathbf{V}}}{dt} = \mathbf{Grad}(\mathbf{P}) \tag{2.2}$$

where Grad = $\frac{\partial}{\partial x}i + \frac{\partial}{\partial y}j + \frac{\partial}{\partial z}k$

C. conservation of Energy

$$\rho \frac{dE}{dt} = \frac{P}{\rho}\frac{d\rho}{dt} \tag{2.3}$$

where P=fluid pressure, E=internal energy of the fluid per unit mass, ρ=mass density of the fluid

D. Pressure-Density Relations

$$\frac{dP}{d\rho} = \frac{\frac{P}{\rho^2} - \frac{\partial E}{\partial \rho}}{\frac{\partial E}{\partial P}} \tag{2.4}$$

Because water is compressible, the conclusions that can be drawn are that pressure applied to a localized region in the liquid is transmitted as a wave disturbance with a finite velocity to other points in the liquid and that this wave disturbance results in local motion of the water and cause a variation in its pressure. If an explosive such as HBX-1, TNT or RDX is detonated in water, several typical phenomena can be observed. Typical phenomena are the shock wave, gas bubble, cavitation etc, and are elucidated in the following sections. Figure 2.2. shows the underwater explosion phenomena.

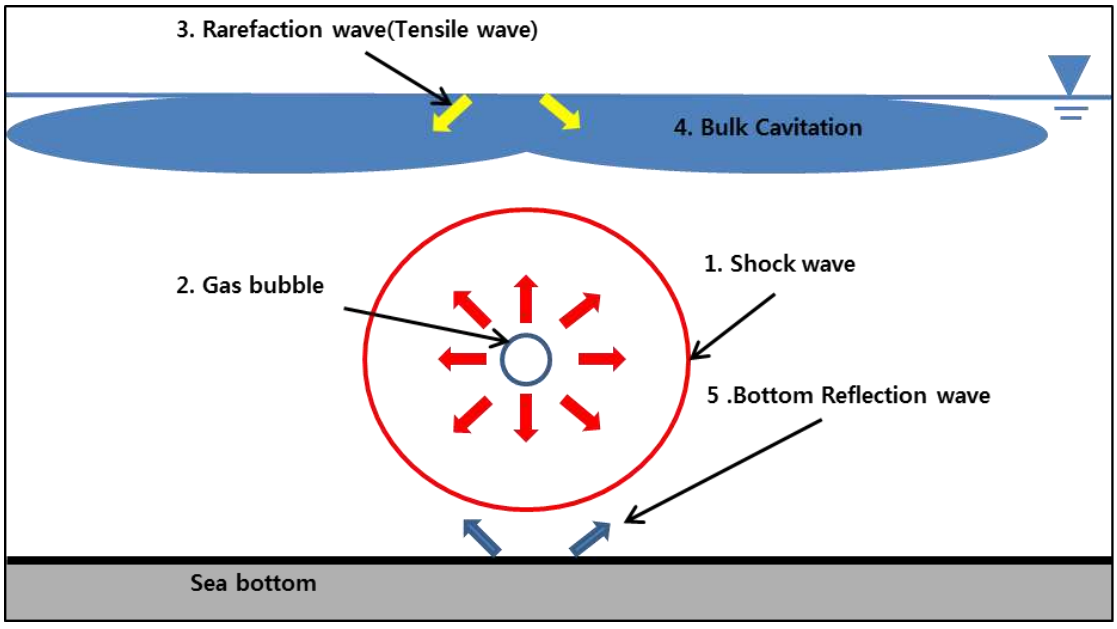

Figure 2.2 Underwater explosion phenomena

2.1.1 Shock wave propagation

During an underwater explosion, the charge instantly converts explosive energy into hot gas of approximately 3000 °C and induces a shock pressure of up to 730000 psi [7]. This shock wave propagates spherically into the water medium. Shock waves are instantaneous and their duration is of the order $10^{-5} \sim 10^{-3}$ s due to a rapid breakdown of an exited unstable explosive mixture into stable solids and gases with an associated release of high heat and energy. The explosion energy is a function of the charge weight and stand-off distance. The pressure time history at any location has an instantaneous pressure increase followed by a decay approximated by an exponential function given by

$$\mathrm{P(t)} = P_{max} e^{-\frac{t-t_1}{\theta}}, (\mathrm{t} \geq t_1) \tag{2.1}$$

$$P_{max} = K_1 \left(\frac{W^{\frac{1}{3}}}{R}\right)^{A_1} (psi) \tag{2.2}$$

$$\theta = K_2 W^{\frac{1}{3}} \left(\frac{W^{\frac{1}{3}}}{R}\right)^{A_2} (msec) \tag{2.3}$$

where W is the explosive weight, R is the standoff distance, and K_1, K_2, A_1 and A_2 are the shock parameters of the explosion.

Table 2.1 Shock wave parameters

	Parameters	HBX-1	TNT	PETN	NUKE
Pmax	K1	22347.6	22505	24589	4.38
	A1	1144	1.18	1.194	1.18
Decay Constant	K2	0.056	0.058	0.052	2.274
	A2	-0.247	-0.185	-0.257	-0.22
Impulse	K3	1.786	1.798	1.674	11760
	A3	0.856	0.98	0.903	0.91
Energy	K4	3086.5	3034.9	3135.2	3.313
	A4	2.039	2.155	2.094	2.04

The velocity of the water particle can be expressed with the following equation, where P(t) is the shock pressure time history, ρ is the water density, and c is the acoustic velocity.

$$u(t) = \frac{P(t)}{\rho c} + \frac{1}{\rho R}\int_0^t P(t)dt \tag{2.4}$$

The first term indicates the plane wave velocity, and second term is the after flow. According to the equation, the after flow is negligible if R is large. Equations (2.5) and (2.6) below indicate impulse per unit area and energy per unit volume. These equations are also a function of W(kg) and R(m). The coefficients K_3, K_4, A_3 and A_4 are empirical parameters.

$$I = \int_0^t p(t)dt = K_3 W^{\frac{1}{3}}\left(\frac{W^{\frac{1}{3}}}{R}\right)^{A_3} \qquad \left(lb - \frac{sec}{in^3}\right) \tag{2.5}$$

$$E = \int_0^t pudt = K_4 W^{\frac{1}{3}}\left(\frac{W^{\frac{1}{3}}}{R}\right)^{A_4} = \frac{W}{R^2} \qquad \left(lb - \frac{sec}{in^3}\right) \tag{2.6}$$

The total energy at the specified standoff distance R can be expressed as

$$E_s = 4\pi R^2 E = 4\pi K_4 W\left(\frac{W^{\frac{1}{3}}}{R}\right)^{A_4-2} \tag{2.7}$$

The value of A_4 is very close to 2, so the effect of $\left(\frac{W^{\frac{1}{3}}}{R}\right)$ in Equation (2.7) is negligible. The total energy E_s in Equation (2.7) can be roughly approximated as

$$E_s = WC_1, \quad C_1 = 4\pi K_4 \tag{2.8}$$

Where C_1 is the shock energy generated per unit mass of the explosive. Figure 2.3 shows the pressure profile of a shock wave

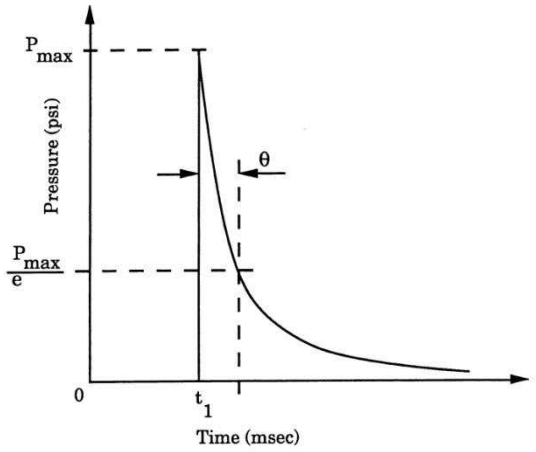

Figure 2. 3 Pressure profile of a shock wave

2.1.2 Gas bubble behavior and bubble pulse loading

Gas bubble behavior is not dealt with in this study on surface shield effects from waterblast waves, gas bubbles are just one factor in understanding underwater explosions. An overview of gas bubble theory is presented as helpful background information in understanding entire UNDEX phenomenon.

Gas bubbles generated by the explosion are almost spherical during their initial stage of expansion and contraction. The maximum bubble radius and the time taken to reach the first bubble-radius minimum can be calculated. Both vary with the size of the explosive charge and the depth at which the explosion occurs. These parameters can be calculated from

$$T = K_5 \frac{W^{\frac{1}{3}}}{(D+33)^{\frac{5}{6}}} \quad (\text{sec}) \tag{2.9}$$

$$R_{max} = K_6 \frac{W^{\frac{1}{3}}}{(D+33)^{\frac{1}{3}}} \quad (\text{ft}) \tag{2.10}$$

The constant values K_5 and K_6 are decided by type of charges and presented in Table 2.2.

Table 2.2 Gas bubble parameters

	Charge type			
Bubble parameter	HBX-1	TNT	PENTOLITE	NUKE
K_5**(Bubble perid)**	4.761	4.268	4.339	515
K_6 **(Bubble radius)**	14.14	12.67	12.88	1500

Where R_{max} is the maximum bubble radius in feet and T is the time to reach maximum radius in seconds. The peak pressure of a bubble, which is achieved during its first minimum, is approximately 10 ~ 15% of the shock-wave peak pressure and can be reduced by large migrations of bubbles towards the water surface. However, the pressure pulse that bubbles produce can result in localized loading effects on a ship's hull. Also, large bubbles often lose their symmetry and can collapse in upon themselves thus forming a toroid-shaped bubble and a column of rapidly moving water. The combination of the water jet and collective bubble pulse can produce extensive damage to ship hulls. Figure 2.4 shows the shock-wave and pressure pulses emitted from a bubble over time.

As a gas bubble expands during its oscillation, it displaces water, as the bubble contracts to a minimum, the water rushes in to surround the volume vacated by the contracting bubble. It would seem that the bubble would be most buoyant at its maximum size, but in fact the opposite is true. When the bubble is large, inertial forces brought on by the surrounding water dominate, cancelling out the buoyancy effect to a large extent. When the bubble is at its minimum, the inertial forces are also at a minimum and thus the buoyancy of the bubble causes it to rise at its maximum rate [8].

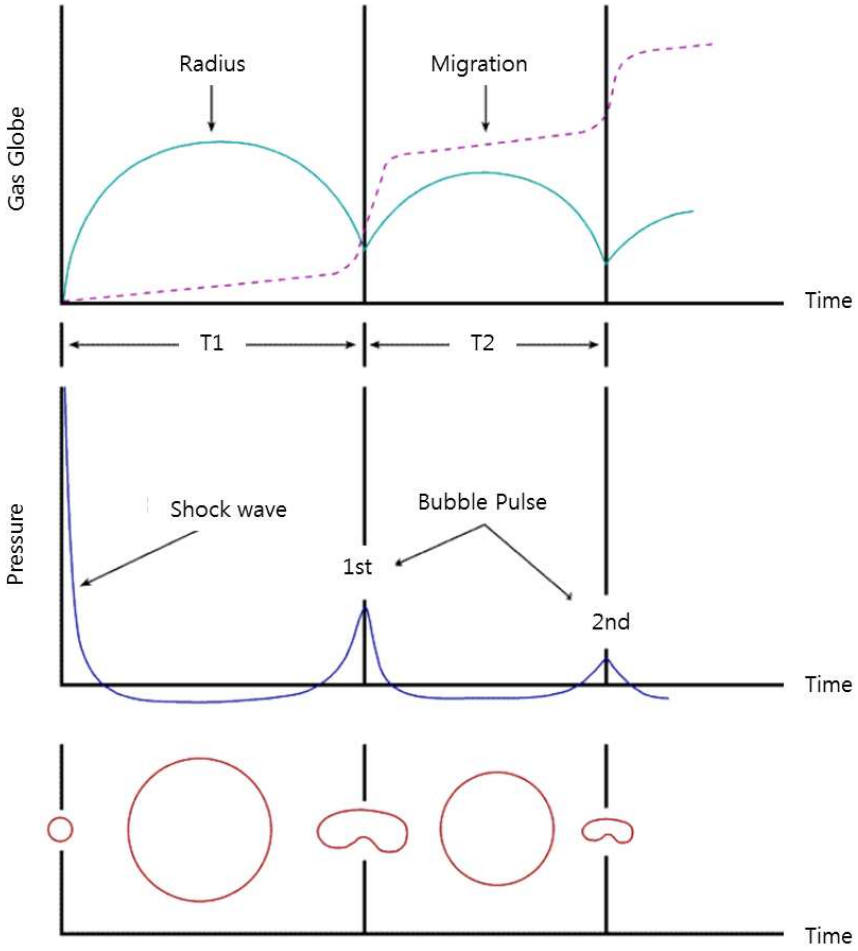

Figure 2.4 Bubble migration behavior versus bubble expansion.[8]

Depending on the initial depth of the explosion the bubble may migrate close to the water surface during its oscillation stage. If the bubble gets close enough to the surface, then the characteristic plumes of water that occur just after a shockwave cavitates the surface (spray dome) can be seen. Each of the plumes matches an outward expansion of the bubble that causes water to be displaced radially outward. If the first bubble expansion does not break through the water surface, then the first plume appears broad and low. The bubble then goes through another oscillation phase, thus migrating closer to the surface. If the bubble is going to breach the water surface it is usually during the second or third oscillation maximums, after which the energy has dissipated quite dramatically. When the bubble does finally breach the surface, the water plume is usually thinner, higher, and blackened due to the venting of carbon rich explosion gases.

2.1.3 Cavitation

Cavitation is a phenomenon which occurs when there is a region of negative absolute pressure present in the water. Since this negative pressure causes the tensile force in the water, and therefore, the water cannot sustain this force, cavitation or separation is formed. During an UNDEX event, there are two types of cavitations present in the water "bulk cavitation" and "local cavitation". Bulk cavitation can be considered a large region of low pressure at the free surface while local cavitation is a small region of low pressure usually occurring at the fluid-structure interface. When cavitation occurs in water, it has a large effect on the overall response of the ship during an UNDEX event. Therefore, this phenomenon must be considered a significant factor, and thus is included in the simulation process for a more accurate prediction [9].

2.1.3.1 Bulk cavitation

The shock wave propagates in a spherical enlarging circle from the charge detonation point in an UNDEX event. As seen in Figure 3, the incident shock wave, which is compressive, reflects from the free surface and results in a tensile reflected (rarefaction) wave. Since the water is unable to sustain a significant amount of tension, due to the reflected wave, the fluid pressure is reduced and bulk cavitation occurs when the absolute pressure drops to zero or below in the water. As a matter of fact, water can support a small quantity of tension (approximately a negative pressure of 3 to 4 psi), but zero psi is normally used for design and calculation purposes [10]. In the guidance of cavitation, the water and the surrounding pressures rise to the vapor pressure of water, which is about 0.3 psi. As shown in Figure 2.5, the reflected wave arrives at the image charge after the incident shock wave. The incident wave pressure has decayed, and then, the arrival of the rarefaction wave causes a sharp drop or so-called "cut-off" in the pressure. Notice that, as mentioned previously, cavitation occurs at cut-off when the absolute pressure in the water drops below the cavitation pressure, which is about a negative pressure of 3 to 4 psi [10]. Although it is not shown in the figures below, a bottom reflection wave may be present due to the reflection of the shock wave from the sea ground as well. Nevertheless, because the bottom reflection wave mostly depends on the properties of the sea ground and its

closeness to the ship, for an UNDEX event, this type of pressure wave is less important [7].

The underwater explosion geometry and shock wave pressure profile are shown in Figures 2.5 and 2.6.

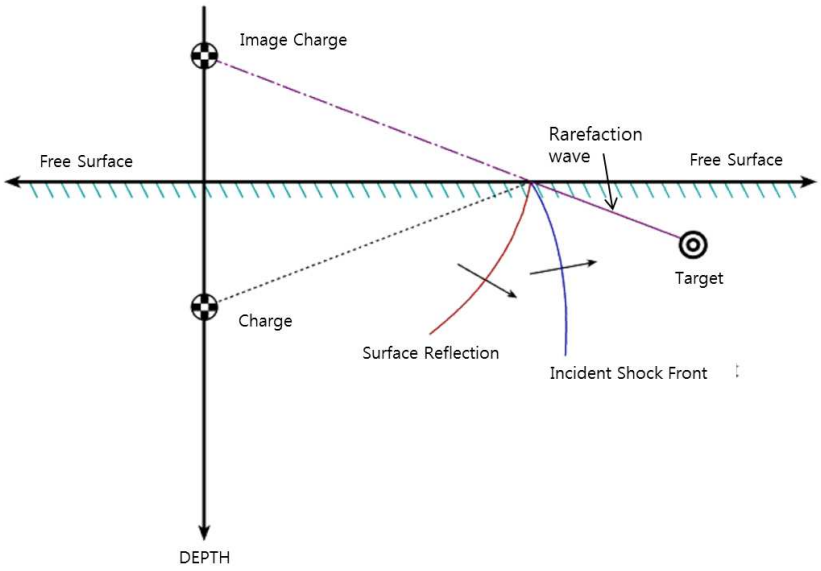

Figure 2. 5 Underwater Explosion Geometry

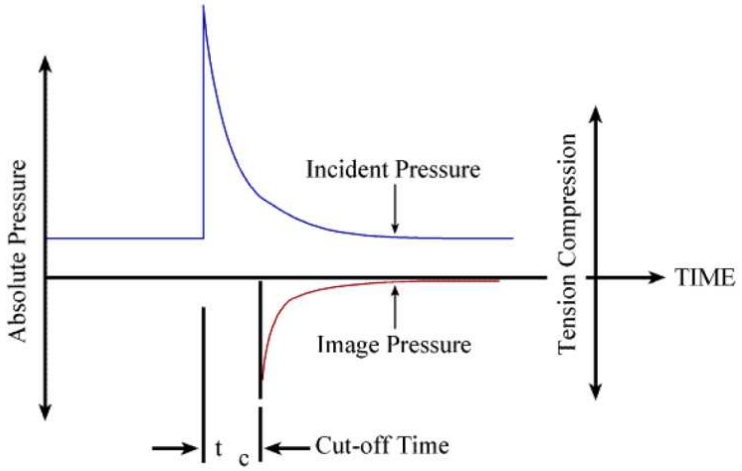

Figure 2.6 Shock Wave Pressure Profile with Cut-off Time [7]

The bulk cavitation region is described by an upper and a lower boundary. These boundaries are a function of the size, type and depth of the charge that is detonated in an UNDEX event [Ref. 9]. By

varying the weights and the depths of TNT charge, this dependency can be shown in Figures 2.7.

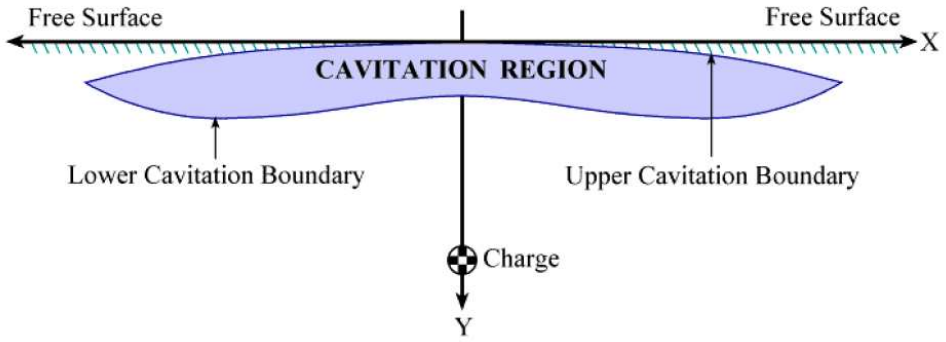

Figure 2.7 The bulk Cavitation Region Produced by an Underwater Explosion [8]

Upper cavitation boundary is defined as the locus of points at which the absolute pressure falls to the cavitation pressure upon arrival of the reflected wave [10]. As long as the absolute pressure does not go higher than the vapor pressure of water, the bulk cavitation area will remain cavitated. Since vapor and cavitation pressures are small enough, they can be taken as zero. To be able to determine the upper cavitation boundary, the total pressure must be considered. The upper cavitation boundary, which is defined as the region in which the total pressure is equal to zero in, is calculated by using Equation (2.11) along with Equations (2.12) and (2.13) [8].

$$F(x,y) = K_1\left(\frac{W^{\frac{1}{3}}}{r_1}\right)^{A_1} e^{-\frac{(r_2-r_1)}{c\theta}} + P_A + \gamma y - K_1\left(\frac{W^{\frac{1}{3}}}{r_2}\right)^{A_1} = 0 \qquad (2.11)$$

$$r_1 = \sqrt{(D-y)^2} \text{ and } r_2\sqrt{(D+y)^2 + x^2} \qquad (2.12), (2.13)$$

x, y = the horizontal range and the vertical depth of the point

r_1 = standoff distance from the charge to the point

r_2 = standoff distance from the image charge to the point

C = acoustic velocity in the water

D = charge depth

θ = decay constant (Equation 2.3)

P_A = atmospheric pressure

γ = weight density of water

W = charge weight

K_1, A_1 = shock wave parameters (depends on charge type, Table 2.1)

If the breaking pressure is defined as the rarefaction or reflected pressure that reduces the absolute pressure at the position to the cavitation pressure, the lower cavitation boundary is computed by making the decay rates of the absolute pressure and breaking pressure equal. The equation for this calculation is demonstrated in Equation (2.14) which makes use of the same variables as in Equations (2.11), (2.12), (2.13) [8].

$$G(x,y) = -\frac{P_i}{c\theta}\left\{1+\left[\frac{r_2-2D\left(\frac{D+y}{r_2}\right)}{r_1}\right]\left[\frac{A_2 r_2}{r_1}-A_2-1\right]\right\}$$
$$-\frac{A_1 P_i}{r_1^2}\left[r_2-2D\left(\frac{D+y}{r_2}\right)\right]+\gamma\left(\frac{D+y}{r_2}\right)+\frac{A_1}{r_2}(P_i+P_A+\gamma y)=0 \qquad (2.14)$$

where P_i, the incident pressure at cut-off time, is provided by the following expression,

$$P_i = P_{max} e^{-\left[\frac{(r_2-r_1)}{c\theta}\right]} \qquad (2.15)$$

Figure 2.8 shows a cross-section view which represents the bulk cavitation region generated by a 5000 lb TNT charge exploded 164 ft. below the free surface. It must be noted that the bulk cavitation region in Figure 2.8 is actually three-dimensional, and normally symmetric about an imaginary vertical axis passing through the charge. The water particles behind the shock wave front have velocities depending on their position 18 relative to the charge location and the free surface at the time of cavitation. For instance, water particles near the free surface will have a primarily vertical velocity

at cavitation. As the reflected wave passes, the particles will be acted upon by gravity and atmospheric pressure.

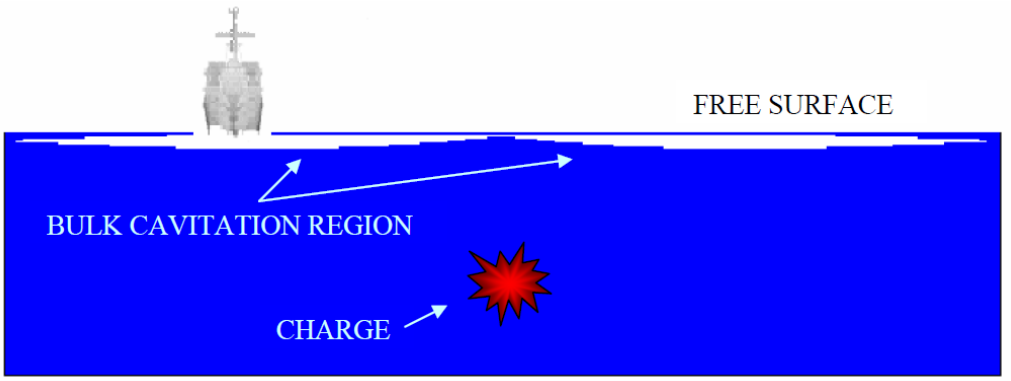

Figure 2.8 Bulk Cavitation Region in an Underwater Explosion Event

This region will remain in the cavitated state until its absolute pressure rises above zero psi [8].

2.1.3.2 Local cavitation

The shock pressure pulses which are created by an underwater explosion impinging on a ship agitate the structure which causes dynamic responses. As long as the pressure pulses impinge the flexible surface of the structure, a fluid-structure interaction takes place. When this fluid-structure interaction occurs, the total pressure throughout the ship's hull turns out to be negative. Since the water can not sustain tension, the water pressure decreases the vapor pressure, and then local cavitation occurs. For the simplest fluid-structure interaction situation, the Taylor flat plate theory will be used to be able to illustrate how the local cavitation occurs. Figure 2.9 shows a Taylor flat plate subjected to a plane wave.

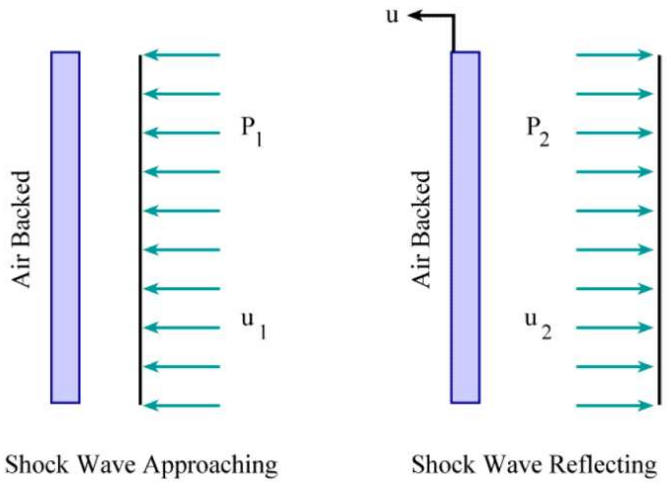

Figure 2.9 Taylor plate subjected to a plane wave [11]

An infinite and air backed plate of mass is subjected to the incident plane shock wave of pressure $P_1(t)$. When the incident plane shock wave interacts with the plate, the reflection wave of pressure $P_2(t)$ will be reflected off the plate. If the velocity of the plate is defined as u(t) , the equation of motion of the plate utilizing Newton's 2nd law can be written as

$$m\frac{du(t)}{dt} = P_1(t) + P_2(t) \tag{2.16}$$

where m is the mass of the plate per unit area.

The fluid particle velocities behind the incident and reflected shock waves are defined as $u_1(t)$ and $u_2(t)$, respectively. The interface between the surface of the plate and the fluid is expressed as

$$u(t) = u_1(t) - u_2(t) \tag{2.17}$$

For a one-dimensional wave, the incident and reflected shock wave pressures can be shown as follows:

$$P_1(t) = \rho C u_1(t) \tag{2.18}$$

$$P_2(t) = \rho C u_2(t) \tag{2.19}$$

where ρ and C are the fluid density and acoustic velocity, respectively. Substituting Equations (2.18) and (2.19) into Equation (2.17) results in the next equation for the velocity of the fluid particle along the fluid-structure interface,

$$u(t) = u_1(t) - u_2(t) = \frac{P_1(t) - P_2(t)}{\rho C} \tag{2.20}$$

Once more, substituting Equation into (2.20) and solving for$P_2(t)$, the reflected pressure wave equation is defined as

$$P_2(t) = P_{max} e^{-\left(\frac{t-t_1}{\theta}\right)} - \rho C u(t) \tag{2.21}$$

and then, the equation of motion, Equation (2.16) can be rewritten as

$$m\frac{du(t)}{dt} + \rho C u(t) = 2P_{max} e^{-\left(\frac{t-t_1}{\theta}\right)} \tag{2.22}$$

If the first order linear differential equation, Equation (2.22) is solved, it results in the following relationship for the plate velocity.

$$u(t) = \frac{2P_{max}\theta}{m(1-\beta)}\left\{e^{-\left[\frac{\beta(t-t_1)}{\theta}\right]} - e^{-\left[\frac{(t-t_1)}{\theta}\right]}\right\} \tag{2.23}$$

Where $\beta\frac{\rho C\theta}{m}$ and $t > 0$. Finally $P_2(t)$ and the total pressure at the plate can then be expressed as

$$P_2(t) = \frac{P_{max}}{(1-\beta)}\left\{(1-\beta)e^{-\left[\frac{(t-t_1)}{\theta}\right]} - 2\beta e^{-\left[\frac{\beta(t-t_1)}{\theta}\right]}\right\} \tag{2.24}$$

$$P_1 + P_2 = P_{max}\left\{\frac{2}{(1-\beta)}e^{-\left[\frac{(t-t_1)}{\theta}\right]} - \frac{2\beta}{1-\beta}e^{-\left[\frac{\beta(t-t_1)}{\theta}\right]}\right\} \tag{2.25}$$

Equation (2.25) illustrates that, as β becomes large, which corresponds to a light weight plate, the total net pressure turns out to be negative at a very early time. Therefore, local cavitation occurs as the vapor pressure of water is reached. This local cavitation essentially separates the plate from the

water [8]. Furthermore, because the pressure in front of the plate occurs at cut-off time, the plate reaches its maximum velocity. The time when the maximum plate velocity occurs can be calculated by setting $P_1 + P_2$ equal to zero and solve for t. By using Equation (2.25), t_0 , the time for the maximum plate velocity is expressed as

$$t_0 = \frac{\ln \beta}{\beta - 1}\theta \tag{2.26}$$

then substituting 0 t into Equation (2.23), the maximum plate velocity results in the following equation.

$$u_{max} = \frac{2P_{max}\theta}{m(1-\beta)}\left\{e^{-\left[\frac{\beta t_0}{\theta}\right]} - e^{-\left[\frac{t_0}{\theta}\right]}\right\} \tag{2.23}$$

It can be noticed that the equations used in the Taylor plate theory are valid only up to the time when the cavitation starts. After that, this problem turns into nonlinear and possibly non conservative. Since the momentum of the plate equals to no more than a fraction of the impulse in the shock wave for the light plate weights, a second loading which increases the plate velocity will arise. This second loading can be more damaging than the first.

2.2 Hull response and damage subjected to underwater explosion

2.2.1 Incident shock wave damage

Shock damage to the hull area of a ship can very quite dramatically, depending on the charge size, orientation and proximity to the hull. If the charge is located directly or almost directly underneath or close by to a ship then there could be a contribution to the damage arising from the bubble collapse onto the ship's hull and also due to whipping damage caused by the bubble pulses [12].

An explosive charge detonating in contact with or in very close proximity to the ship's hull will also generally tear a large hole given that the hull thickness is not too great and that the charge is of a sufficient size. The bulkheads close to the point of attack will also often rupture due to direct exposure to the shockwave, or to deformation caused in the bulkhead by hull deformation. Fragmentation of the shell of the explosive charge may also cause severe damage to equipment in the immediate vicinity. Although the damage may quite often be severe it usually does not extend far into the ship or in the fore-and-aft direction [12].

As the stand-off increases, the point at which the hull just ruptures is reached. Past this point the hull is still water tight but heavily deformed with the level of deformation decreasing as the stand-off continues. Eventually a point is reached where only elastic hull deformation occurs. At large stand-off distances, the shock-wave front is essentially planar and the ship is more or less loaded as a whole rather than in localized areas as with a smaller charge close in to the hull. However different portions of the ship will respond at different velocities depending upon the mass per unit area. Most ship shock trials are performed at large stand-off distances for this reason [12].

When a shock-wave arrives at a ship's hull, the pressure loading on the plating shows an almost instantaneous rise to a peak pressure followed by an exponential decay period. If the plating is relatively light it responds by accelerating until a point is reached where the plating moves faster than the water adjacent to the plating can respond. Because water cannot sustain tension a localized cavitation region is produced and the maximum velocity which the hull has picked up is the kick-off velocity At some later stage the cavitation envelope adjacent to the hull closes and the plate is reloaded again but usually not at the previous loading level. However it is not uncommon for further deformation to take place due to cavitation closure.

2.2.2 Bubble jet damage

Another damage mechanism which follows on closely to that of bubble-pulse loading is bubble collapse. If the oscillating gas bubble is close enough to a rigid body surface such as a submarine or ship hull then the pressure differential created as the bubble decreases in volume (caused by resistance to water low close to the hull) will result in the bubble collapsing onto the hull and producing a high speed water jet, which in some instances is capable of holing the hull. Much research is currently being performed to model the collapse and formation of the water jet, using hydro codes and finite element models [12].

2.2.3 Cavitation damage

Surface cut-off occurs when a plane compressive wave hits a free surface, is then reflected off that surface as a tensile wave, and then interacts with (cancels out) the compressive wave so as to produce a slightly negative pressure. For ships and submarines near the surface it means that the shock-wave pressure loading (which is decreasing in an exponential fashion after the initial loading phase) on the hull may suddenly drop to the ambient pressure. This may be significant if another reloading occurs (eg. due to bubble pulse) and the hull is moving down towards the water surface [12].

The phenomenon of bulk cavitation occurs when a shock-wave is reflected off a free surface such as the air/water interface. The compression shock-wave reflects off the free water surface as a tensile wave and since water can only sustain a very small level of tension it begins to cavitate. The cavitated region forms a bulk cavitation envelope which has an upper and lower boundary and extends in a radial direction away from the centre of the explosive burst position. The extent and duration of the cavitated region that forms can be generated from equations in which the negative pressure distribution with time is determined [14].

Eventually the bulk cavitated region closes (like a zipper) and the water layer above the cavitated region closes down onto the lower layer causing a water hammer (effect) which sends out a pressure wave (cavitation pulse). If the point of closure of the cavitation region lies close to the hull of a ship or submarine then reloading may occur. In certain circumstances this may result in higher recorded strains, than the original pressure pulse resulting from the detonation of the charge [12]..

2.3 Arbitrary Lagrangian Eulerian(ALE) Method

Explosions involve liquid and gas flow, as well as high-pressure shock waves. A Lagrangian finite element mesh in the explosive charge region is not always feasible. The surrounding fluid medium elements around the explosive charge deform severely in Lagrangian based meshes. Consequently, the time step size per iteration becomes extremely small resulting in large computational time [15].

Furthermore, numerical approximation inaccuracies can exist due to mesh distortions [16].

Eulerian based finite element modeling advance solutions in time on a fixed mesh using Navier-Stokes equations. When the solutions are progressed on a fixed mesh, the Eulerian hydrocodes avoid mesh distortions as presented in the Lagrangian hydrocodes. Additionally, algorithms have been developed to prevent the diffusion between two material types at a higher computational expense. Furthermore, solving the Navier- Stokes equations (Eulerian) are generally more expensive computationally and complicated than the Lagrangian formulation [17]. As a result, a hybrid numerical formulation technique has been developed which tries to utilize the advantages of both the Eulerian and Lagrangian schemes.

The numerical analysis processor conducted in this study utilizes an ALE finite element code. LS-DYNA [18] was used for the numerical analysis during this investigation. ALE hydrocodes utilize

both Lagrangian and Eulerian hydrocodes that perform automatic rezoning [19]. An ALE hydrocode involves a Lagrangian time step followed by a remap or advection phase. The advection phase may pursue one of three avenues in which the spatial mesh is (a) not rezoned due to reasonable mesh deformation (Lagrangian), (b) rezoned to its original shape due to severe mesh deformation (Eulerian), or (c) rezoned to a more suitable form (Lagrangian and Eulerian) thus allowing the topology of mesh to remain fixed. [18], [20]. It provides suitable material models and essential equations of state (EOS) for underwater and air explosions. Furthermore, the code provides advection and coupling algorithms in the ALE method in order to provide accurate, stable, conservative, and monotonic results. Mass, momentum, and energy transport is systematically computed for all elements in the model. Each element's density, velocity, and energy will be updated. Pressure in each element is computed using the updated density and specific internal energies in the model's EOS. The figures from 2.10 to 2.12 show the difference of the lagrangian, eulerian and ALE method.

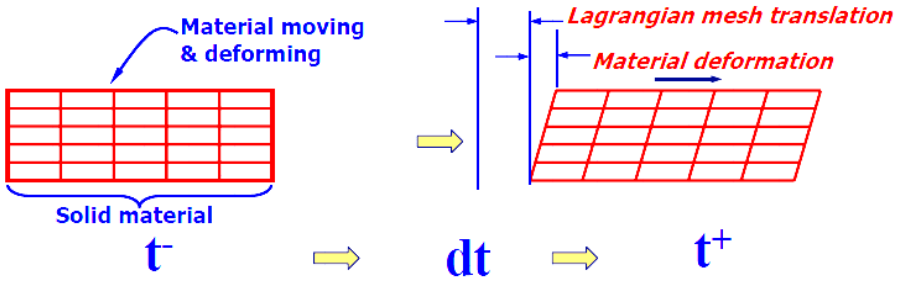

Figure 2. 10 Lagrangian method[21]

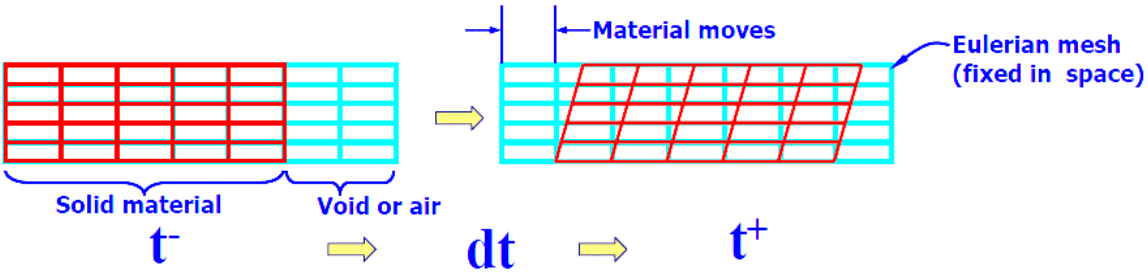

Figure 2.11 Eulerian method [21]

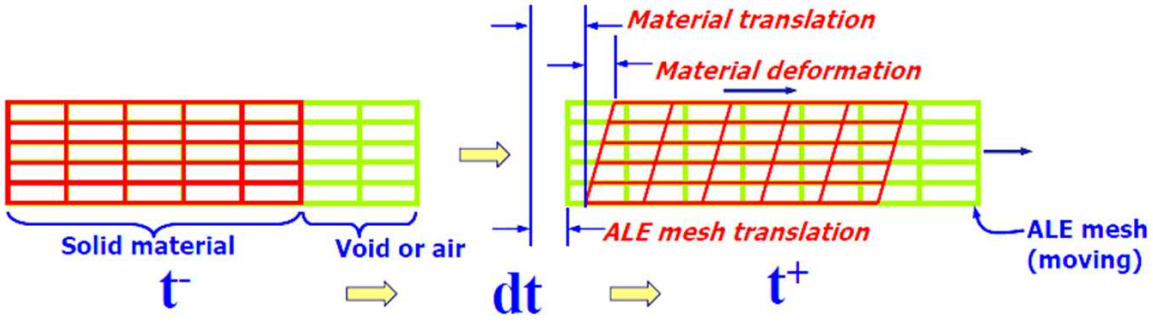

Figure 2.12 Arbitrary Lagrangian-Eulerian method [21]

2.4 Ship system damping

Damping is the energy dissipation mechanism that causes vibrations to diminish over time and eventually stop. Amount of damping mainly depends on the material, velocity of motion, and frequency of vibration [22].

Almost all of the damping within a structure is a result of frictional energy that is being dissipated at physical connection points such as bolted or riveted joints. However, in a ship the majority of connections are welded rather than mechanically joined, so there is much less energy dissipation through the welds. Ships do however provide a viable means for energy to escape the system. This occurs through long cable runs, hangers, snubbers and out to the fluid surrounding the hull itself [23].

LS-DYNA allows Rayleigh damping constants α and β only. Damping can be classified as viscous damping and hysteresis(solid) damping. The viscous damping is rayleigh mass-weighted damping constant αand the hysteresis(solid) damping is rayleigh stiffness-weighed damping constant β. Rayleigh damping constant α and β are used as multipliers of [M] and [K] to calculate [C]

$$[C] = \alpha[M] + \beta[K] \tag{2.24}$$

$$\frac{\alpha}{2\omega} + \frac{\beta\omega}{2} = \xi \tag{2.25}$$

where ω is the frequency, and ξ is the damping ratio.

Since there are two unknowns, assume that the sum of alpha and beta damping gives a constant damping ratio ξ over the frequency range $\omega 1$ to $\omega 2$. This gives two simultaneous equations from which you can solve for α and β.

$$\frac{\alpha}{2\omega_1} + \frac{\beta\omega_1}{2} = \xi \tag{2.26}$$

$$\frac{\alpha}{2\omega_2} + \frac{\beta\omega_2}{2} = \xi \tag{2.27}$$

where the damping ratio ξ can be obtained from test data as follows

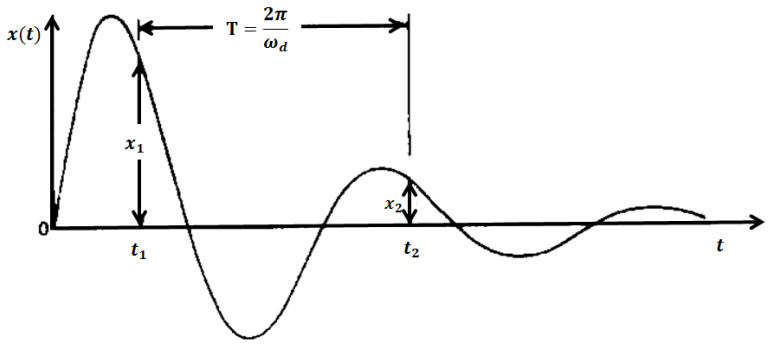

Figure 2.13 Damping rate

calculate the logarithmic decrement, δ, as follows

$$\delta = \ln\left(\frac{x_1}{x_2}\right) \tag{2.28}$$

x_1 and x_2 are two consecutive displacements, one cycle apart. And ξ is follows

$$\xi = \frac{\delta}{\sqrt{(2\pi)^2+\delta^2}} \tag{2.29}$$

2.5 Equation of state (EOS)

The solid elements for the water and air are employed by equation of state(EOS). An equation relating the pressure, temperature, and specific volume of a substance is known as an EOS. Property relations involving other properties of a substance at equilibrium states are also known as an equation of state [19]. This investigation utilized two different EOS in the modeling and simulation. The EOS involved were the linear polynomial and Jones Wilkins and Lee (JWL) equations.

2.5.1 Linear Polynomial equation[19]

Air and water are modeled using the linear polynomial EOS. The linear polynomial EOS is linear in internal energy per unit initial volume, E. The pressure is given by

$$p = C_0 + C_1\mu + C_2\mu^2 + C_3\mu^3 + (C_4 + C_5\mu + C_6\mu^2)E \quad (2.30)$$

Here, C_0, C_1, C_2, C_3, C_4, C_5 and C_6 are user defined constants and

$\mu = (\rho-\rho0)/\rho0$ = Acoustic condensation

E = internal energy per volume

$$\mu = \frac{1}{V} - 1 \quad (2.31)$$

where V is the relative volume. In expanded elements, the coefficients of μ^2 are set to zero, i.e.,

$$C_2 = C_6 = 0$$

The linear polynomial equation of state may by used to model gas with the gamma law equation of state. This may be achieved by setting

$$C_0 = C_1 = C_2 = C_3 = C_6 = 0$$

And

$$C_4 = C_5 = \gamma - 1$$

Where γ is the ratio of specific heats. The pressure is then by

$$p = (\gamma - 1)\frac{\rho}{\rho_0}E$$

2.5.2 Jones Wilkins and Lee (JWL) equations[19]

The JWL equation is employed for the explosive. The JWL EOS defines the pressure as a function of the relative volume, V, and initial energy per initial volume, E, such that

$$p = A\left(1 - \frac{\omega}{R_1 V}\right)e^{-R_1 V} + B\left(1 - \frac{\omega}{R_1 V}\right)e^{-R_2 V} + \frac{\omega E}{V}$$

※ $\eta = \rho/\rho 0$ ($\rho 0$ = Initial density)

E = Specific internal energy per mass

A, B, ω, R1, R2 = Constants for explosive

The parameters ω, A, B, R_1 and R_2 are constants pertaining to the explosive. This EOS is well suited because it determines the explosive's detonation pressure in applications involving structural metal accelerations [24].

2.6 Coupling method

Fluid-Structure Interactions(FSI) between ALE(Fluid) and lagrangian(structure) material, each modeled with separate meshes. LS-DYNA searches for the interections between the lagrangian parts and ALE parts. If a coupled Lagrangian surface is detected inside an ALE element, LS-DYNA marks the Lagrangian-Eulerian coupling points(NQUAD) at t-. It then tracks the independent motion of the 2 materials over dt(ALE material interface is tracked based on its volume fraction in the element). Then

it computes the penetration distance of the ALE material across the Lanrangian surface. Coupling forces are calculated based on this penetration and re-distributed back on to both materials.

The coupling forces are usually computed based on a penalty method(similar to that used for standard lagrangian contact).

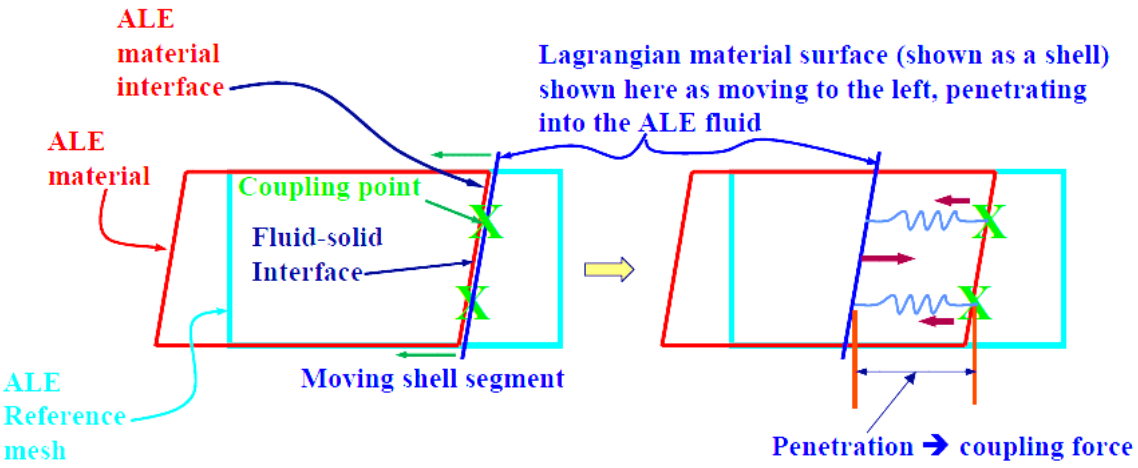

Figure 2.14 Coupling method based penetration

2.7 Scaling

2.7.1 Hopkinson scaling law

A deformable structure immersed in a fluid subjected to a shock wave loading imparted through the fluid is common to refer to Hopkinson scaling(baker, 1991) [25].

The down Scaling model experiment is used to save time and money and extract as much useful information as possible as quickly and efficiently as possible and at minimum cost. Since we normally Construct models of the same material as prototype we must keep density and failure stress invariant. Also we wish to scale geometrically so that the length scales linearly. This means that out scale factor, λmust be related to length, density, and stress as follows

Table 2. 3 Hopkinson scaling law [8]

Parameters	Dimensions	Scale Factor
Length(L)	L	λ^1
Time(T)	T	λ^1
Force(F)	F	λ^2
Velocity(v)	LT^{-1}	λ^0
Displacement(S)	L	λ^1
Acceleration(a)	LT^{-2}	λ^{-1}
Grav.Const(g)	LT^{-2}	λ^0
Mass(m)	FT^2L^{-1}	λ^3
Density(ρ)	FT^2L^{-4}	λ^0
Stress(σ)	FT^2	λ^0
Pressure(p)	FT^2	λ^0
Failure Stress(σ)	FT^2	λ^0
Strain(ε)	-	λ^0
Strain rate($\dot{\varepsilon}$)	T^{-1}	λ^{-1}
Volume(Vol)	L^3	λ^3
Energy(E)	FL	λ^3
Impulse(I)	FT	λ^3

Chapter 3 Modeling and Simulation

Pre-processing, analysis, and post-processing are used for the modeling and simulation. A flow chart for the model building and simulation procedure is shown in figure 3.1. For this simulation, the models are generated using TrueGrid and VPG. LS-DYNA is used for the analysis. LS-POST is used for the post-processing.

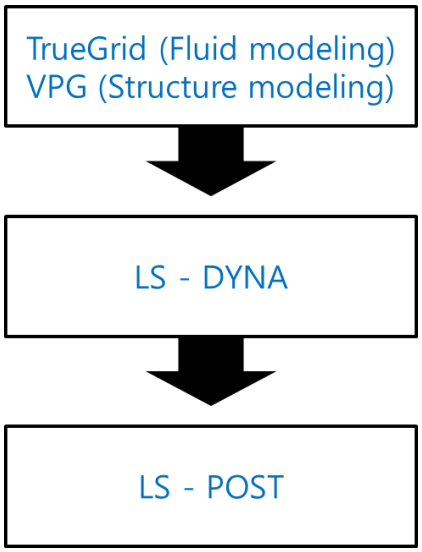

Figure 3.1 Flow chart of simulation.

3.1 Modeling

3.1.1 Water and air modeling

The finite element models of the fluid parts are made using TrueGrid, which is a smart grid generator. The fluid groups are separated into the air part and water part. The nodes in the air and water boundaries must be merged.

The fluid models are made similar to the experimental environment, because the objective is to compare the test results with numerical analysis results. The depth of the modeled water is 10 m,

which is almost the same as the test site. To avoid the impact of reflected waves from the side boundary, the width of the free surface is modeled at approximately 20 m. The air area is modeled at 5 m to see the plume caused by bubbles.

Application of too many elements for the fluid area would increase the computation time drastically. To avoid this scenario, the area that contains the ship and explosive is the only densely generated area. The smallest size of elements of the water area is 4 cm. As a result of the fluid modeling, the number of fluid elements is 4,447,710. Figure 3.2 shows the fluid model.

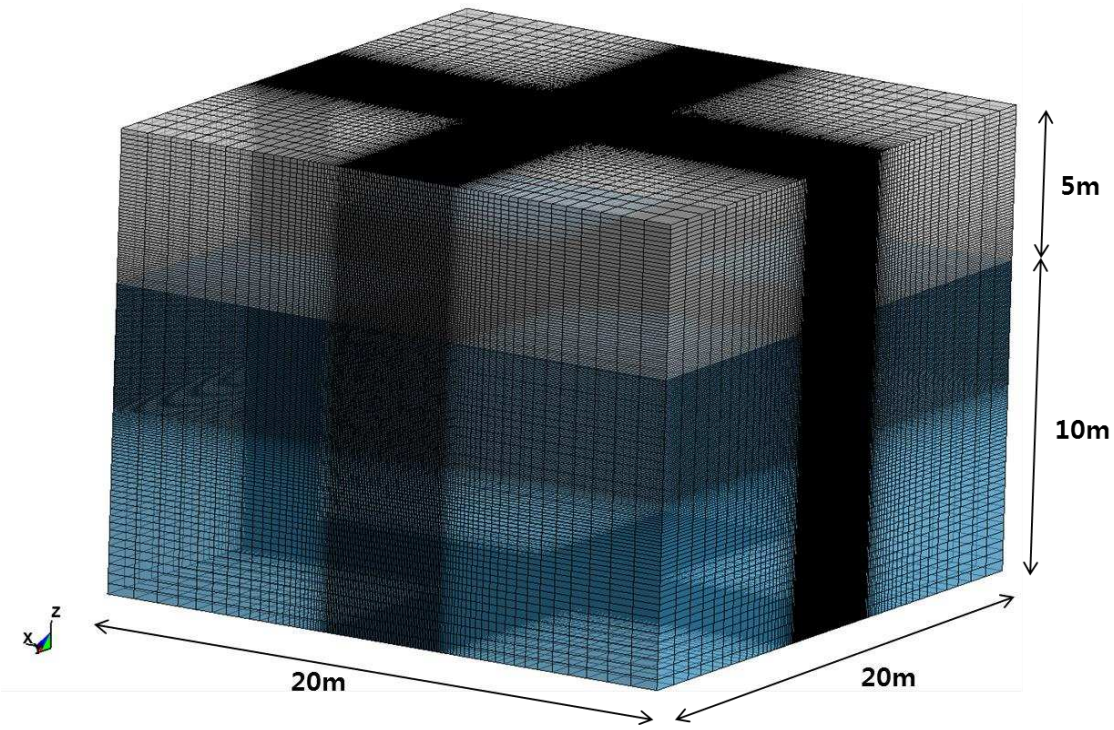

Figure 3.2 Fluid model (air and water).

Because fresh water is used for the real explosion test, fresh water's equation of state is employed for the water area model. Air's well-known equation of state is also employed. The basic units employed in this paper are g, mm, and ms. The values of equation of state are described in table 3.1.

Table 3.1 Parameters of linear polynomial equation of state.

Properties	Fresh water	Air
Density (g/mm^3)	1	0.001
C_0 **(MPa)**	0	0
C_1 **(MPa)**	2002	0
C_2 **(MPa)**	8436	0
C_3 **(MPa)**	8010	0
C_4	0.4394	0.4
C_5	1.3937	0.4
C_6	0	0
E_0	0.2086	0.25
V_0	1	1

$$p = C_0 + C_1\mu + C_2\mu^2 + C_3\mu^3 + (C_4 + C_5\mu + C_6\mu^2)E \quad \text{(Pressure in compression)} \tag{3.1}$$

$$p = C_1\mu(C_4 + C_5\mu + C_6\mu^2)E \quad \text{(Pressure in tension)} \tag{3.2}$$

Where, $\mu = \frac{\rho - \rho_0}{\rho_0}$

E : Unit of pressure

E_0 : Initial internal energy per unit reference specific volume

V_0 : Initial relative volume

3.1.2 Explosive modeling

Many kinds of explosives are available, including HBX-1, TNT (trinitrotoluene), and PENT. This study employed TNT (trinitrotoluene), which is shown as being in the center of water in figures 3.3 and 3.4. There are three ways to model an explosive: as a solid, as a spherical shell, or by using the keyword of the initial_volume_fraction_geometry in LS-DYNA. Using solid modeling provides the advantage of modeling the exact mass of the explosive. However, in this method, generation of the model is complicated. It is suitable for checking the shock wave pressure. Figure 3.3 shows a solid explosive model.

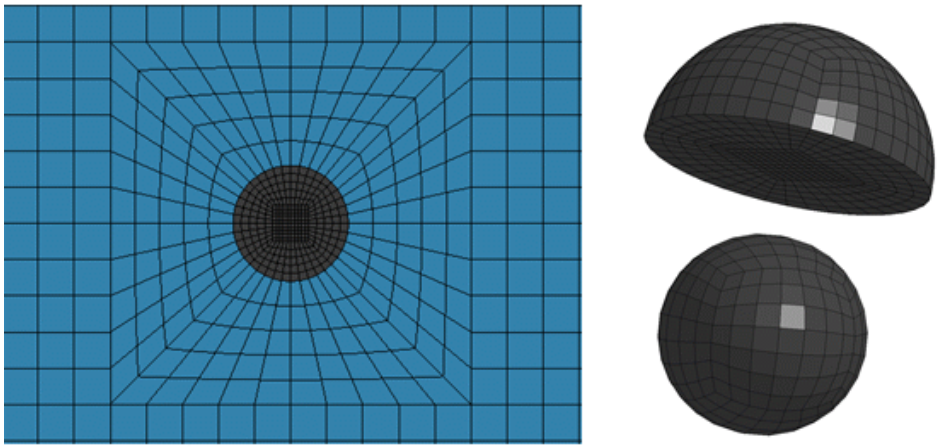

Figure 3.3 Solid explosive model.

As mentioned above, the other two ways are the use of a spherical shell for the explosive and employing the keyword of the initial_volume_fraction_geometry in LS-DYNA. The hydrostatic pressure is essential for detecting bubble oscillation. It requires 0.2 s to stabilize the hydrostatic pressure. However, when the solid model is used, the explosive sinks in 0.2 s. One way of avoiding this problem is to make a spherical shell and fix it by employing the boundary_spc_set keyword. Next, the tail side of the spherical shell's normal vector is defined as TNT by using the initial_volume_fraction_geometry keyword. The use of this method enables maintaining the explosive without sinking. This way is easier than making a solid explosive. Figure 3.4 shows a spherical shell and the normal vectors.

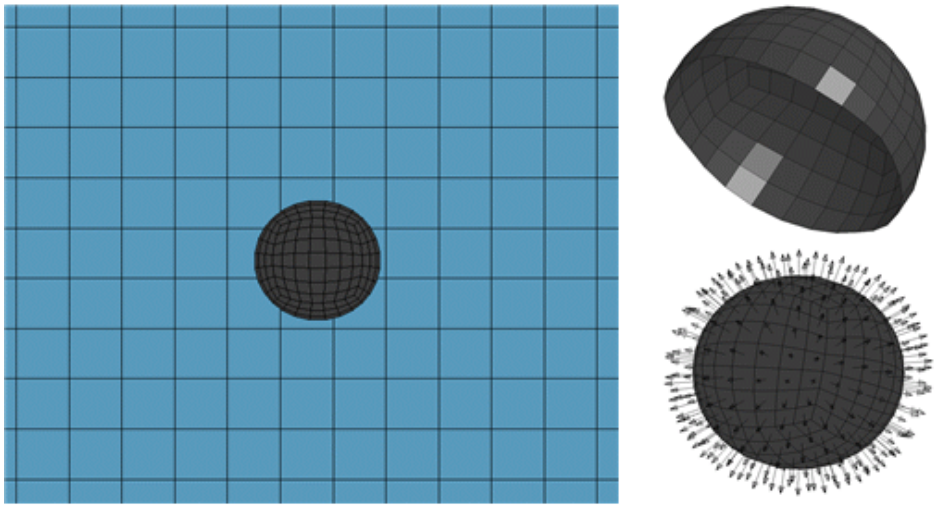

Figure 3.4 Spherical shell model for explosive.

The density of TNT is 1630 kg/m^3. The TNT model employs the Jones-Wilkins-Lee (JWL) equation of state (EOS), which defines the pressure as eq. 3.3 and is usually employed for detonation products of high explosives. The JWL equation of state defines a function of the relative volume, E, as

$$p = A\left(1 - \frac{\omega}{R_1 V}\right)e^{-R_1 V} + B\left(1 - \frac{\omega}{R_1 V}\right)e^{-R_2 V} + \frac{\omega E}{V} \tag{3.3}$$

where ω, A, B, R_1 and R_2 are user-defined input parameters. The JWL equation of state is used to determine the pressure of the detonation products of high explosives in applications involving metal accelerations. The input parameters for this equation have been given by Dobratz [24] for a variety of high explosive materials.

This equation of state is used with the explosive burn material model, which determines the lighting time for the explosive element [12]. The parameters of JWL are described in table 3.2.

Table 3.2 Parameters of the JWL EOS.

Parameters	TNT
Density (g/mm^3)	1630
Detonation velocity	6930
Chapman-Jouget pressure	2.1E+4
A	3.371E+5
B	3231
R_1	4.15
R_2	0.95
OMEGA	0.3
E_o	7000
V_0	1

3.1.3 Ship-like structure modeling

To verify the response of the ship-like structure in a numerical simulation, the simulation conditions and cases used are almost the same as the conditions employed for the experiment. A finite

element model for the simulation is developed using VPG.

To compare the simulation results with ship shock test results, a ship-like structure is constructed as a finite element model. The hull-form of this ship-like structure is a double hull called a catamaran. The reasons for using a double hull form are the assumption that the tested structure is a high-speed ship and the need to maintain the restoring force of the structure. The catamaran form is usually used for a high-speed ship and hence selected here. The catamaran's specifications are listed in table 3.3 and figures 3.5 and 3.6.

Table 3.3 Modeling specifications of ship-like structure.

Properties	Value
Length	2000 mm
Width	1000 mm
Height	250 mm
Weight	32.71 kg
Displacement	27.23 L
Material	AL5052_H32

To confirm the deformation, aluminum is selected as the material for constructing the ship-like structure. Aluminum's properties are listed in table 3.4. The ship-like structure's water line is shown in figure 4.8.

Table 3.4 Mechanical properties of AL5052_H32.

Properties	AL5052_H32	Conditions (°C)
Density (×1000 kg/m^3)	2.68	
Poisson's Ratio	0.33	
Elastic Modulus (GPa)	70–80	
Tensile Strength (MPa)	230	
Yield Strength (MPa)	195	25
Elongation (%)	12	
Hardness (HB500)	60	
Shear Strength (MPa)	140	
Fatigue Strength (MPa)	115	

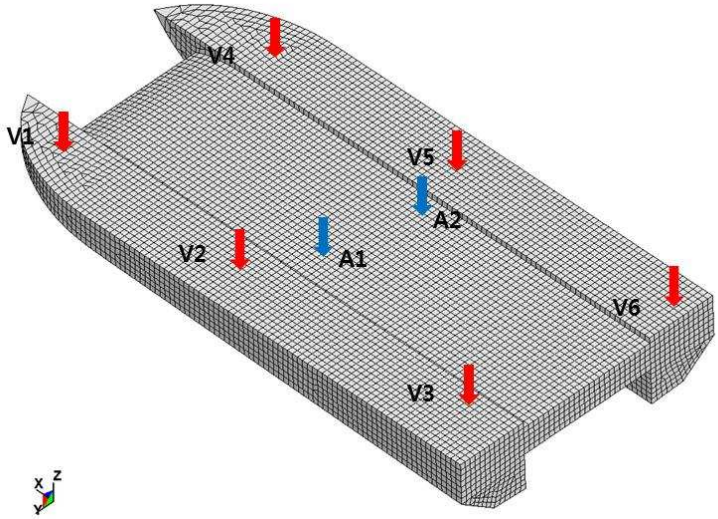

Figure 3.5 Outer hull of ship-like structure and measurement positions.

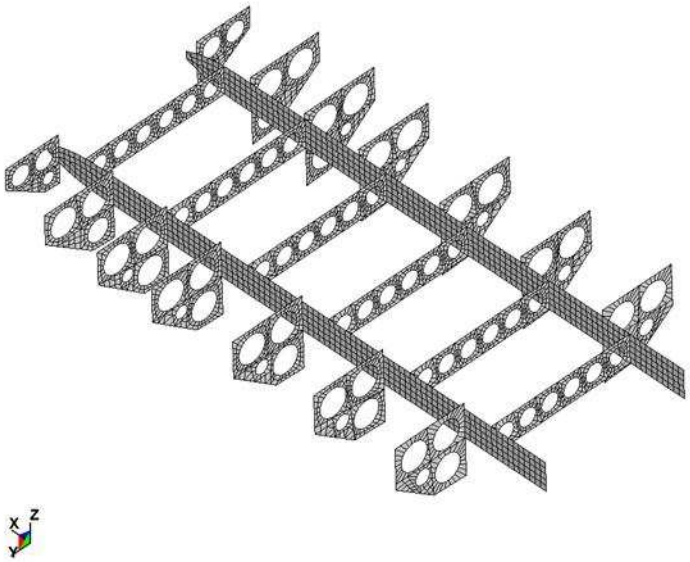

Figure 3.6 Bulkheads and girders in ship-like structure.

The center of mass of the structure is described in table 3.5. Next, an analysis is conducted with LS-DYNA by employing the designed finite element models. The results of the simulation are described in the next chapter.

Table 3.5 Center of mass.

Axis	Coordinate(mm)
X	-80
Y	0
Z	78

3.2 Simulation

3.2.1 Bulk Cavitation

As explained in chapter 2, the bulk cavitation phenomenon occurs at the time of an underwater explosion. In this chapter, the bulk cavitation phenomenon is verified by the simulation. Two hundred and fifty grams of TNT are employed for this simulation. The depth of the explosive from the free surface is 1.5 m. The explosive is constructed using solid elements generated by TrueGrid. Figure 3.7 shows the bulk cavitation area. As shown in figure 3.7, the bulk cavitation zone is generated at 1.8 ms, and the closing bulk cavitation pulse is generated at 11 ms. The closing pulse pressure is very large because the duration is longer than the incident shock wave. It can also impact the structure. Figure 3.8 shows the closing pulse pressure.

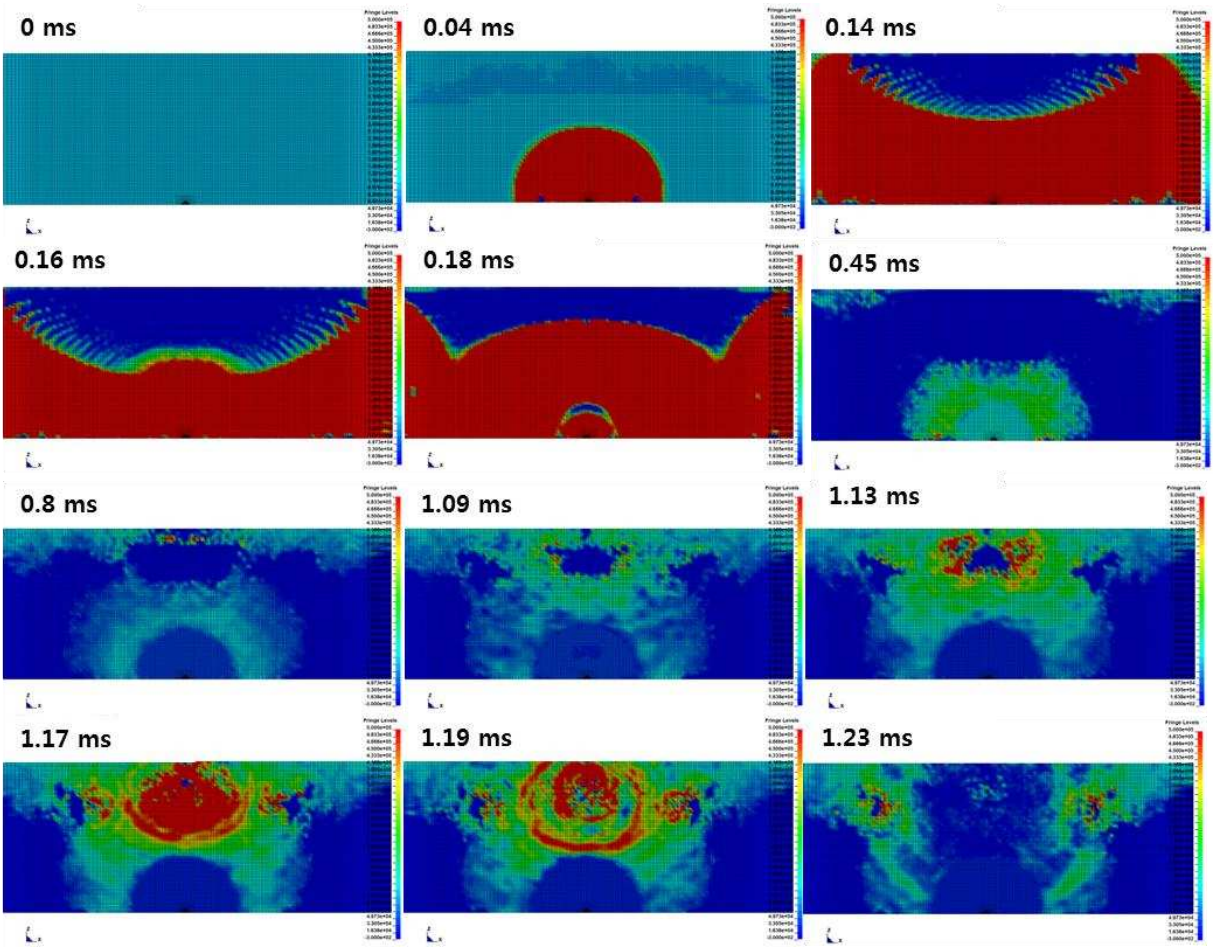

Figure 3.7 Bulk cavitation and closure pulse caused by shock wave.

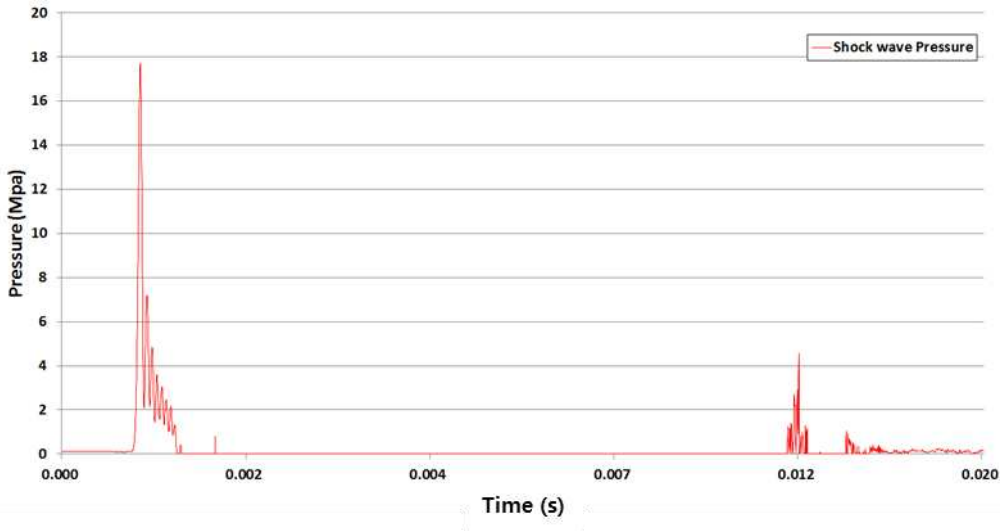

Figure 3.8 Incident shock and closure pulse pressure.

3.2.2 Effect of element size on shock wave propagation

It is beneficial to keep the solid element as small as possible for enabling shock wave pressure propagation. In particular, the accuracy of the pressure increases as distance to the explosive decreases. However, this small-element effect reduces as the distance increases.

As shown in figure 3.9, there is not much difference in pressures at distances greater than 2 m. Hence, to reduce the number of elements, 4-cm solid elements are employed to simulate the response of a structure subjected to an underwater explosion.

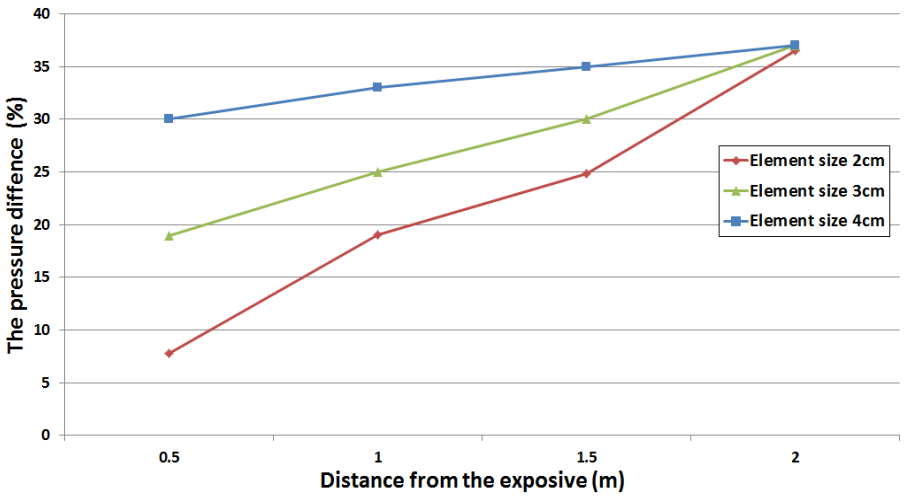

Figure 3.9 Effect of element size on shock wave propagation.

3.2.3 Comparison of empirical and simulated bubble sizes

The maximum diameter of a bubble is measured from the simulation results, as shown in figure 3.10. A comparison of the empirical and simulated values of the maximum bubble diameter and bubble oscillation period (T) is presented in table 3.6.

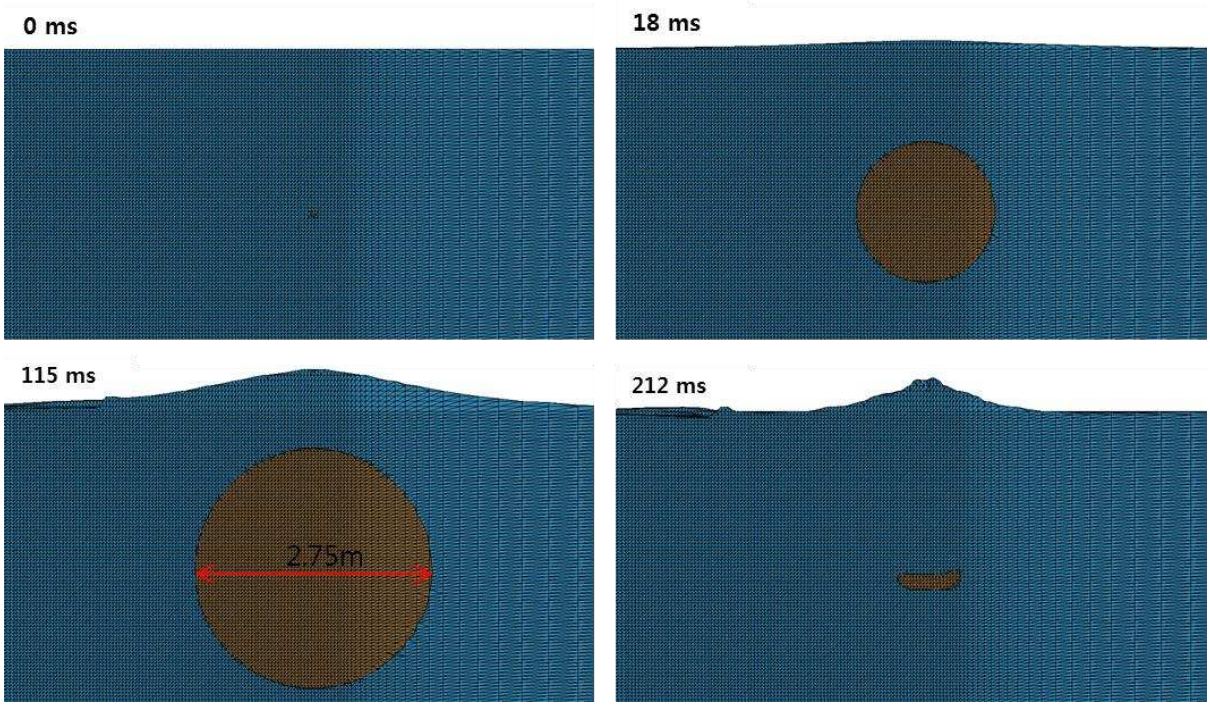

Figure 3.10 Simulation results for maximum diameter of bubble.

Table 3.6 Comparison of bubble parameters.

	Empirical value (A)	Simulated value (B)	B/A
Bubble diameter (m)	2.34	2.75	117%
Bubble oscillation period (s)	0.205	0.212	103%

3.2.4 Structure response caused by shock wave

In this study, a solid explosive model is used only to check the structure's dynamic response to the shock wave caused by the underwater explosion. When modeling the explosive at the edge of the

water model, the boundary condition is very important for the shock wave propagation. Chapter 3.2.4.1 discusses the boundary condition.

3.2.4.1 Boundary condition

If all of the water boundary conditions are fixed, the shock wave will not propagate. For the shock wave to propagate, the water boundary needs to slip conditions.

As shown in figure 3.11, for the edge of the explosive, the X and Z coordinates need to be set up for the translation constraint, and the X, Y, and Z coordinates need to set up for the rotational constraint. For the side of the explosive, the X coordinate needs to be set up as a translation constraint, and the Y and the Z coordinates need to be set up for rotational constraint. For the bottom of the explosive, the Z coordinate is needed to set up for the translation constraint, and the X and Y need to set up for the rotational constraint. Next, to simulate an infinite fluid area environment, the entire fluid area should be set to a nonreflecting boundary surface. Figure 3.11 explains the boundary conditions briefly.

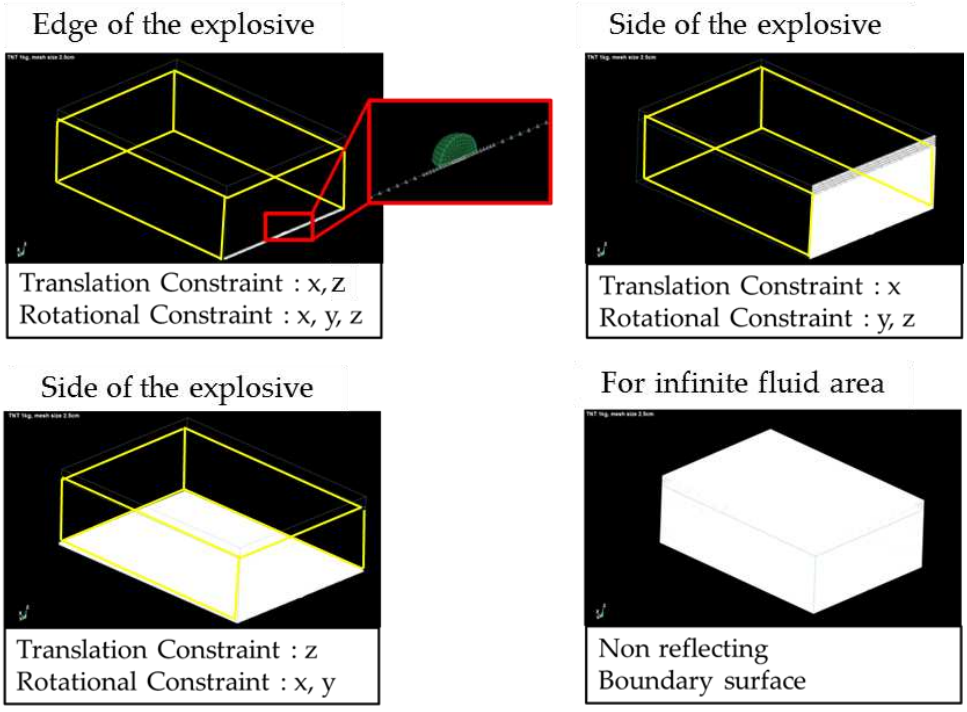

Figure 3.11 Boundary conditions for edge-modeled explosive.

3.2.4.2 Combining structure with water, air, and explosive models

Chapters 3.1.1 to 3.1.3 explain the method used for each model. Next, these models are combined by the LS-preprocessor. In this simulation, the number of solid elements used for the fluid models is 1,939,968 and the number of shell elements for the structure model is 15,659. The solid element formulation option (eq. 11) is employed, which is a one-point ALE multi-material element.

For solving the problem of a Lagrangian material contacting another Lagrangian material, the keyword “contact” should be employed. For solving the problem of an ALE material contacting another ALE material (advection), the nodes of each ALE material should be merged. For solving the problem of a Lagrangian material contacting an ALE material (fluid-structure interaction (FSI) problem), the keyword Constrained_Lagrange_in_solid should be employed [21]. In this simulation, the problem of a Lagrangian material contacting an ALE material (FSI problem) should mainly be considered. Separate elements are modeled between the ALE material (fluid model) and Lagrangian material (structure model). Therefore, two models should be defined for the correlation. LS-DYNA searches for the intersections between the Lagrangian parts and ALE parts. If a coupled Lagrangian surface is detected inside an ALE element, LS-DYNA marks the Lagrangian-Eulerian coupling points (NQUAD). It then tracks the independent motion of the two materials over dt (the ALE material interface is tracked based on its volume fraction in the element). Then, it computes the penetration distance of the ALE material across the Lagrangian surface. Coupling forces are calculated based on this penetration and are re-distributed onto both materials [21]. Next, by using the keyword Initial_Volume_fraction_geometry in LS-DYNA, the structure is filled with air. Figure 3.12 shows the merged model. There is an explosive at the right edge of the water.

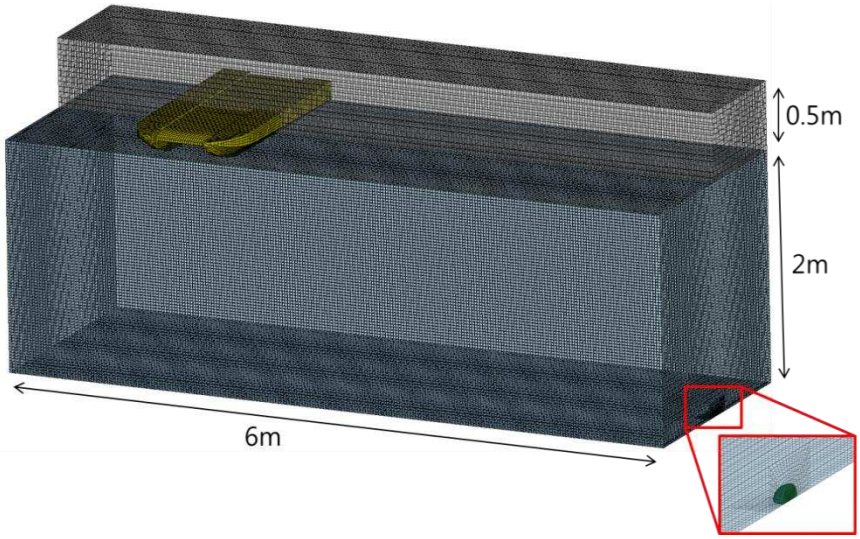

Figure 3.12 Combination of water, air, explosive, and structure.

3.2.4.3 Simulation results for shock wave

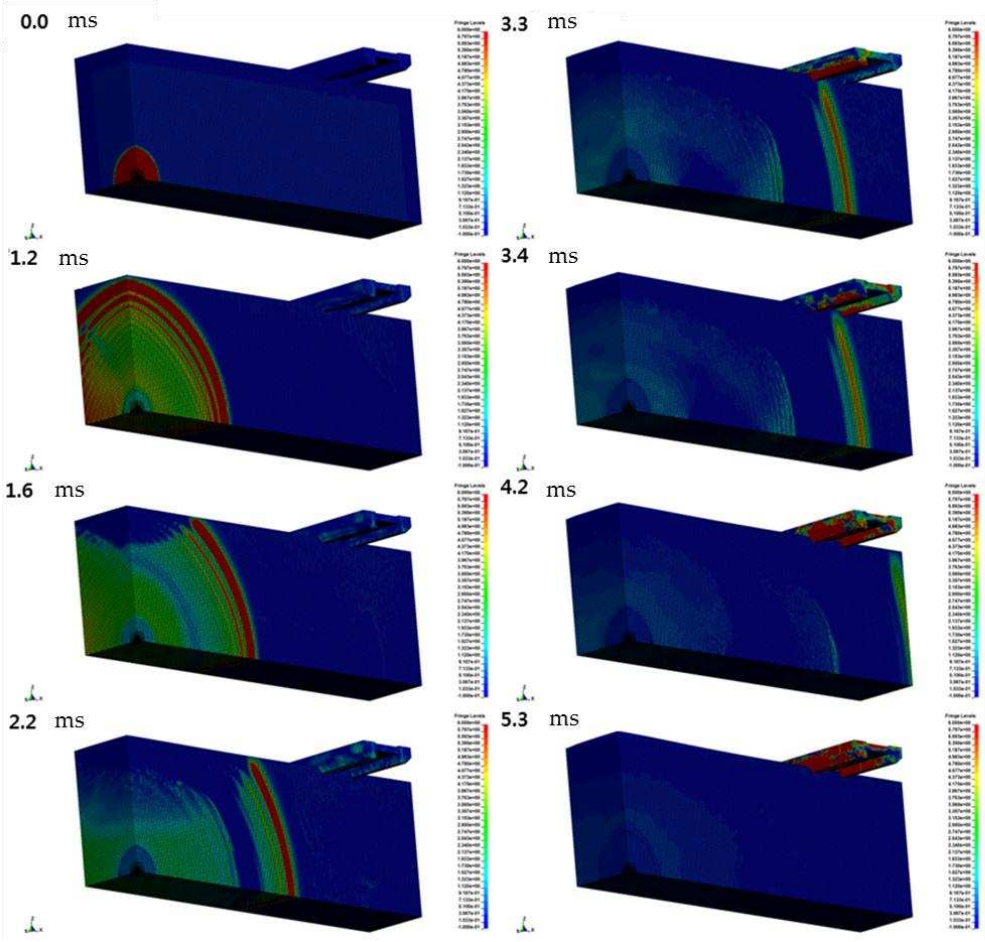

Figure 3.13 Shock wave propagation.

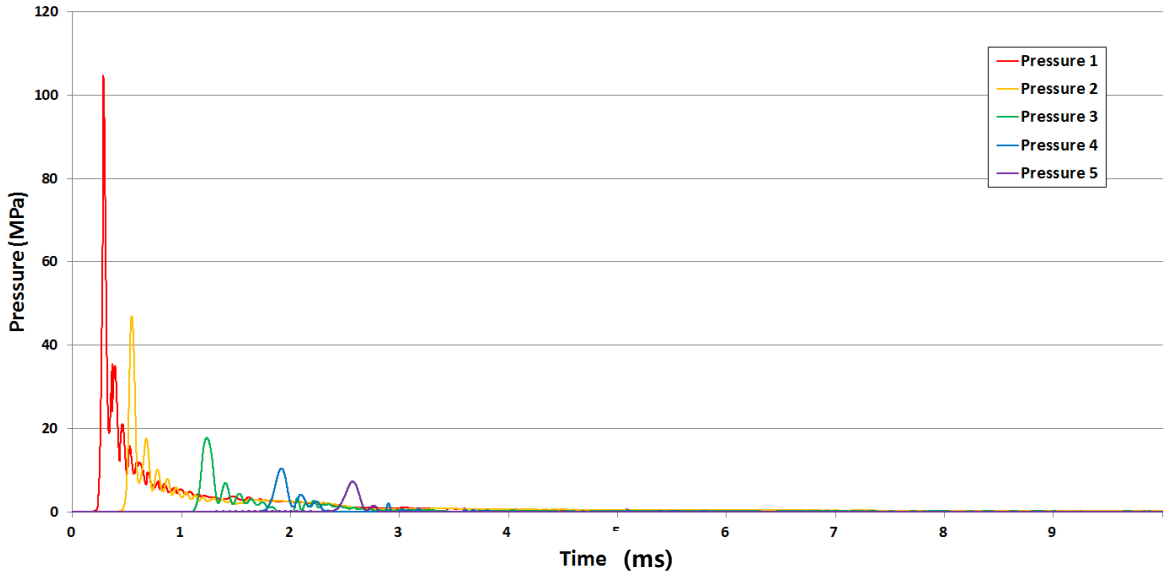

Figure 3.14 Simulation results for incident peak shock pressure.

In this case, 1 kg of TNT is employed. The shock wave propagation is shown in figure 3.13, and the pressure of the shockwave is summarized in table 3.7. As explained in chapter 3.2.2, the results of the simulation are lower than the empirical data when the distance from the explosive is greater than 2 m. The velocity response of the structure to the shockwave is shown in figures 3.14 and 3.15.

Table 3.7 Comparison of empirical and simulation values.

Distance (m)	Empirical value(A) (MPa)	Simulation value(B) (MPa)	(B/A)×100 (%)
Pressue1 (0.5)	112.728	104.69	92%
Pressue2 (1)	52.114	46.984	90%
Pressue3 (2)	23.001	17.778	77%
Pressue4 (3)	14.254	10.466	73%
Pressue5 (4)	10.151	7.296	71%

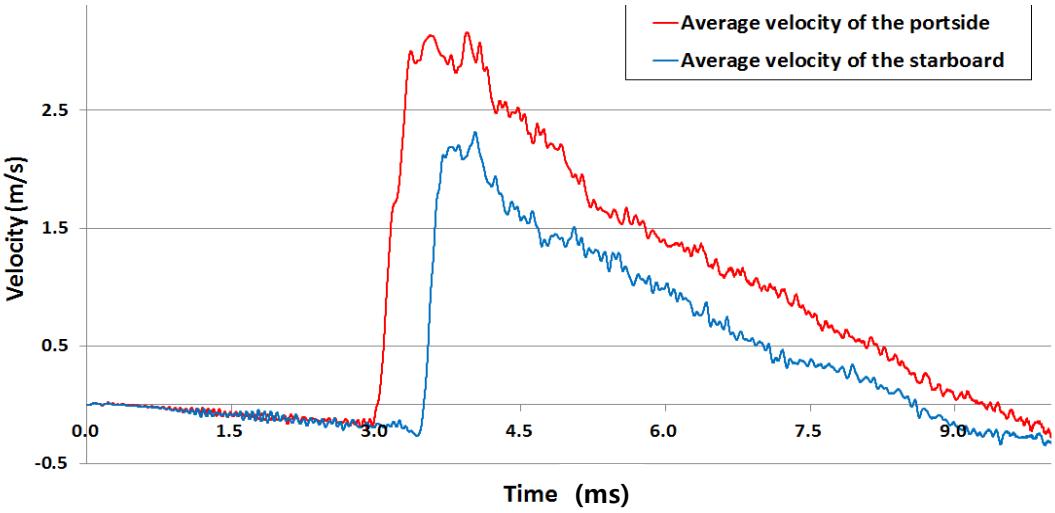

Figure 3.15 Average velocities at portside and starboard (left).

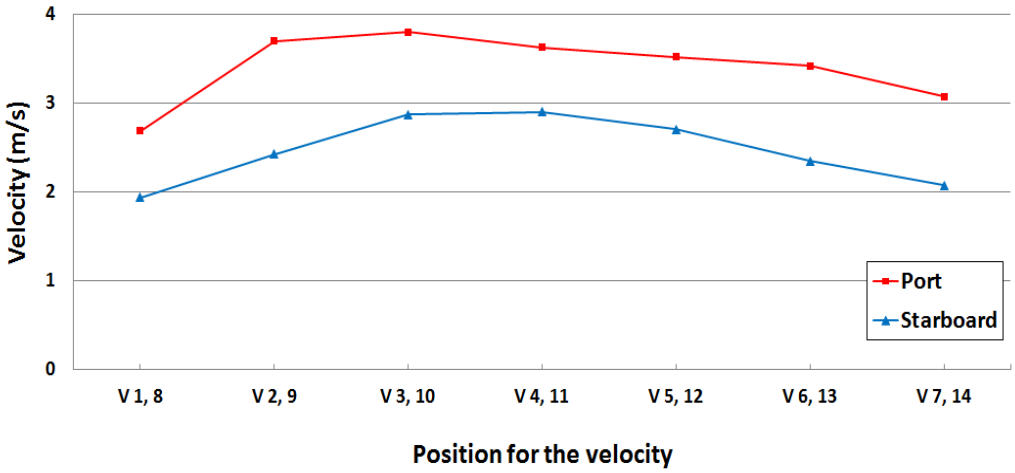

Figure 3.16 Peak velocities at portside and starboard (right).

The average velocities at portside and starboard are shown in figure 3.15 and 3.16. In the case of catamaran-like structure is difference between portside and starboard in velocity. The velocity of shocked side is bigger than starboard about 1m/s.

3.2.5 Structure response caused by underwater explosion

3.2.5.1 Models of water, air, explosive, and structure

As explained in chapter 3.1, the TNT shell technique for modeling the explosive is adopted to verify the bubble effect. The stand-off distance from the structure is 4 m. The geometry of the explosive test is shown in figure 3.17.

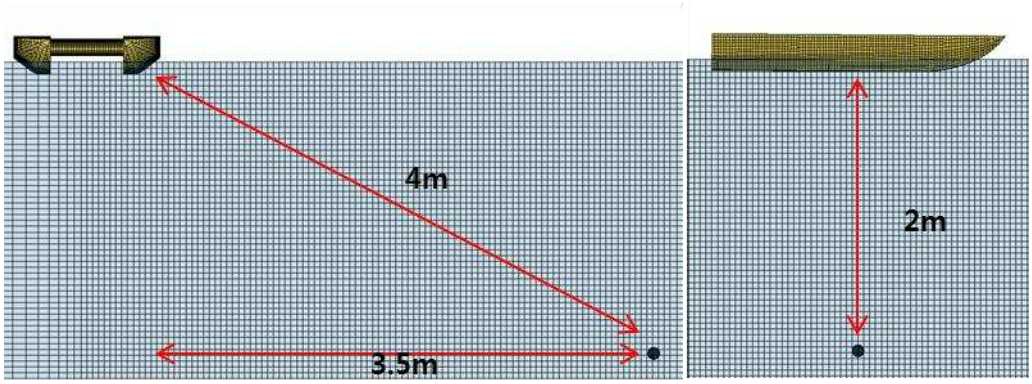

Figure 3.17 Geometry of explosive test.

3.2.5.2 Boundary condition

For the assumption of an infinite boundary for the water area, the boundary of the fluid is set to a boundary with no reflection, and all of the boundary nodes are set to fix all of the translations and rotations.

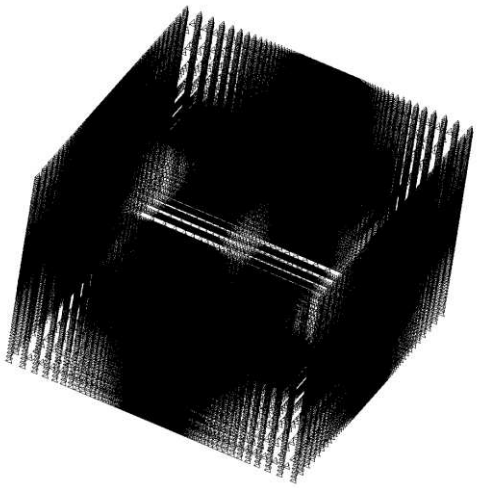

Figure 3.18 Boundary condition for fluid.

3.2.5.3 Simulation results

3.2.5.3.1 Stand-off distance of 4 m

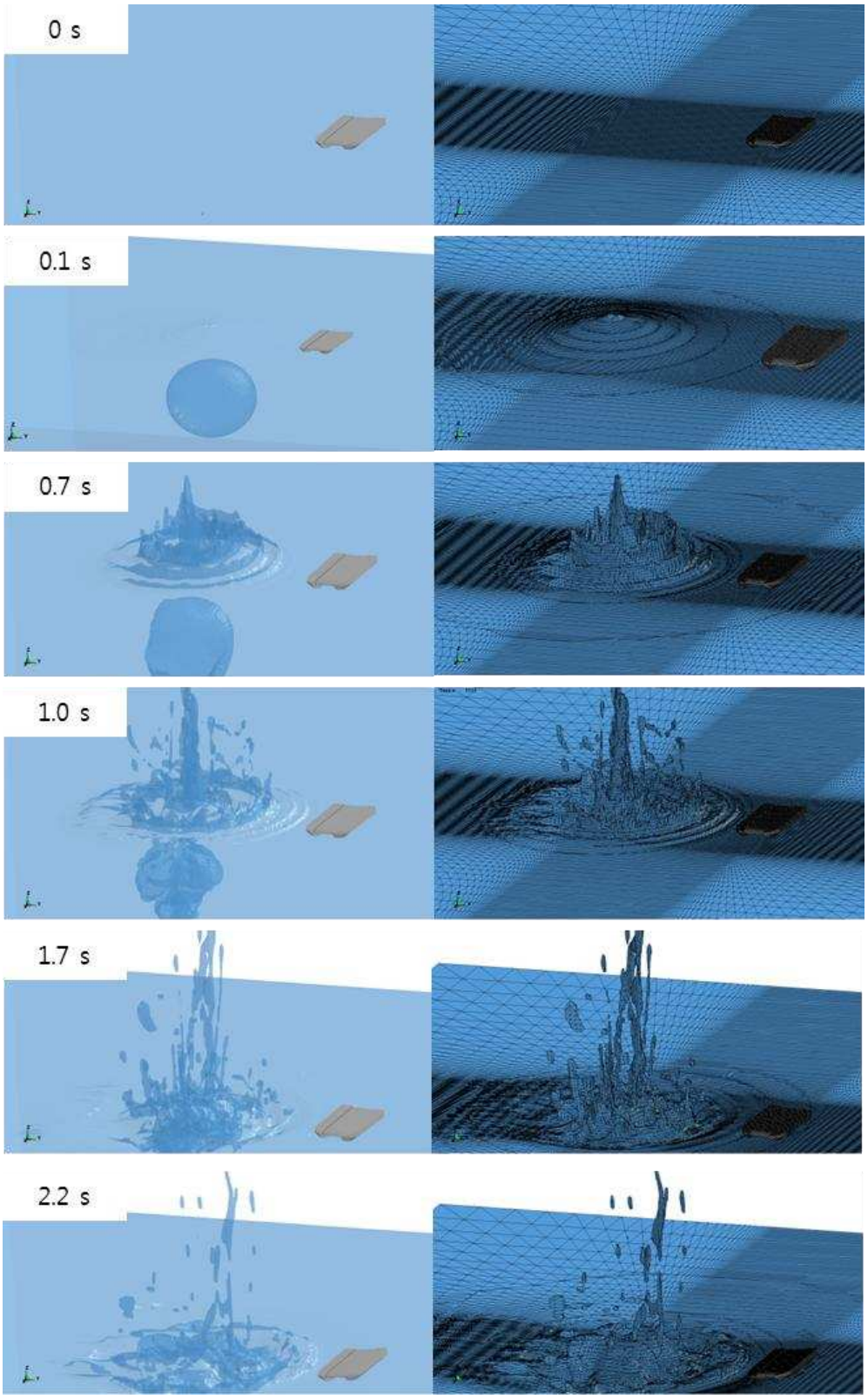

Figure 3.19 Simulation result (stand-off distance of 4 m).

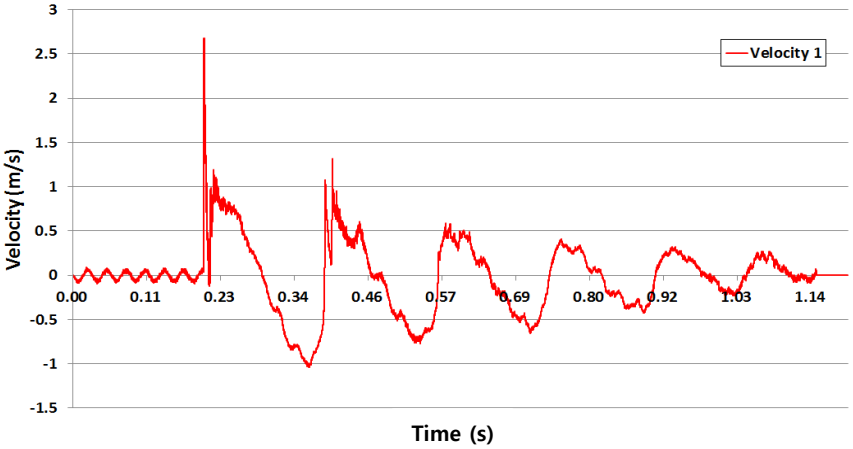

Figure 3.20 Velocity of shock response.

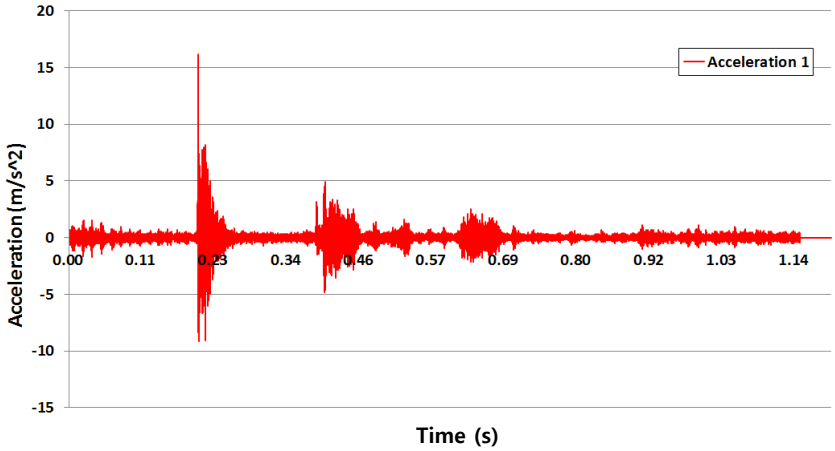

Figure 3.21 Acceleration of shock response.

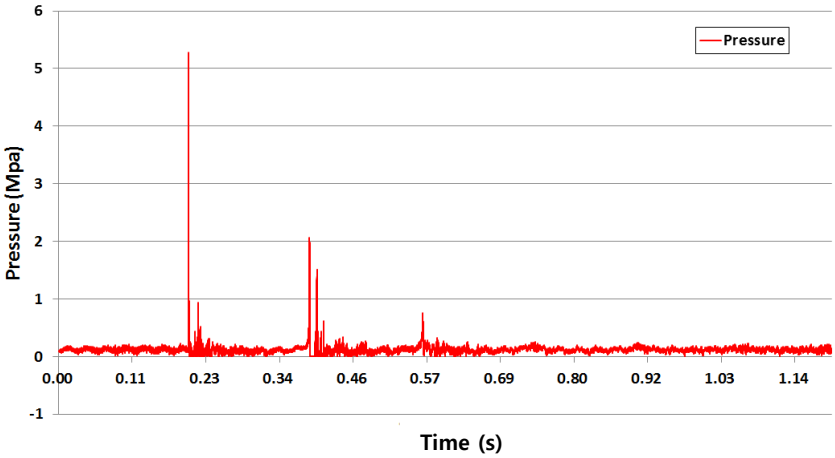

Figure 3.22 Pressure generated by underwater explosion.

As shown in figure 3.22, the incident shockwave pressure reaches the structure. The velocity and acceleration of the structure's response are shown in figures 3.20 and 3.21, respectively. As shown in these results, the acceleration and velocity values are affected by the bubble pulse pressure.

3.2.5.3.2 Stand-off distance of 3.5 m (vent out phenomenon)

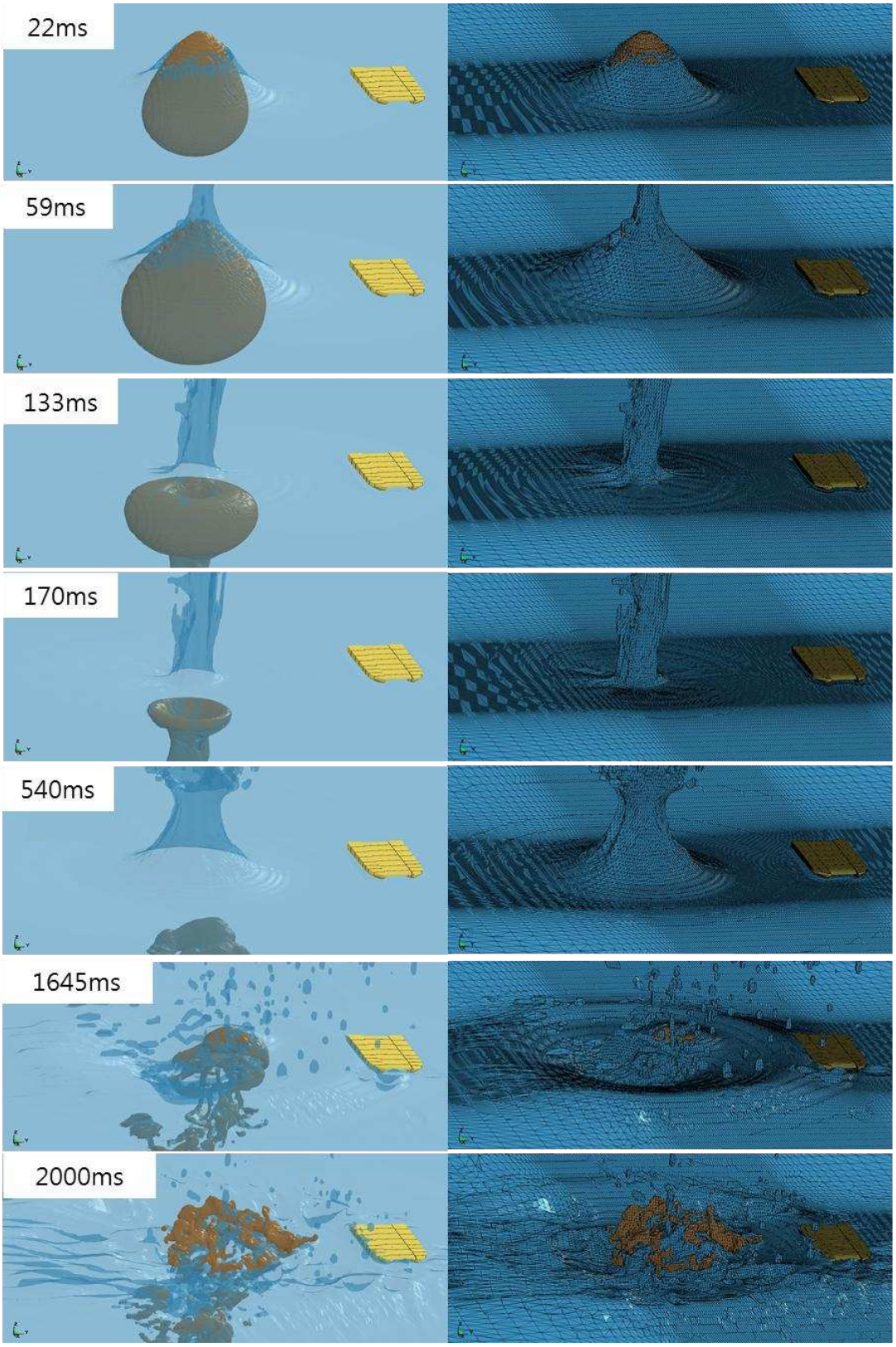

Figure 3.23 Effect of vent out phenomenon.

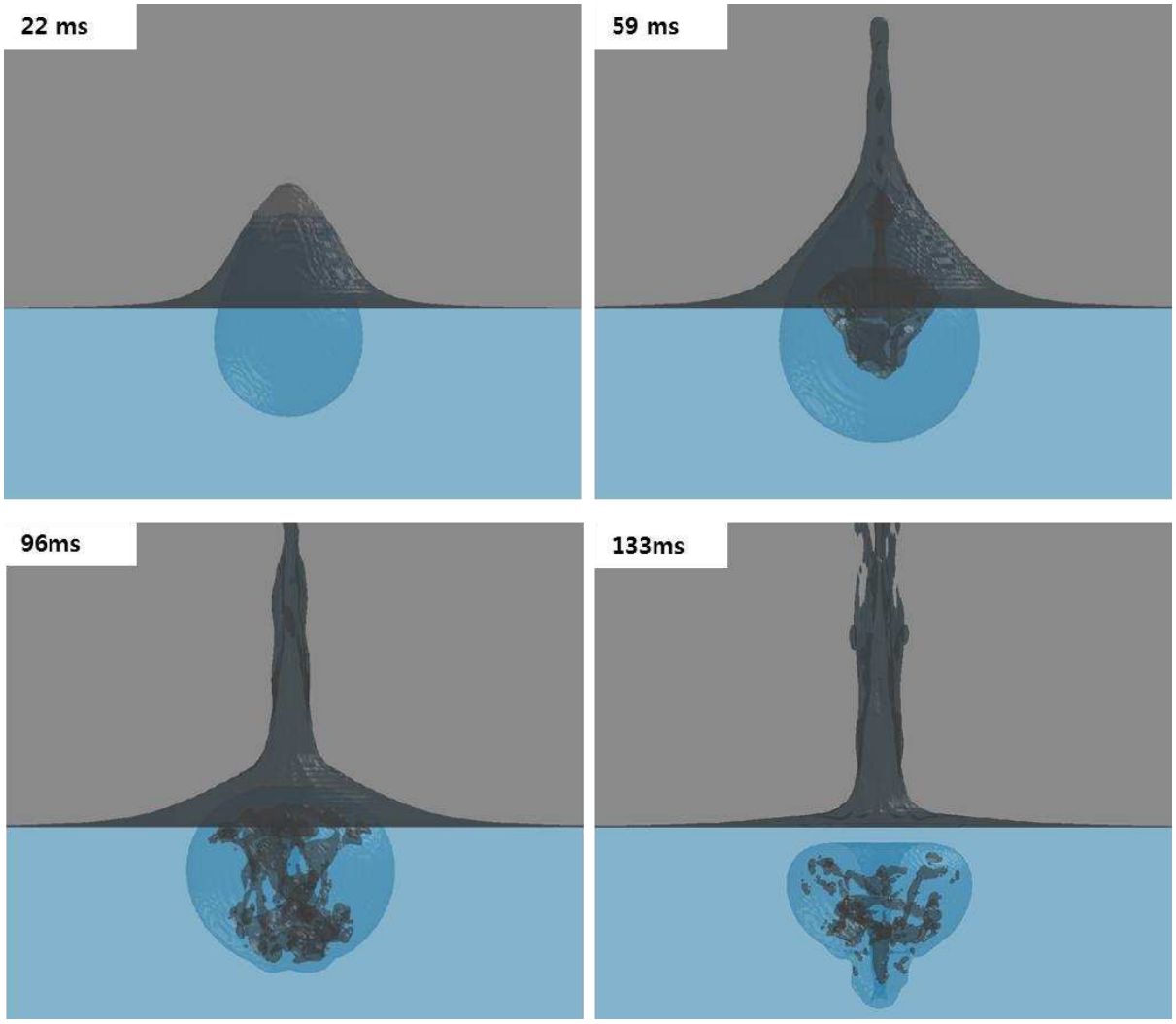

Figure 3.24 Venting out of bubble.

As shown in figures 3.23 and 3.24, when the bubble reaches the free surface at the first oscillation, the air (black color) interpenetrates the bubble because the bubble contains a vacuum.

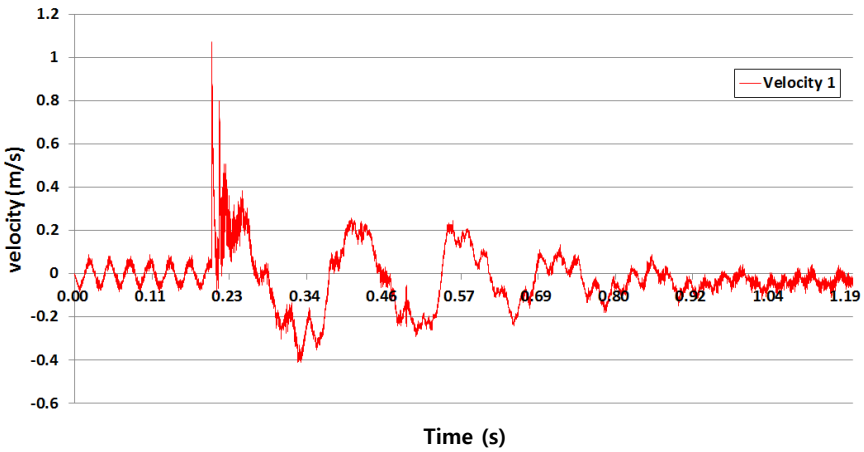

Figure 3.25 Velocity of shock response.

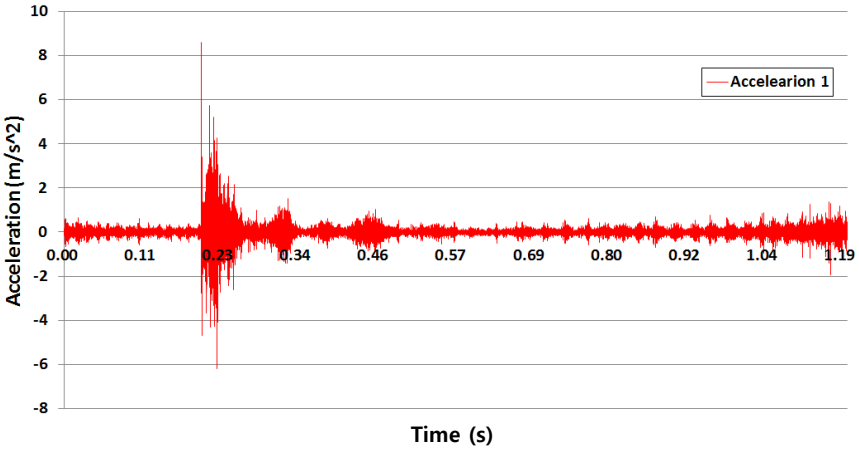

Figure 3.26 Acceleration of shock response.

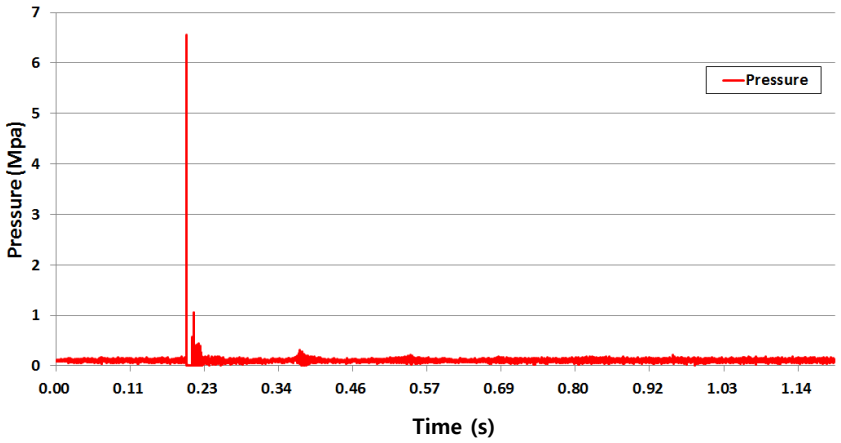

Figure 3.27 Pressure generated by underwater explosion.

As shown in figure 3.27, the incident shockwave pressure reaches the structure. The velocity and acceleration of the structure's response are shown in figures 3.25 and 3.26, respectively. Because of the vent out phenomenon, the bubble pulse is not seen clearly.

3.2.5.3.3 Stand-off distance of 2.2 m

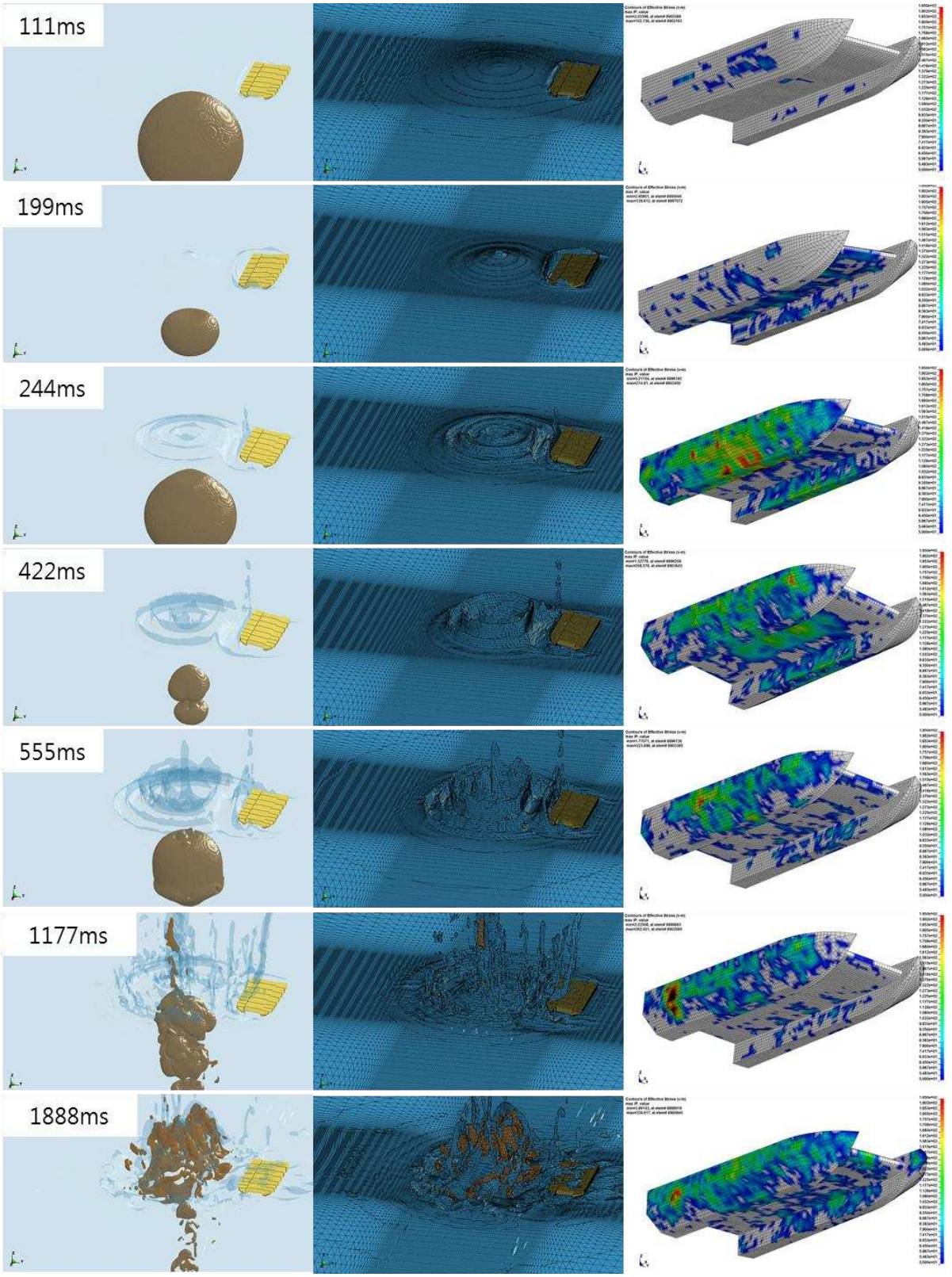

Figure 3.28 Simulation results (stand-off distance of 2.2 m).

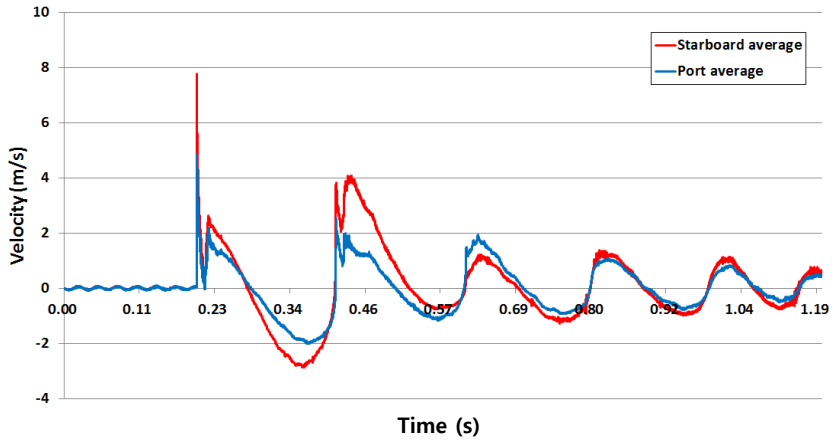

Figure 3.29 Velocity of shock response.

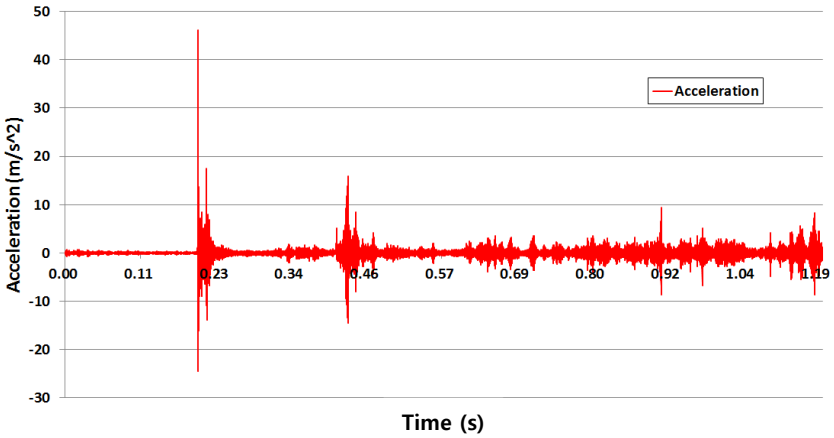

Figure 3.30 Acceleration of shock response.

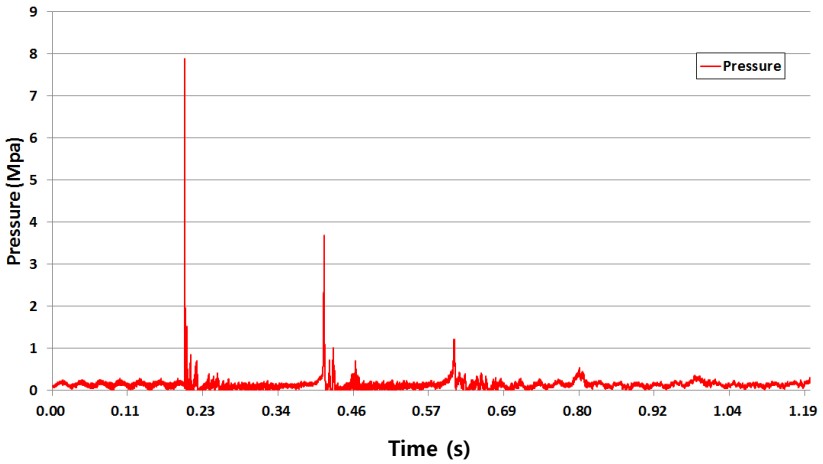

Figure 3.31 Pressure generated by underwater explosion.

In this case, the structure and explosive are very close together. Hence, the effective stress on the structure is shown in figure 3.28. The structure is deformed as a result of the shock wave and bubble impact. The deformed structure is shown in figure 5.4.

3.2.5.3.4 Explosion behind structure

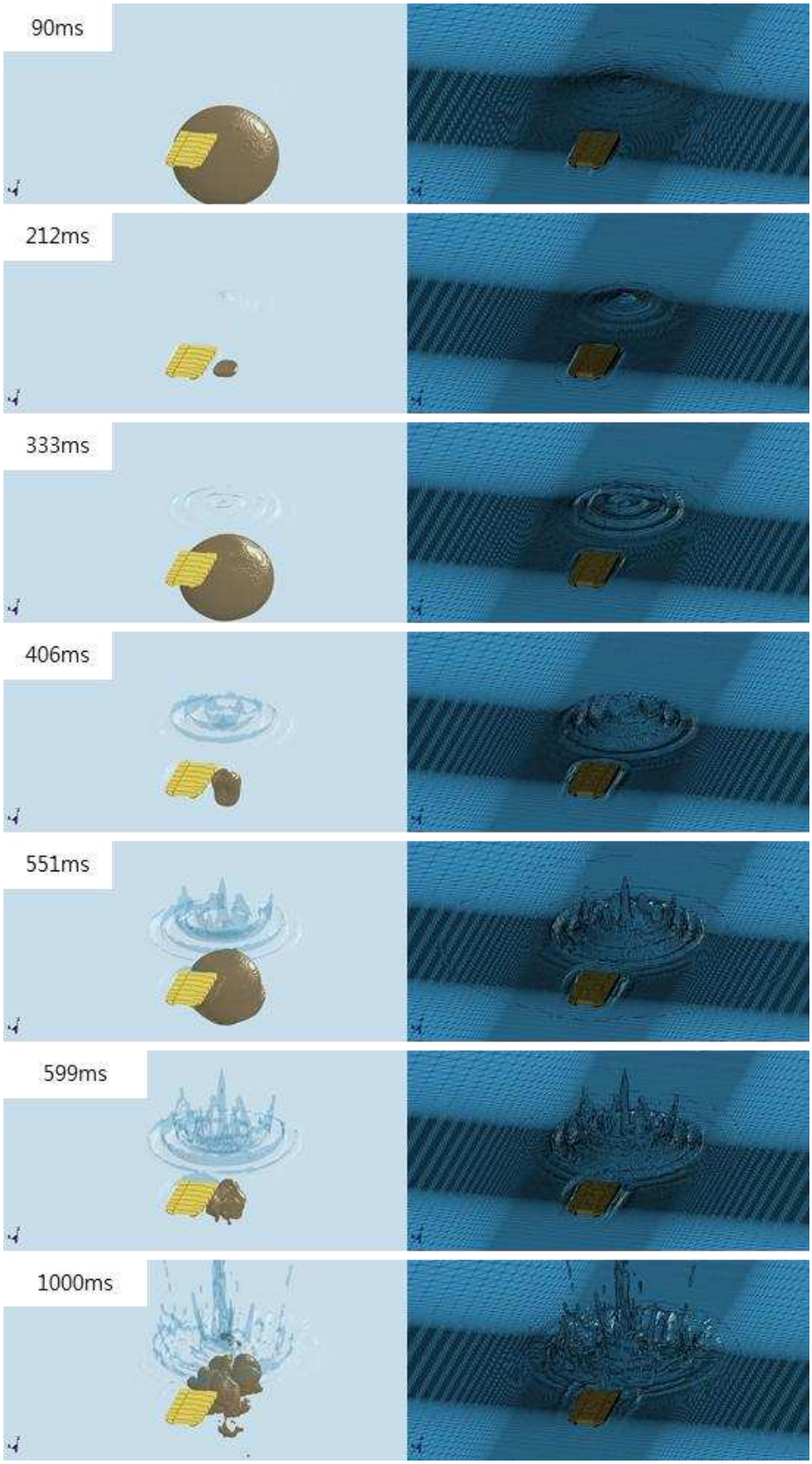

Figure 3.32 Explosion behind structure.

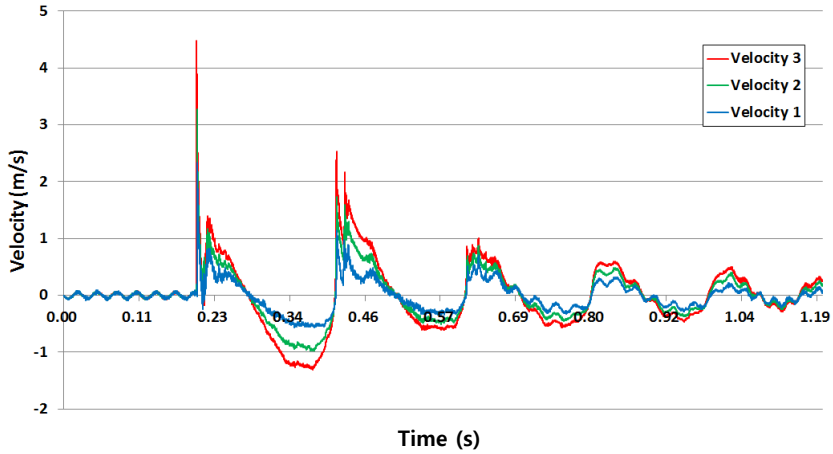

Figure 3.33 Velocity of shock response.

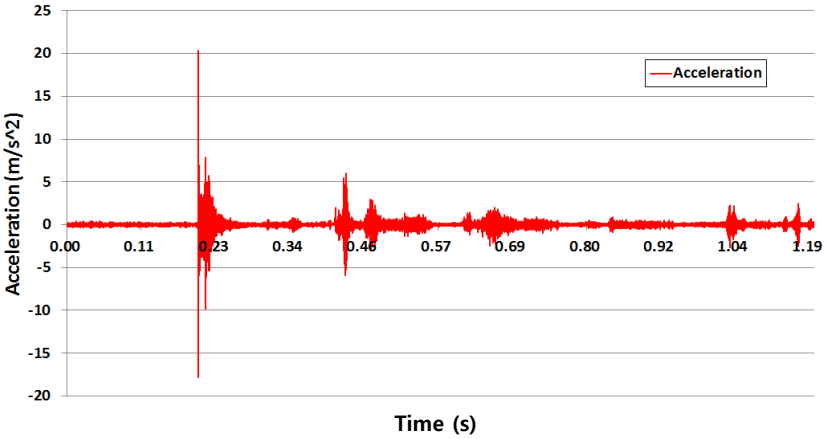

Figure 3.34 Acceleration of shock response.

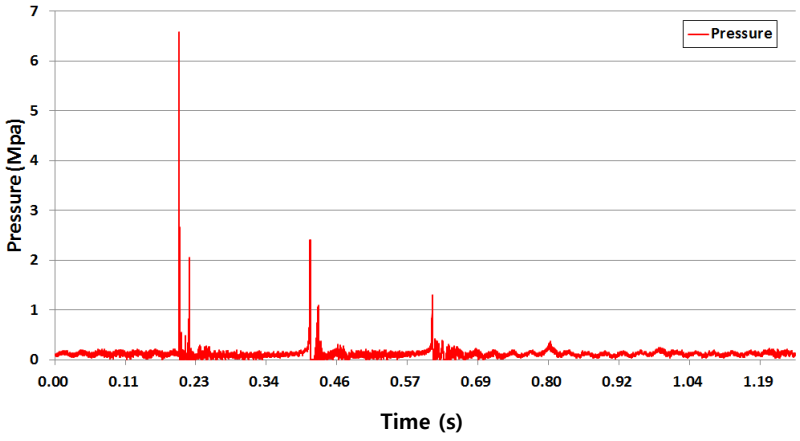

Figure 3.35 Pressure generated by underwater explosion.

As shown in figure 3.35, the incident shockwave and bubble pulse pressure reach the structure. The velocity and acceleration of the structure's response are shown in figures 3.33 and 3.34, respectively. Because of the bubble pulse pressure, a second velocity peak appears.

Chapter4 Underwater explosion testing

4.1 Pressure test

TNT is an explosive used for the military application, it is not allowed to use in this experiment. Therefore, MegaMEX is used for the explosion experiments. MegaMEX's basic properties are listed in table 4.1. However, MegaMEX's JWL (Jones-Wilkins-Lee) EOS (equation of state) is not disclosed. The feasibility of using MegaMEX as an alternative for TNT is verified by a pressure test.

Table 4.1 Comparison of properties of TNT and MegaMEX.

Explosive	Specific Energy (N-mm)	Specific Density (g/mm^3)	Detonation velocity (m/s)
TNT	11.076	1.63	6930
MegaMEX	9.613	1.25	6000

As shown in figure 4.1, the experimental site is a reservoir in the city of Gimhae. The deepest depth of this reservoir is about 10 m. The area of the site is 30 m × 50 m. This reservoir is filled with fresh water, and the bottom consists of fine sand. The procedures for the experiment are described in chapter 4.1.1.

Figure 4.1 Experimental site.

4.1.1 Plan for shock pressure test

To avoid bottom reflection, the explosive is set up in the deepest part of the reservoir. The explosive is placed at a depth of about 2 m. Various quantities are used for the explosives (250–500 g), and they are formed into balls. To protect the water, the explosives are wrapped in vinyl stockings. The explosive materials and prepared explosives are shown in figure 4.2.

Figure 4.2 Explosives for pressure test.

To fix the explosive in the water, aluminum profiles are set up on buoys on the free surface. The explosive is placed 2 m from the free surface of the water. The explosive is installed at the end of the aluminum profile, and pressure gauges are set up at another end of the profile. The pressure gauge properties are described in table 4.2.

Table 4.2 Properties of underwater blast pressure sensors.

Model	Type	Serial #	Sensitivity
137A22	ICP	9523	1402 mV/MPa
	ICP	9524	1379 mV/MPa
	ICP	9525	1354 mV/MPa

The underwater blast pressure gauges are connected to water resistant cables with a length of approximately 20 m. To accurately measure the experiment results, a 51.2-kHz analyzer is set up. It can accurately measure the maximum pressure caused by the underwater explosion. For safety and to allow the sensors to stabilize, the detonation fuse has to cause the explosion to occur at least 30 s after turning on the recorder. A mimetic diagram of the underwater explosion pressure test is shown in figure 4.3. The aluminum profiles are assembled to reach a length of 6 m. The procedure for installing the aluminum profile is shown in figure 4.4.

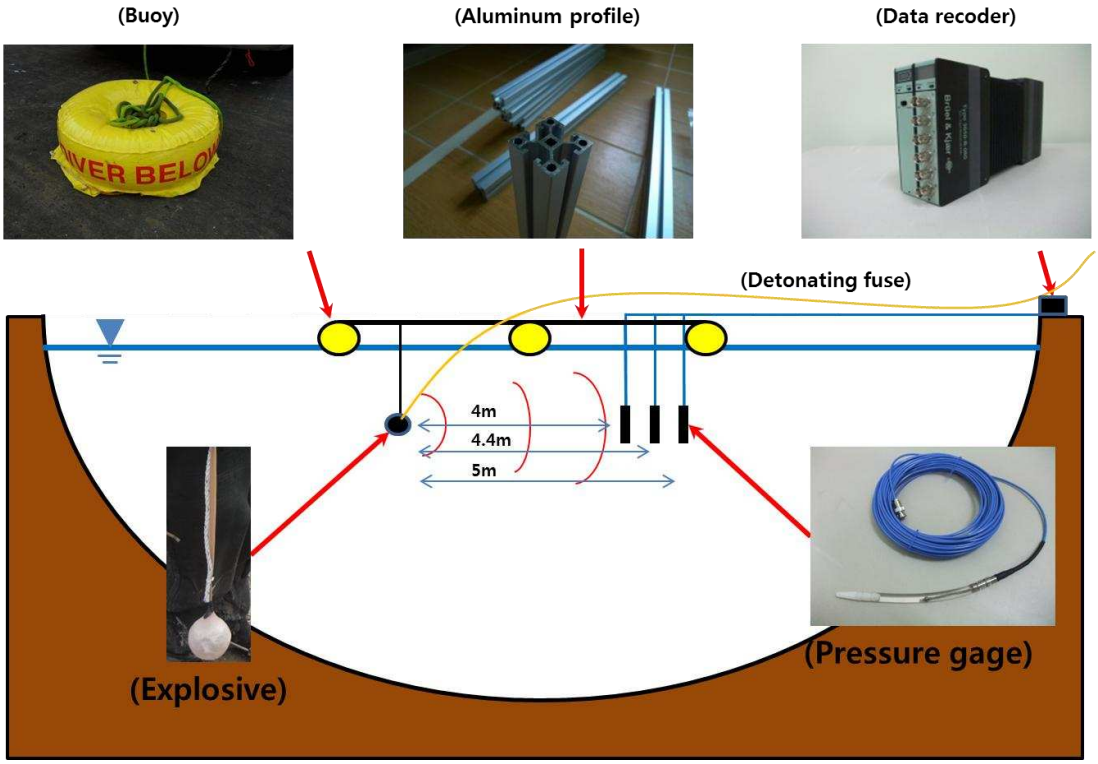

Figure 4.3 Test plan (two dimensions).

The tests are carried out as described in table 4.3. The first three tests are preparation tests. Therefore, the results of these tests are not shown in this dissertation. Three underwater blast pressure sensors are used for tests 4, 5, 6, and 7. The results of these tests are described in chapter 4.1.2.

Table 4.3 Summary of tests.

No.	Explosive weight (g)	Depth (m)	Number of channels	Distance of sensor from explosive (m)		
				4	4.4	4.5
1	500	2	1	o	x	x
2	500	4	1	x	x	o
3	250	2	1	o	x	x
4	250	2	3	o	o	o
5	300	2	3	o	o	o
6	500	2	3	o	o	o
7	500	2	3	o	o	o

O : sensor on, X : sensor off

Figure 4.4 Installing buoys and aluminum profiles.

4.1.2 Results of underwater shock pressure tests with MegaMEX

4.1.2.1 Results of test #4

Two hundred and fifty grams of MegaMEX is used for test #4. The explosive is placed 2 m from the free surface. Three underwater blast pressure sensors are installed at the end of the profile, as shown in figure 4.3.

Table 4.4 Summary of test #4.

No.	Explosive weight (g)	Depth (m)	Number of channels	Distance of sensor from explosive (m)		
				4	4.4	4.5
4	250	2	3	o	o	o

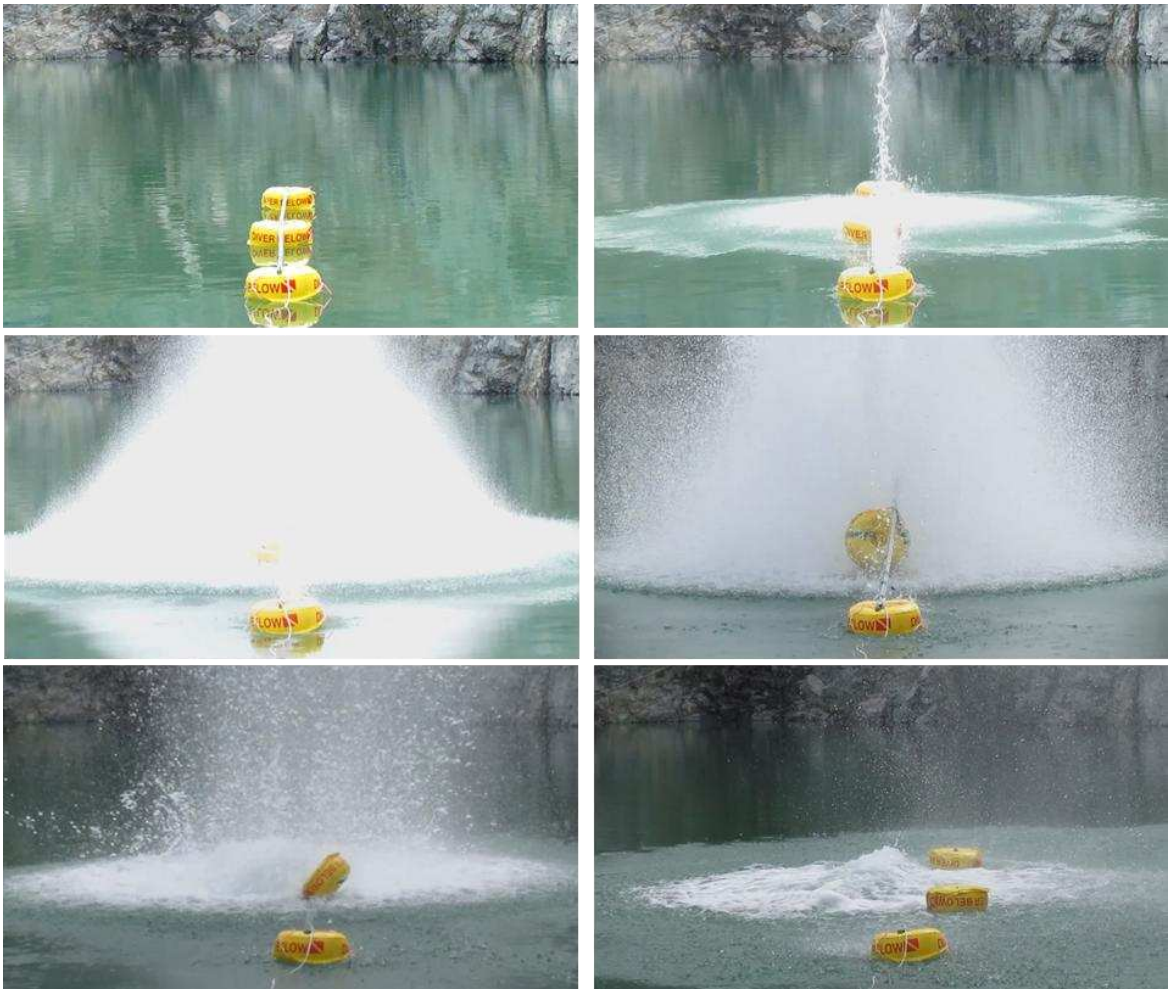

Figure 4.5 Underwater explosion shock wave pressure test #4.

Because of the stabilization of the underwater blast pressure sensors, the MegaMEX is exploded 30 s after setting up the sensors. Shortly after the explosion, a bulk cavitation area and spray dome are observed on the free surface caused by the shock wave. Then, a column of water called a flume, which is caused by bubble oscillation, penetrates the spray dome. Afterward, the surface phenomena caused by the explosion end.

The highest measured pressures (P_{max}) at 4 m, 4.4 m, and 5 m are 5.422 MPa, 4.922 MPa, and 4.739 MPa, respectively. The data measured by the recorder are shown in figure 4.6. The shock wave propagation speed is calculated as 2 Mm/s from 4 m to 4.4 m and 1.2 Mm/s from 4.4 m to 5 m. The incident shock wave is measured at 30 s 660 ms, and bubble pulses caused by bubble oscillation are measured at 30 s 810 ms and 30 s 930 ms. Based on the bubble pulse pressure, the first bubble's pulse period is inferred as being 150 ms. The exponential decay (θ) of MegaMEX is measured at about 0.08 ms. The surface cutoff caused by the reflected tension wave is reached 1.4 ms after the incident wave. Figure 4.6 and table 4.5 present a comparison of the empirical values of TNT and the test results for the MegaMEX.

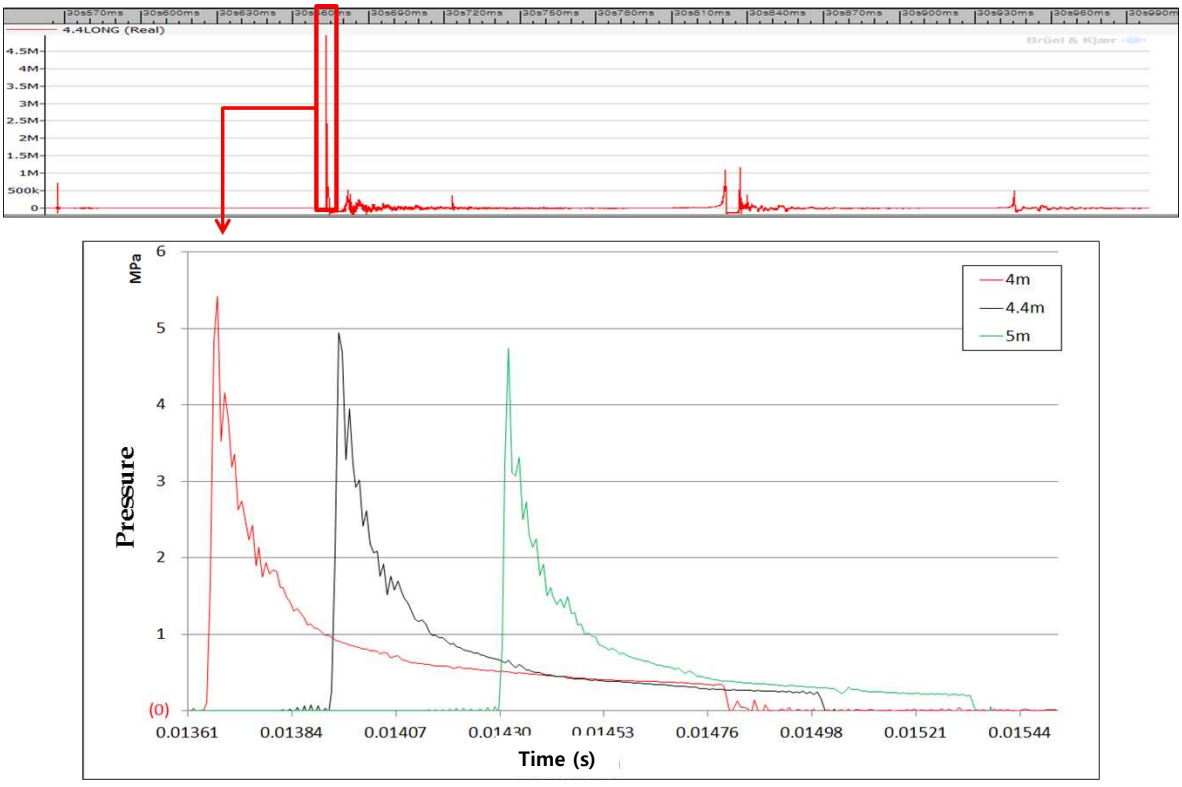

Figure 4.6 Results of test #4 (Explosive : 250 g).

Table 4.5 Comparison of empirical values of TNT and test results for MegaMEX.

Distance (m)	Empirical values of TNT		Test results for MegaMEX		Similarity (%)	
	P_{max}(MPa)	θ (ms)	P_{max}(MPa)	θ (ms)	P_{max}	θ
4	5.885	0.079	5.422	0.077	92	97
4.4	5.257	0.081	4.943	0.083	94	102
5	4.522	0.083	4.739	0.082	104	99

4.1.2.2 Results of test #5

To find an appropriate explosive weight for the structure shock response experiment, the weight of MegaMEX is gradually increased. Hence, 300 g of MegaMEX is used for test #5.

Table 4.6 Summary of test #5.

No.	Explosive weight (g)	Depth (m)	Number of channels	Distance of sensor from explosive (m)		
				4	4.4	4.5
5	300	2	3	o	o	o

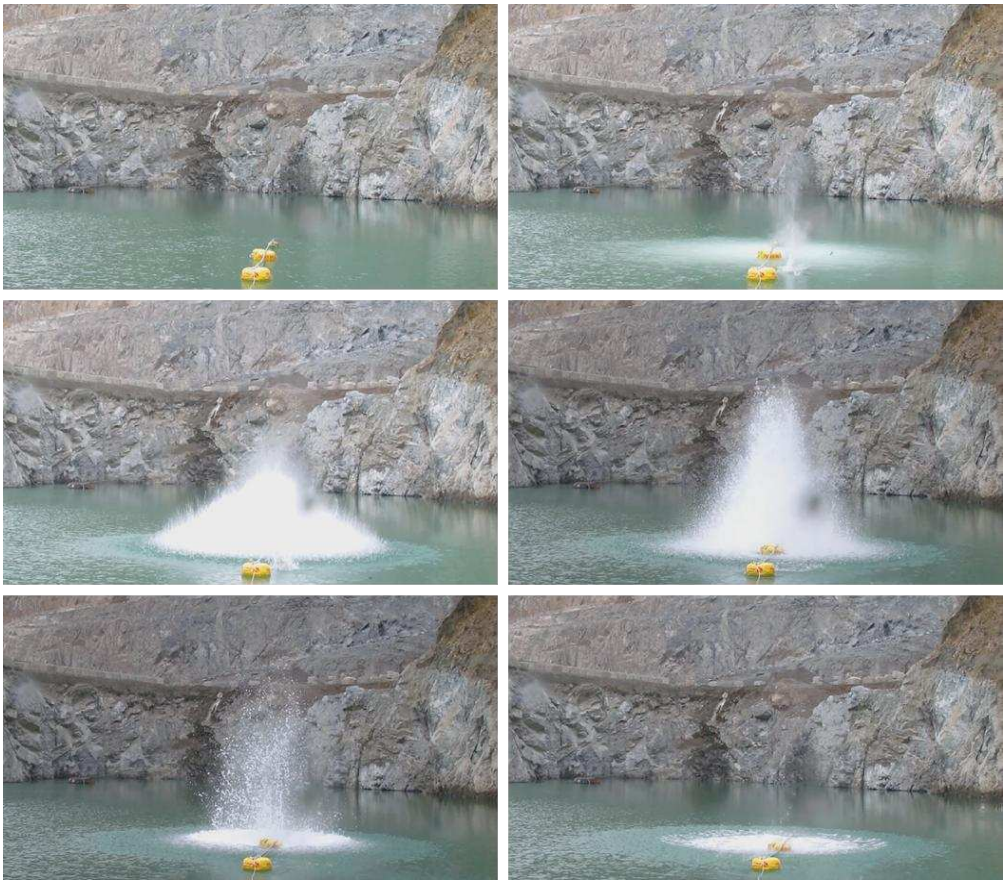

Figure 4.7 Underwater explosion shock wave pressure test #5.

Just as with test #4, for the stabilization of the underwater blast pressure sensors, MegaMEX is exploded 34 s after setting up the sensors. The phenomena of the test are similar to those for test #4.

The highest pressures (P_{max}) and exponential decay are presented in figure 4.8 and table 4.7. The data measured by the data recorder are shown in figure 4.8. The shock wave propagation speed shows a trend similar to test #4. The incident shock wave is measured at 34 s 987 ms, and the bubble pulses caused by bubble oscillation are measured at 35 s 153 ms and 35 s 273 ms. Based on the bubble pulses, the first bubble's pulse period is inferred as being 166 ms. The exponential decay (θ) of the 300 g of MegaMEX is measured at about 0.083 ms. The surface cut-off caused by the reflected tension wave is measured 1.4 ms after the incident wave. Table 4.7 presents a comparison of the empirical values for TNT and the test results for MegaMEX.

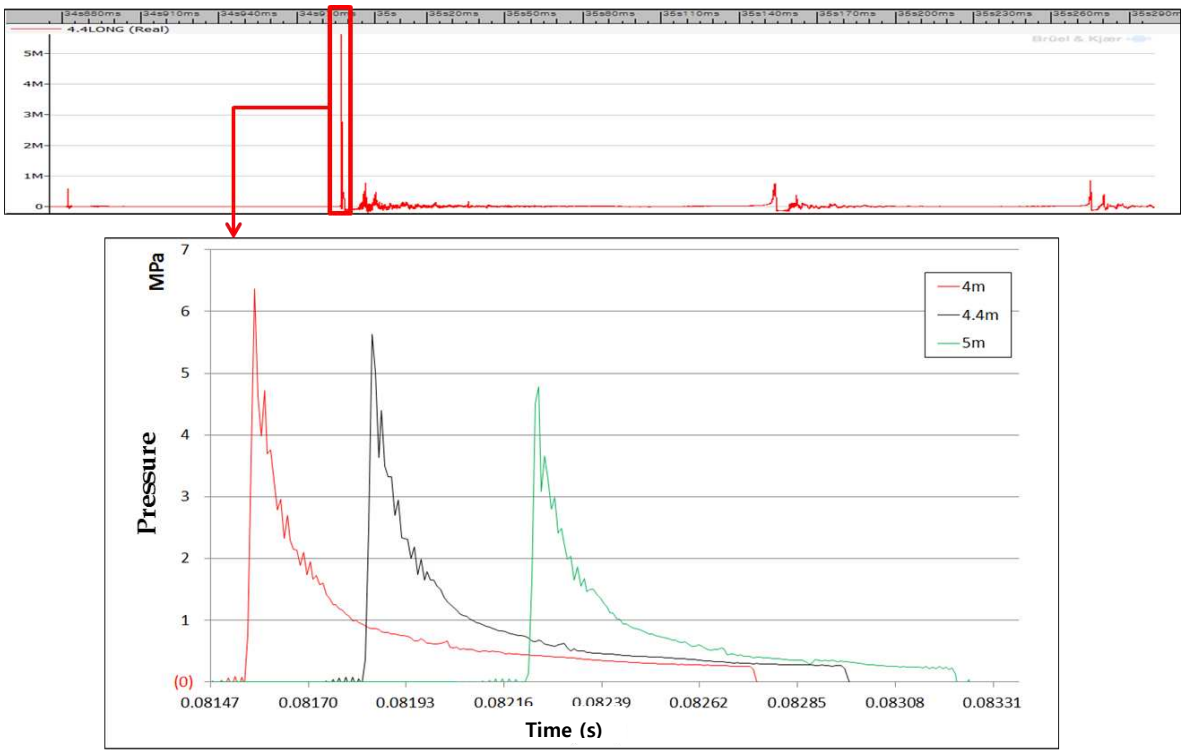

Figure 4.8 Results of test #5 (Explosive : 300 g).

Table 4.7 Comparison of empirical values of TNT and test results for MegaMEX.

Distance (m)	Empirical values of TNT		Test result for MegaMEX		Similarity (%)	
	P_{max}(MPa)	θ (ms)	P_{max}(MPa)	θ (ms)	P_{max}	θ
4	6.322	0.083	6.374	0.080	101	96
4.4	5.649	0.085	5.626	0.083	100	98
5	4.858	0.087	4.783	0.085	98	98

4.1.2.3 Results of test #6

For the same reason given for test #5, the weight of the MegaMEX explosive is increased. Hence, 500 g of MegaMEX is used for test #6.

Table 4.8 Summary of test #6.

NO.	Explosive weight (g)	Depth (m)	Number of channels	Distance of sensor from explosive (m)		
				4	4.4	4.5
6	500	2	3	o	o	o

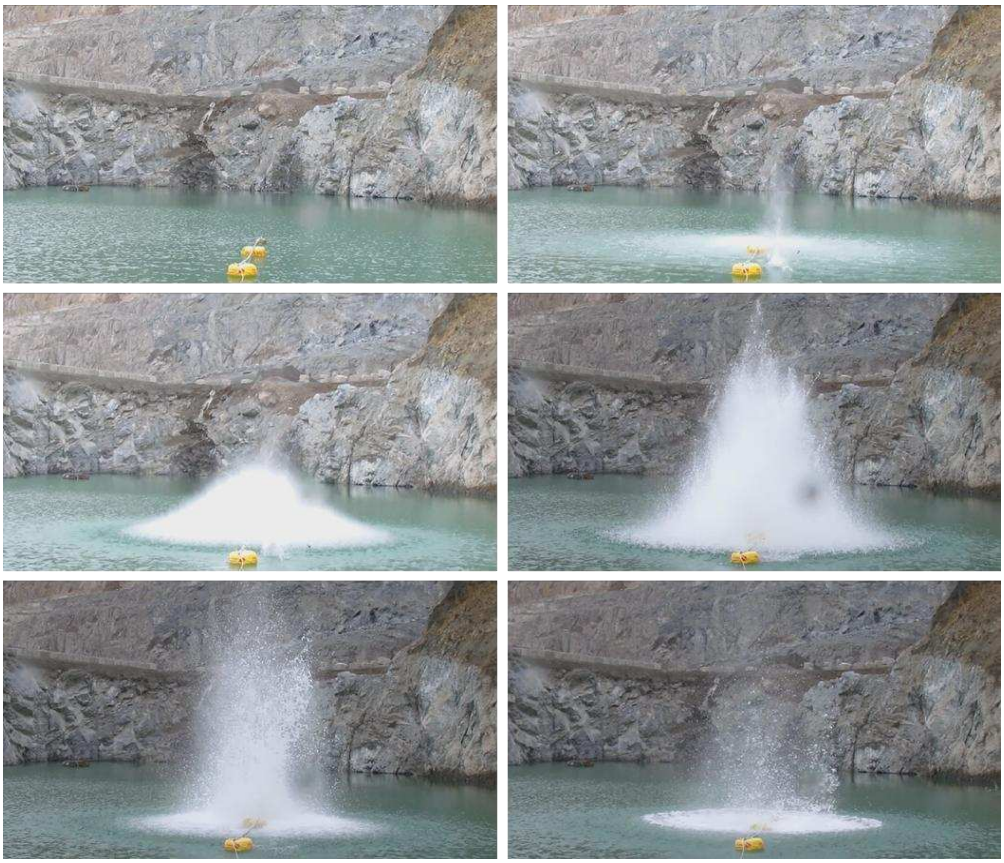

Figure 4.9 Underwater explosion shock wave pressure test #6.

Test #6 is conducted in the same way as tests 4 and 5. The phenomena of the bulk cavitation area, spray dome, and flume are observed to occur on the free surface.

The highest pressures (P_{max}) and exponential decay are presented in figure 4.10 and table 4.9. The incident shock wave is measured at 30 s 425 ms, and the bubble pulses generated by bubble oscillation are measured at 30 s 618 ms and 30 s 757 ms. Based on the bubble pulses, the first bubble's pulse period is inferred as being 193 ms. The exponential decay (θ) of the 500 g of MegaMEX is measured at about 0.01 ms. The surface cutoff caused by the reflected tension wave is measured 1.4 ms after the incident shock wave. Table 4.9 presents a comparison of the empirical values of the TNT and the test results for MegaMEX.

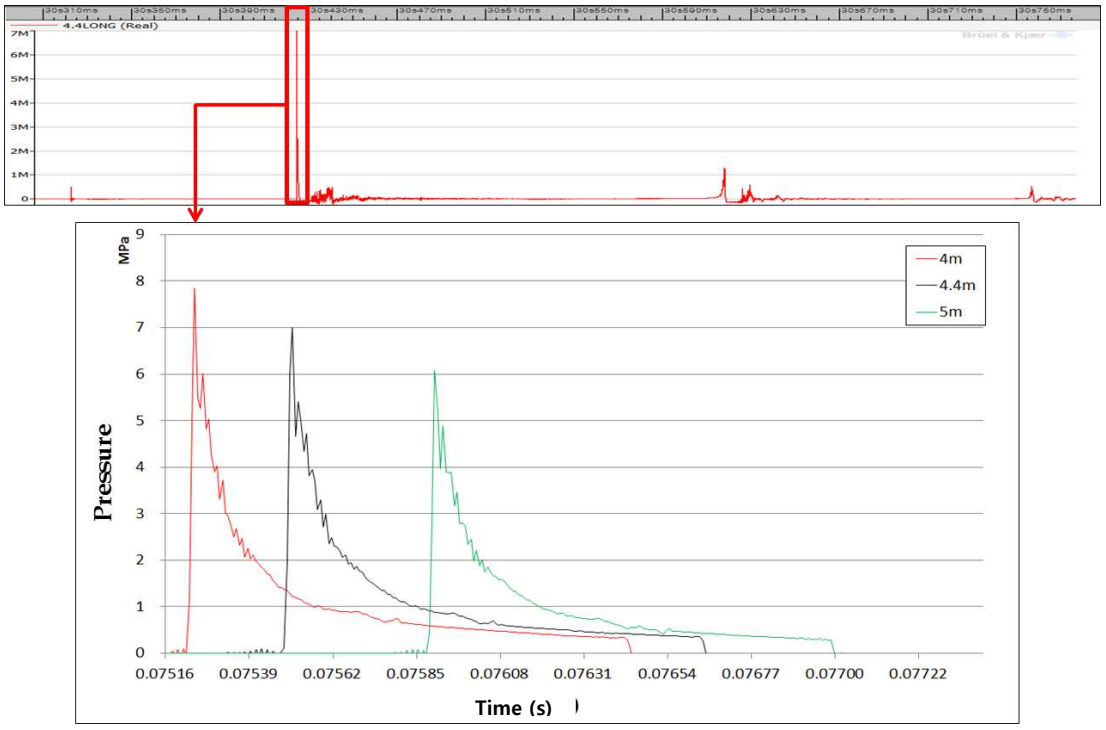

Figure 4.10 Results of test #6 (Explosive : 500 g).

Table 4.9 Comparison of empirical values of TNT and test results for MegaMEX.

Distance (m)	Empirical values of TNT		Test results for MegaMEX		Similarity (%)	
	P_{max}(MPa)	θ (ms)	P_{max}(MPa)	θ (ms)	P_{max}	θ
4	7.729	0.096	7.849	0.10	101	104
4.4	6.907	0.097	7.005	0.11	101	113
5	5.940	0.099	6.083	0.11	102	111

4.1.2.3 Results of test #7

Five hundred grams of MegaMEX is used for test #7. To verify the accuracy of the measured data, test #6 and test #7 are compared. Figure 4.11 shows the underwater blast pressure tests.

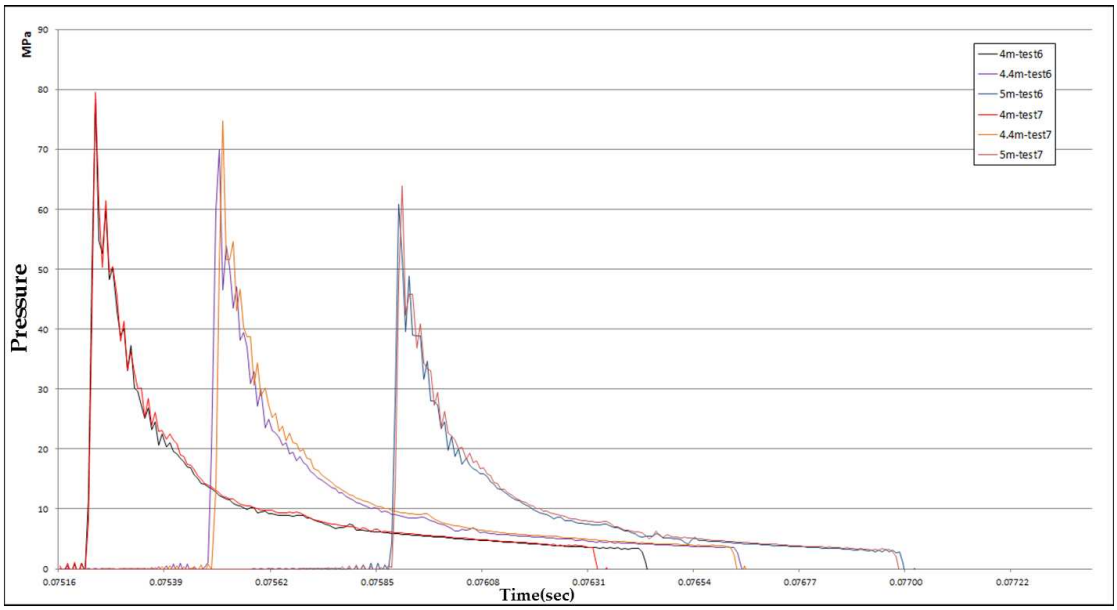

Figure 4.11 Comparison of pressures of test #6 and test #7 (Explosive : 500 g).

Because of the influence of wind, the data of the tests are slightly different. However, the trends for the underwater shock wave phenomena are in agreement. As shown in table 4.9, 500 g of MegaMEX is almost equal to 500 g of TNT. Hence, 500 g of MegaMEX is adopted as the explosive for testing the dynamic response of the structure.

4.2 Response of test structure subjected to underwater explosion

To compare the simulation results and ship shock test results, a ship-like structure is constructed. This ship-like structure has a double hull form called a catamaran. A catamaran is used because of the assumption that the tested structure is a high-speed ship. The catamaran form is usually used for high-speed ships. Table 4.9 lists the boat's specifications. Specifications of a catamaran are presented in table 3.3 and figure 3.4

To confirm the deformation, aluminum is selected for the construction of the ship-like structure. Properties of aluminum are listed in table 3.4. The ship-like structure's drawings and waterline are shown in figures 4.12 and 4.13, respectively.

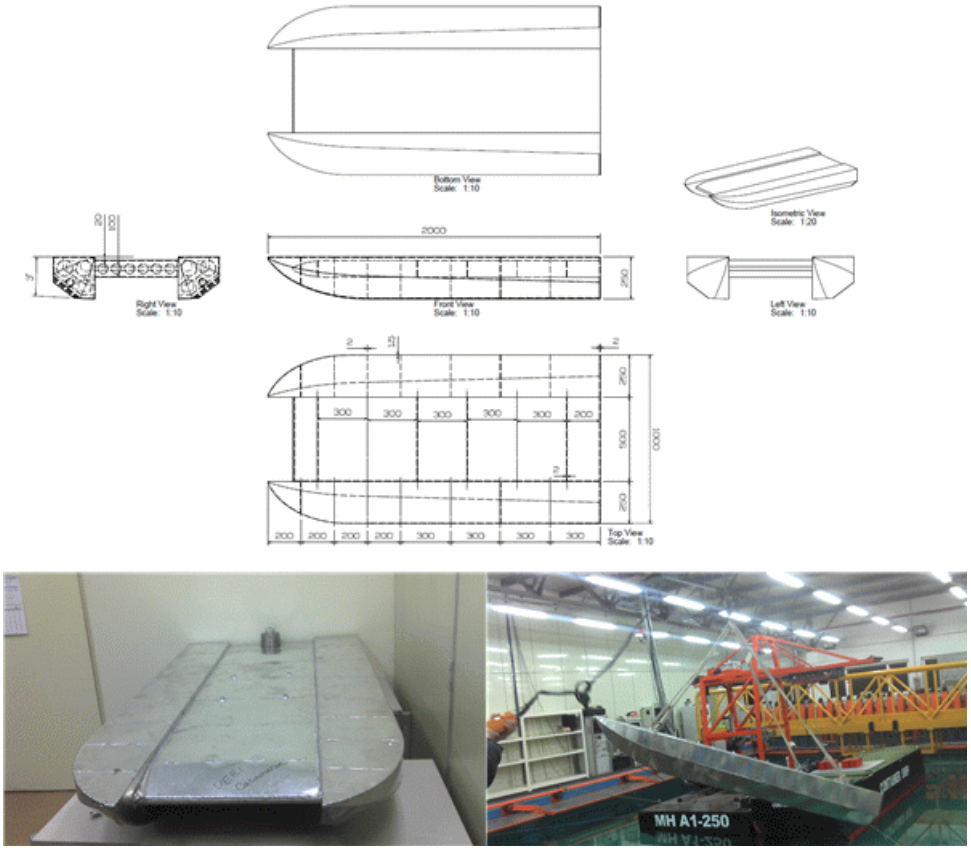

Figure 4.12 Drawings of structure and photographs of completed structure.

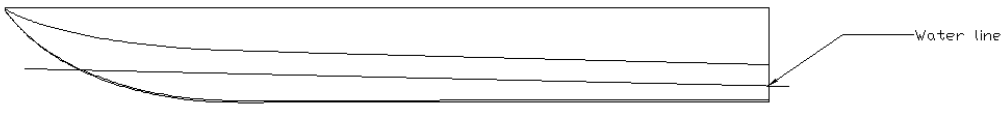

Figure 4.13 Waterline of ship-like structure.

4.2.1 Procedure for shock test

A shock response test for the ship-like structure is conducted at the same site as the shock pressure test, as shown in figure 4.1. The aluminum profile and buoy are installed on the free surface, and the explosive is suspended from the aluminum profile. A twelve-channel data recorder is used for measuring the velocity, acceleration, and pressure. The ship-like structure is tied to the aluminum profile. The structure is not strongly fixed to minimize the effect of the shock response. To measure the experimental data, six velocity output vibration sensors, four shock accelerometers, and two blast pressure sensors are used. The first two sensors' specifications are described in tables 4.10 and 4.11. The specifications of the blast pressure sensors are described in table 4.2. The analyzer used for recording is a LAN-XI, with the frequency range set to 51.2 kHz. The locations of the sensors are shown in figure 4.14. The variable V denotes velocity and A denotes acceleration.

Figure 4.14 Locations of sensors and analyzer.

Table 4.10 Specifications of velocity output vibration sensors.

Position	Model number	Serial number	Sensitivity
Velocity 1	VO622A01	37230	4.0 mV/mm/s
Velocity 2	VO622A01	37228	4.0 mV/mm/s
Velocity 3	VO622A01	37227	4.0 mV/mm/s
Velocity 4	VO622A01	37226	4.0 mV/mm/s
Velocity 5	VO622A01	37234	4.0 mV/mm/s
Velocity 6	VO622A01	37232	4.0 mV/mm/s

Table 4.11 Specifications of shock accelerometers.

Position	Model number	Serial number	Sensitivity
Acceleration 1	8339	57505	0.02830 mV/ms^2
Acceleration 2	8339	57506	0.02883 mV/ms^2

To prevent tension in the cable connected sensors and data recorder, the cables are tied to the aluminum profile. Figure 4.15 provides a brief overview. If the sensors are installed on the deck in an area other than the bulkhead spot, the measured data are incorrect because of the elasticity of the aluminum deck. Therefore, the sensors are installed on the bulkhead spot. If the sensors were attached using glue, they could accidentally fall over because of the shock wave impact. Therefore, nuts are welded to the deck at specific locations, and the sensors are attached to these nuts. However, velocity 6 around the nut decreases because of the shock wave during the test.

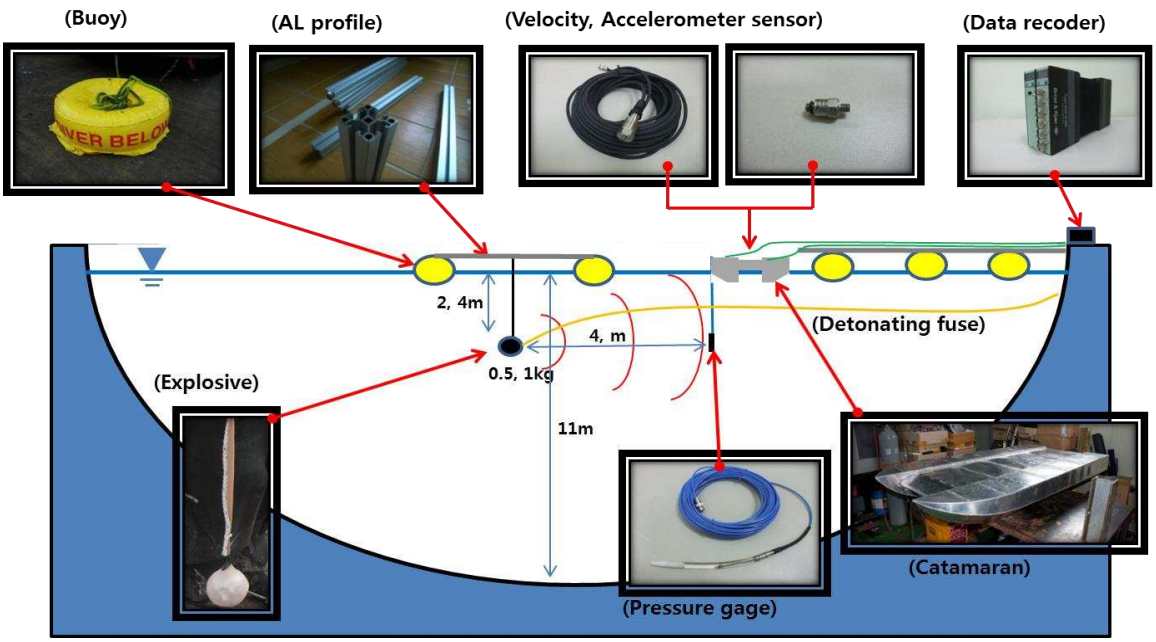

Figure 4.15 Test plan (two dimensions).

4.2.2 Results of response for structure subjected to underwater explosion

4.2.2.1 Response for structure subjected to underwater explosion test 1

Table 4.12 Summary of test 1.

No.	Explosive Weight (g)	Depth (m)	Number of channels	Relation of structure and explosive		
				Position	Distance (m)	Trim (°)
1	500	2	12	Right	3.7	0

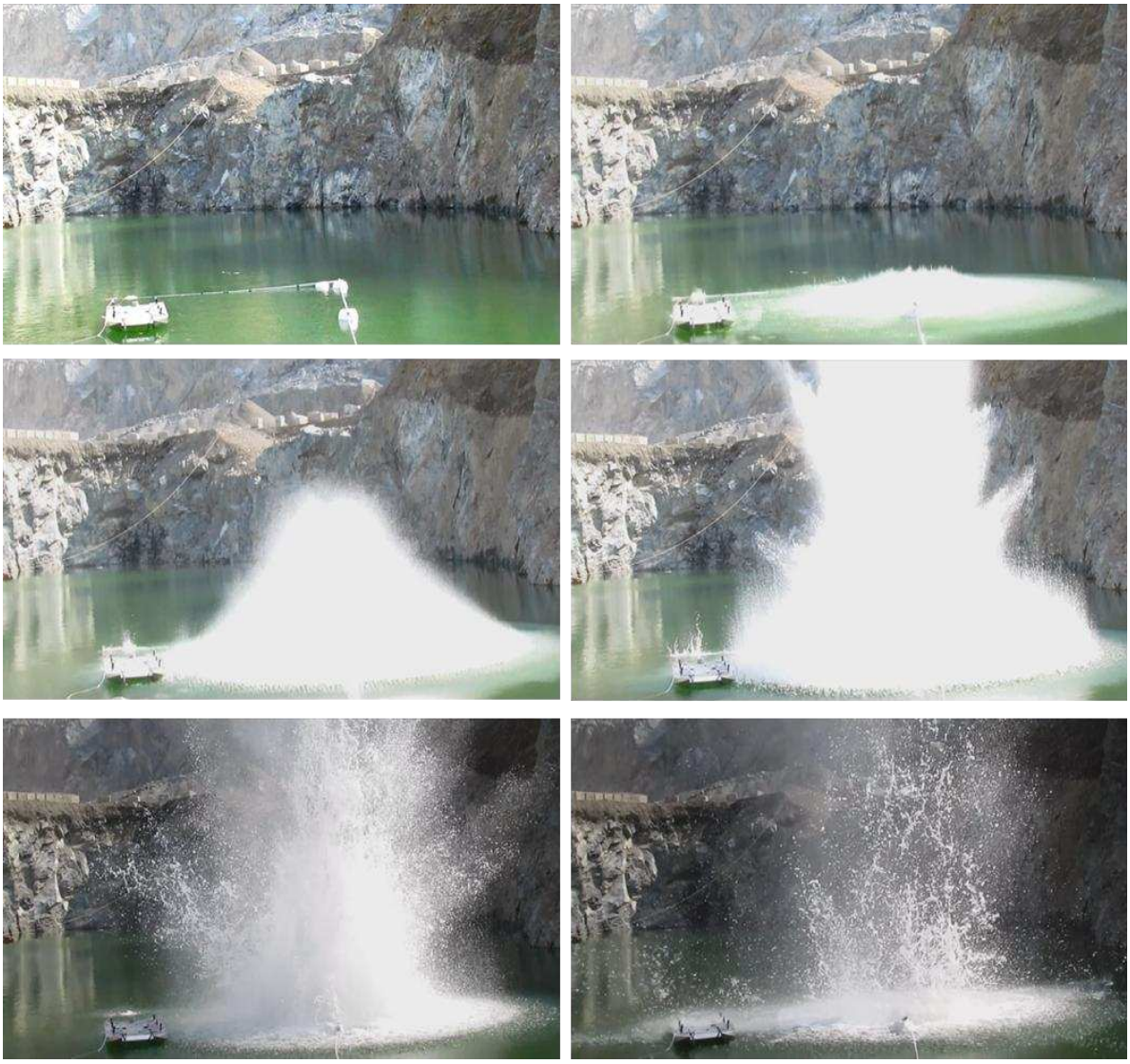

Figure 4.16 Response test for structure subjected to underwater explosion, test 1.

Five hundred grams of MegaMEX is used for the test based on the underwater blast pressure test. The depth of the explosive is 2 m, and the distance between the explosive and structure is 4.47 m. The locations of the sensors are shown in figure 4.14. The total number of channels is twelve. Six velocity output vibration sensors and 4 shock accelerometers are installed on the deck of the ship-like structure. However, two of the acceleration sensors are out of range at all times.

Because of the stabilization of the sensors, the explosive is detonated 30 s after setting up the sensors. Shortly after the explosion, the structure experiences the highest z-velocity and z-acceleration caused by the shock wave. The bulk cavitation area and spray dome are observed on the free surface caused by the shock wave, and then a column of water called a flume, which is caused by the bubble pulse, penetrates the spray dome. The response of the structure is recorded by the 12 channel analyzer. The measured data from the recorder are shown in figures 4.17, 4.18, and 4.19, and the responses are highly impacted by the bubble pulse pressure.

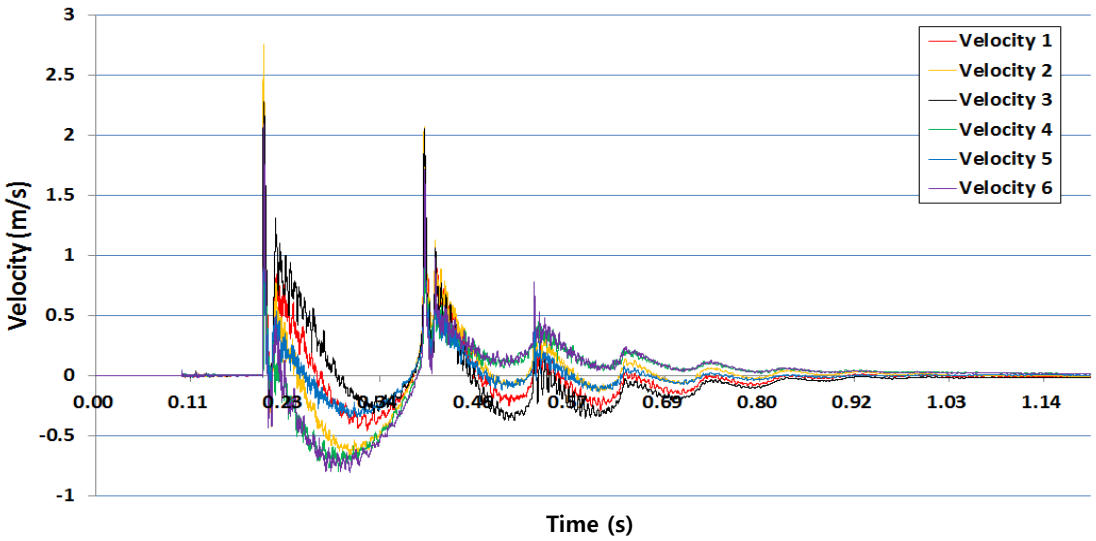

Figure 4.17 The results of structure velocity.

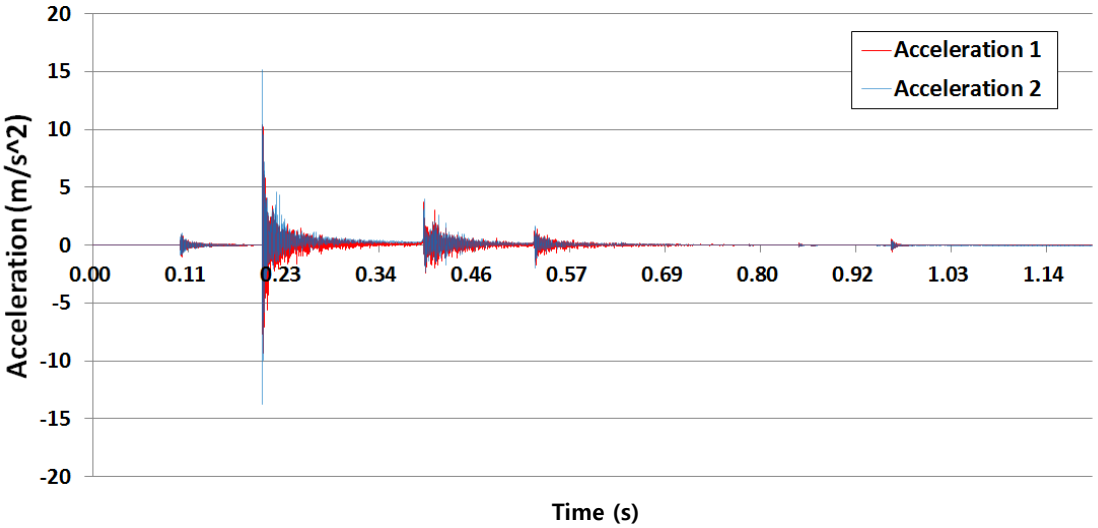

Figure 4.18 The results of structure acceleration.

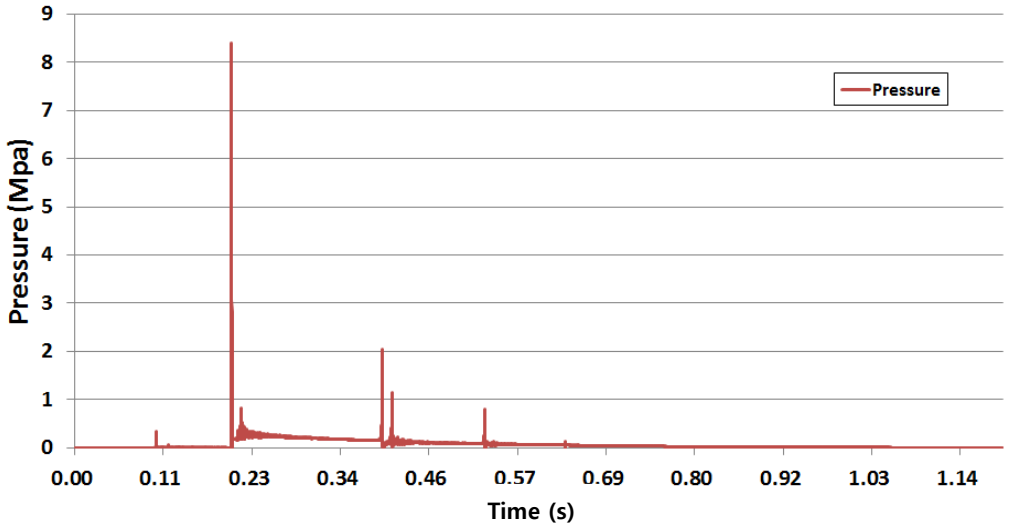

Figure 4.19 Input shockwave and bubble pulse pressure, max: 8.40 MPa (3.7 m).

When the explosive is detonated underwater, the structure experiences a shock caused by the incident shock wave. As shown in figures 4.17 and 4.18, the dynamic responses in terms of the velocity and acceleration depend on the shock wave and bubble pulse pressure. Figure 4.18 shows the acceleration of the structure's response caused by three bubble pulses.

4.2.2.2 Response for structure subjected to underwater explosion test 2

The basic procedure is the same as in test 1. However, the depth of the explosive is 1 m to detect the vent out phenomenon at the bubble's first growth, because the first bubble radius is 1.11 m, as calculated by the empirical equation. Because of the vent out phenomenon, the flume is higher than in other circumstances. A summary of test 2 is given in table 4.15.

Table 4.13 Summary of test 2.

No.	Explosive weight (g)	Depth (m)	Number of channels	Relation of structure and explosive		
				Position	Distance (m)	Trim (°)
2	500	1	12	Right	3.9	0

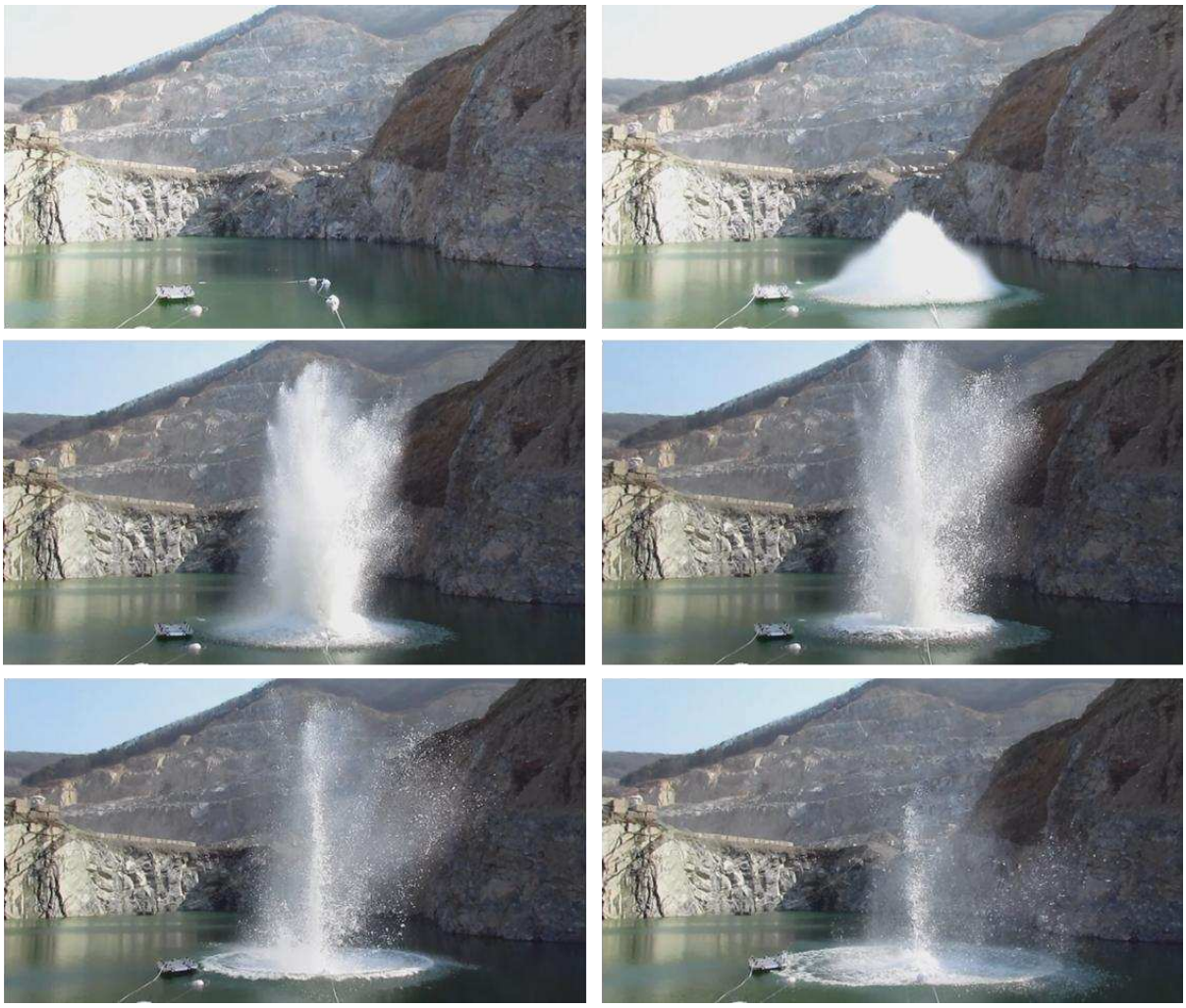

Figure 4.20 Response test for structure subjected to underwater explosion, test 2.

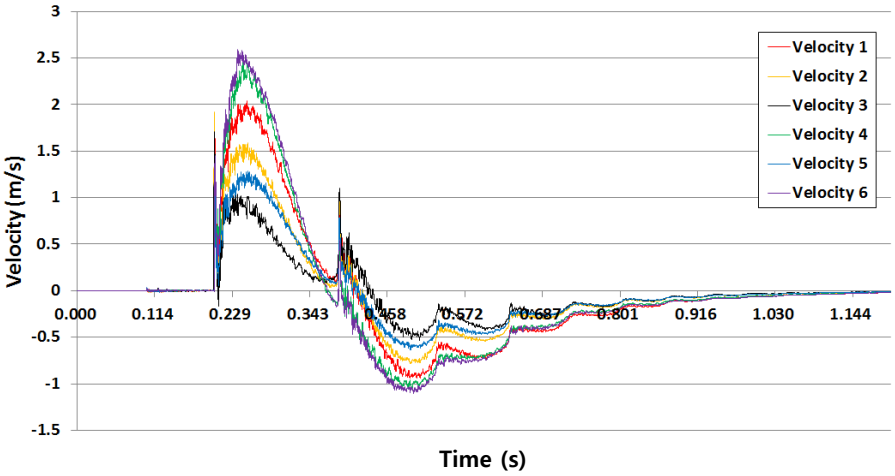

Figure 4.21 The results of structure velocity.

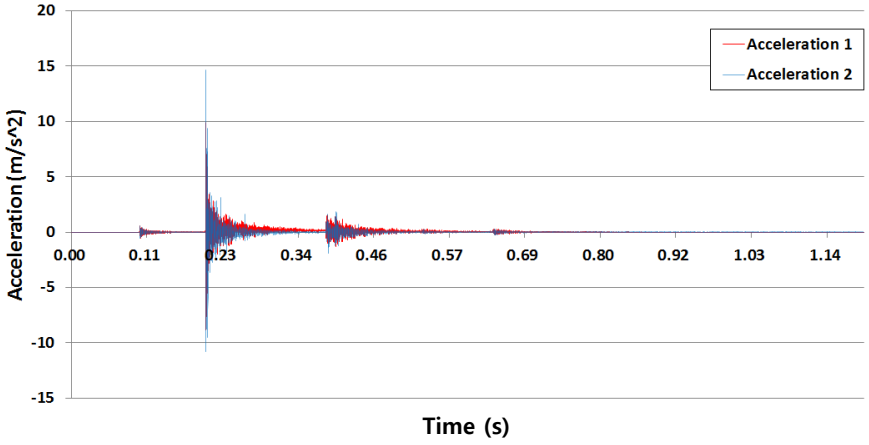

Figure 4.22 The results of structure acceleration.

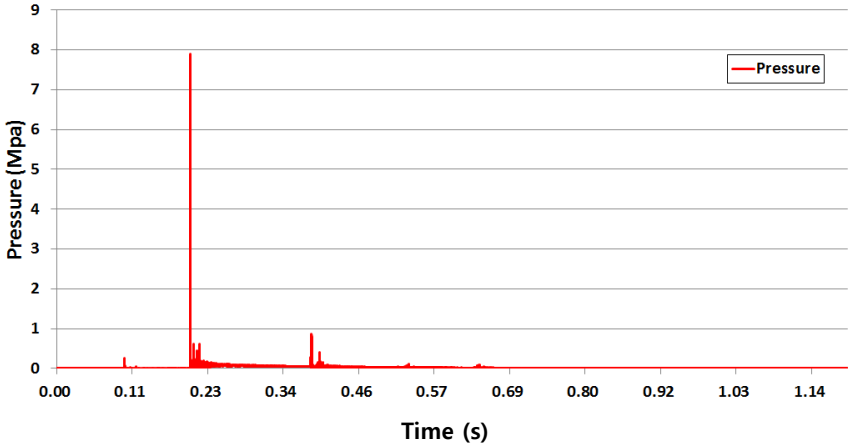

Figure 4.23 Input shock wave pressure, max: 7.9 MPa (3.9 m).

The purpose of test 2 is an examination of the vent out phenomenon of the bubble effect and the dynamic response of the structure. At first, the plan is to use the same conditions as test 1. However,

the structure is out of control because of the effect of the wind. Thus, the distance between the structure and the explosive is increased to 3.9 m. As a result of this changed condition, the first response of the velocity is lower than test 1. As shown in figure 4.20, when the bubble is vented out, the velocity of the structure's response is increased without the bubble pulse. Next, the first bubble pulse occurs. Before the test, the bubble pulse is not expected. However, the bubble pulse appears.

4.2.2.3 Response for structure subjected to underwater explosion test 3

Table 4.14 Summary of test 3.

No.	Explosive weight (g)	Depth (m)	Number of channels	Relation of structure and explosive		
				Position	Distance (m)	Trim (°)
3	500	2	12	Right	4.5	4

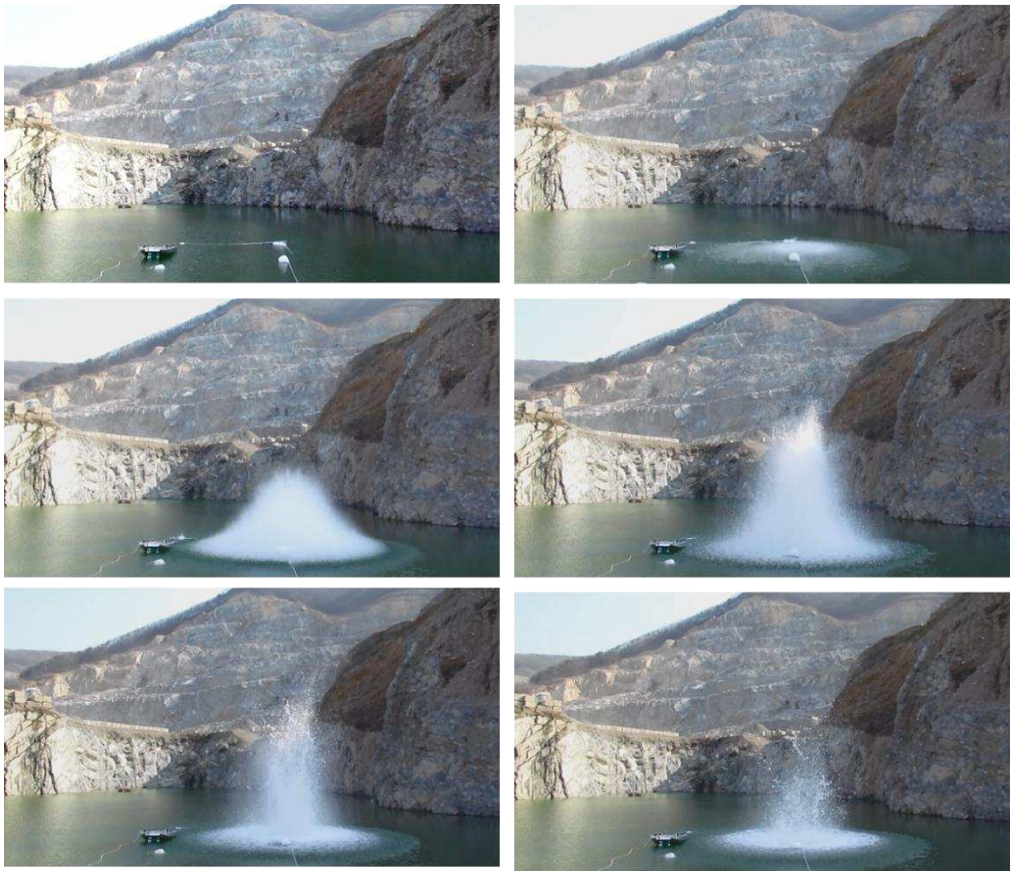

Figure 4.24 Response test for structure subjected to underwater explosion, test 3.

The basic procedure is the same as in test 1. However, the ship-like structure has a 4° angle

because it is assumed to be moving at high speed. When a ship moves at high speed, it has a trim angle. Thus, the characteristics of high-speed craft can be predicted by these test results. A summary of test 3 is given in table 4.14, and the measured data are shown in figures 4.25, 4.26, and 4.27.

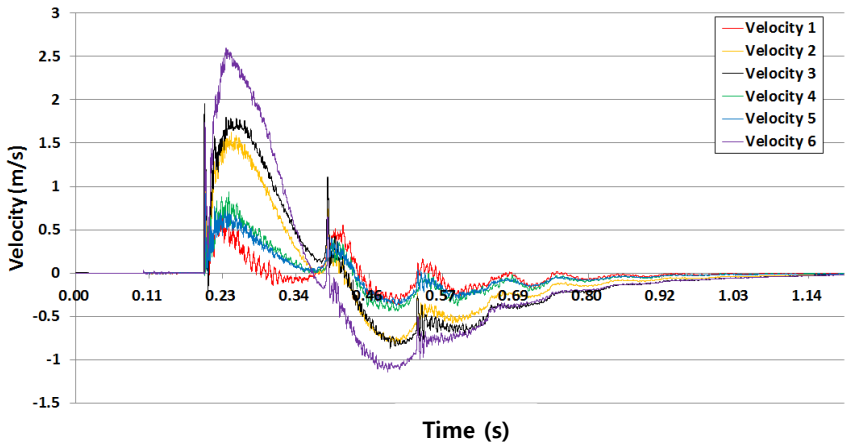

Figure 4.25 The results of structure velocity.

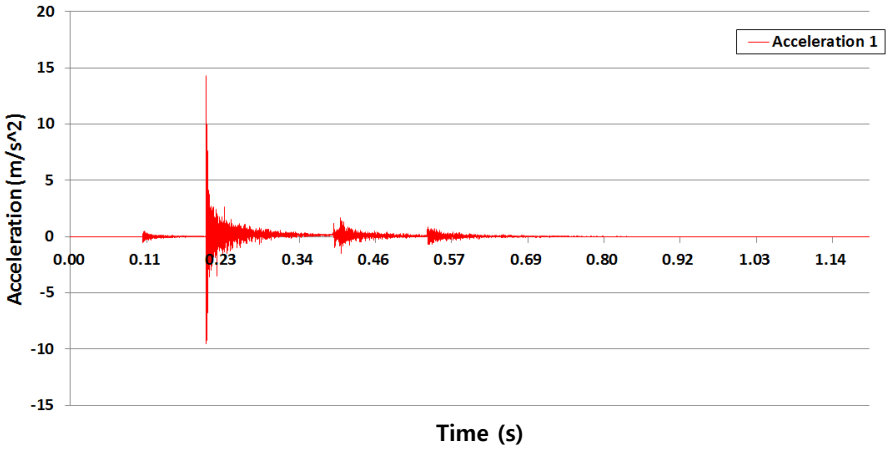

Figure 4.26 The results of structure acceleration.

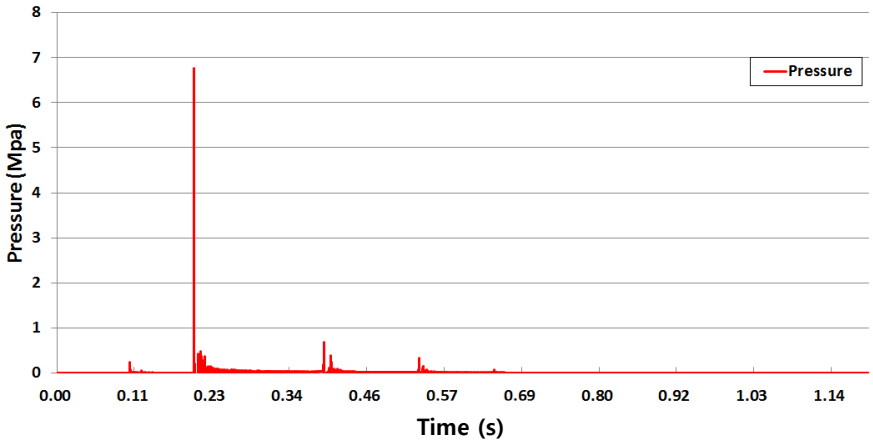

Figure 4.27 Input shock wave and bubble pulse pressure, max pressure: 6.77 MPa (4.5 m).

As shown in figures 4.25 and 4.26, the results of test 3 are affected by the trim angle of the structure. Velocities 1, 4, and 5 are affected very little by the trim angle. However, the wetted surface points (velocities 2, 3, and 6) are affected by the trim angle. As shown in figure 4.26, these points are affected by the second bubble pulse. In addition, the bubble pulse is measured as shown in figure 4.26. Acceleration 2 is not measured, because the acceleration sensor is overloaded for unknown reasons.

4.2.2.4 Response for structure subjected to underwater explosion test 4

Table 4.15 Summary of test 4.

No.	Explosive weight (g)	Depth (m)	Number of channels	Relation of structure and explosive		
				Position	Distance (m)	Trim (°)
4	500	1	12	Right	4.17	4

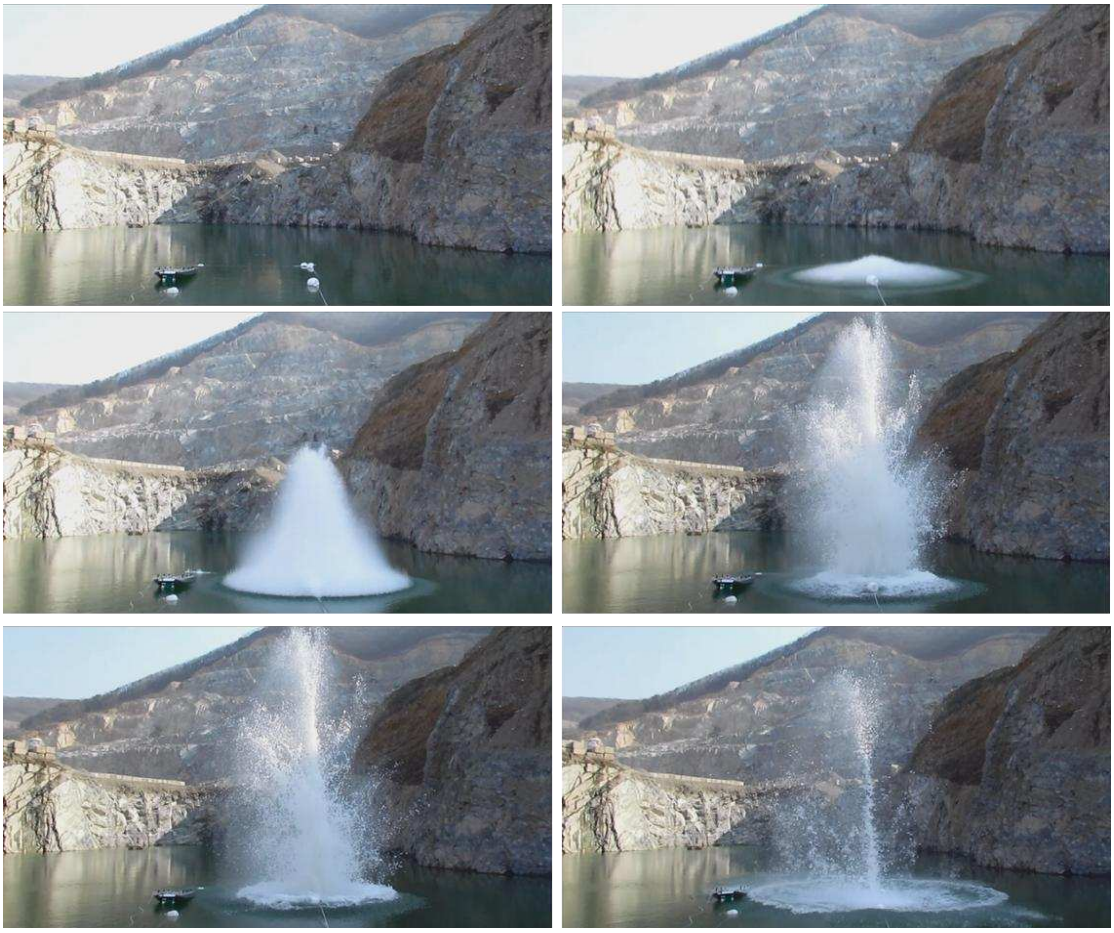

Figure 4.28 Response test for structure subjected to underwater explosion, test 4.

The basic procedure is the same as in test 1. However, the ship-like structure has a 4° angle because high speed is assumed. Test 4 is conducted for comparison with test 2 to verify the impact of the trim angle. A summary of test 4 is given in table 4.15, and the measured data are shown in figures 4.29 and 30.

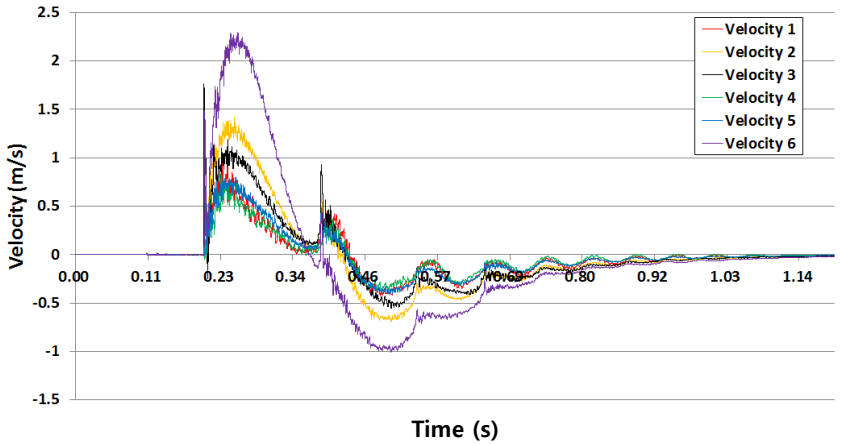

Figure 4.29 The results of structure velocity.

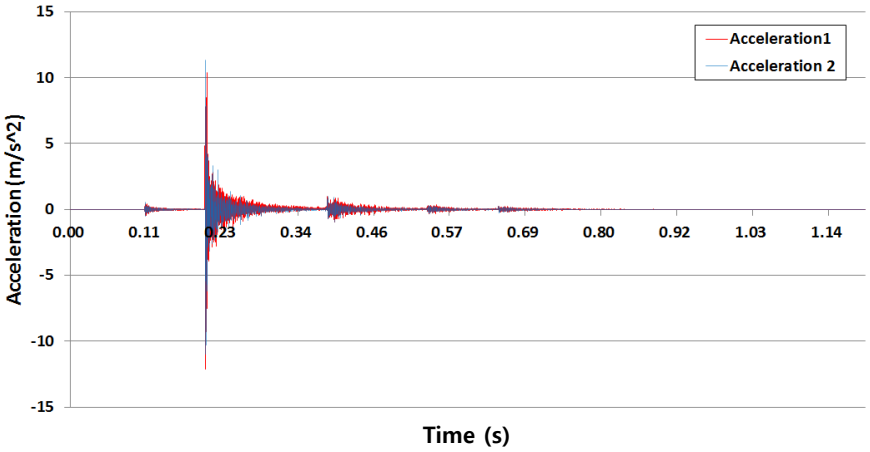

Figure 4.30 The results of structure acceleration.

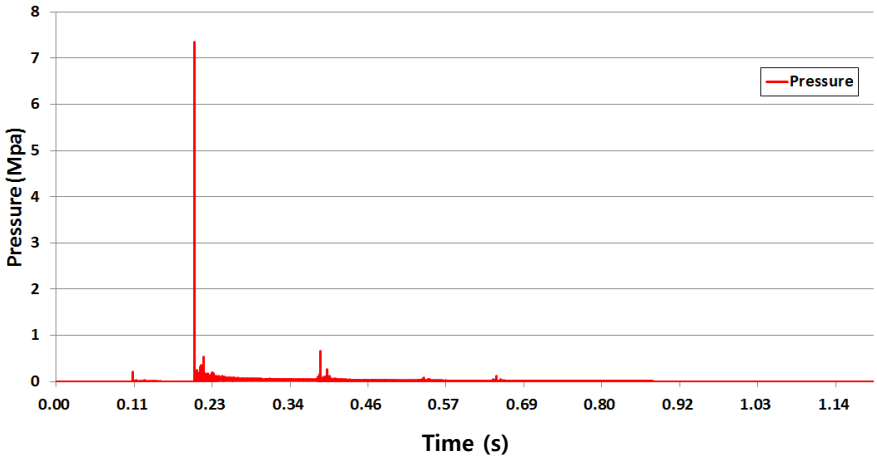

Figure 4.31 Input shock wave and bubble pulse pressure, max: 7.35 MPa (4.17 m).

This test has a trim angle and shows the vent out phenomena of the bubble. Hence, the results of test 4 are a mixture of the results of tests 2 and 3. Velocity sensor 6 is overloaded for unknown reason.

4.2.2.5 Response for structure subjected to underwater explosion test 5

Table 4.16 Summary of test 5.

No.	Explosive Weight (g)	Depth (m)	Number of channels	Relation of structure and explosive		
				Position	Distance (m)	Trim (°)
5	1000	4	12	Right	4.1	0

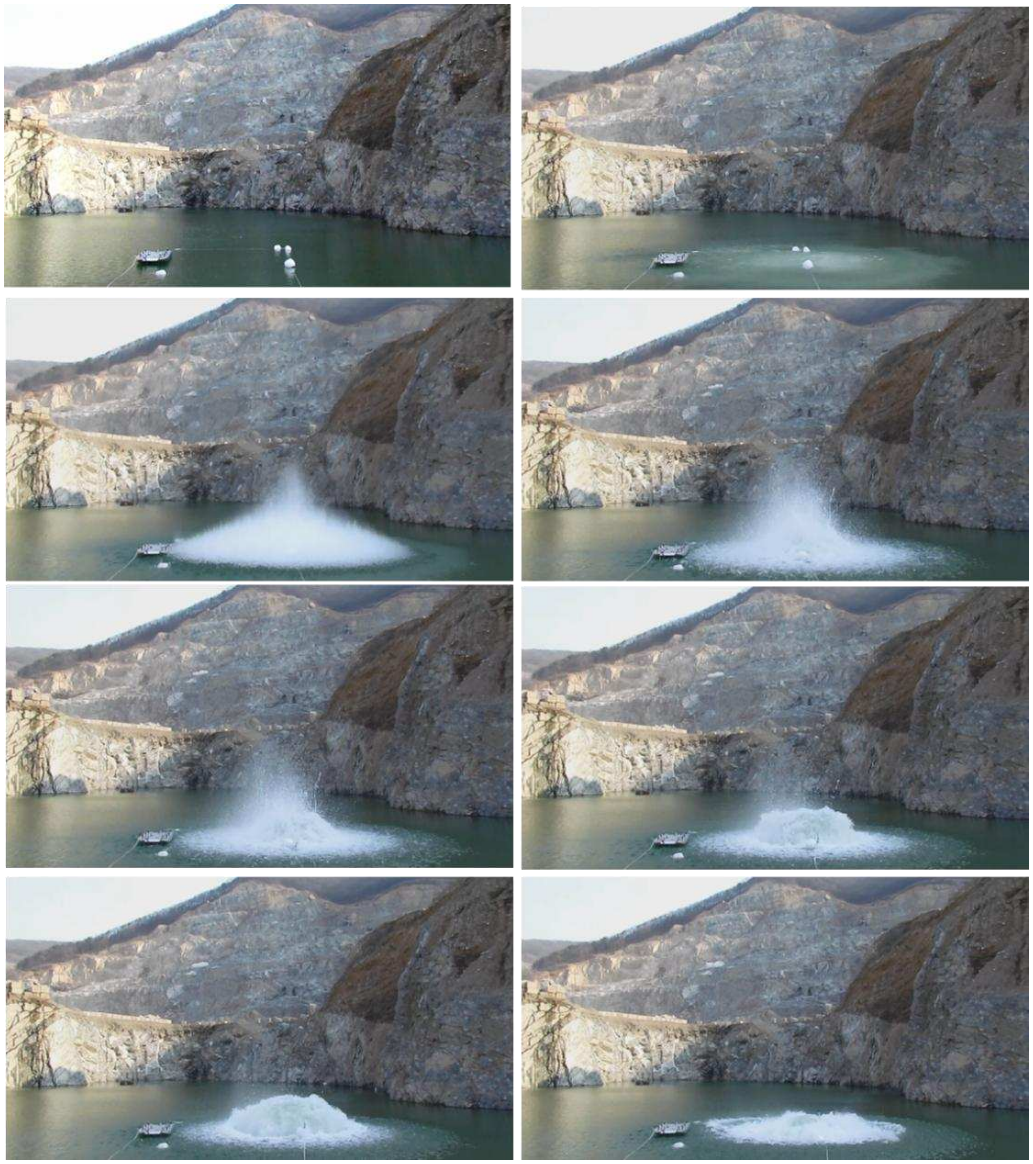

Figure 4.32 Response test for structure subjected to underwater explosion, test 5.

This test is conducted to confirm the bubble motion effect. The velocity results are not measured because the shock response of the structure exceeds the measurement range. The acceleration response results for the structure are shown in figure 4.33.

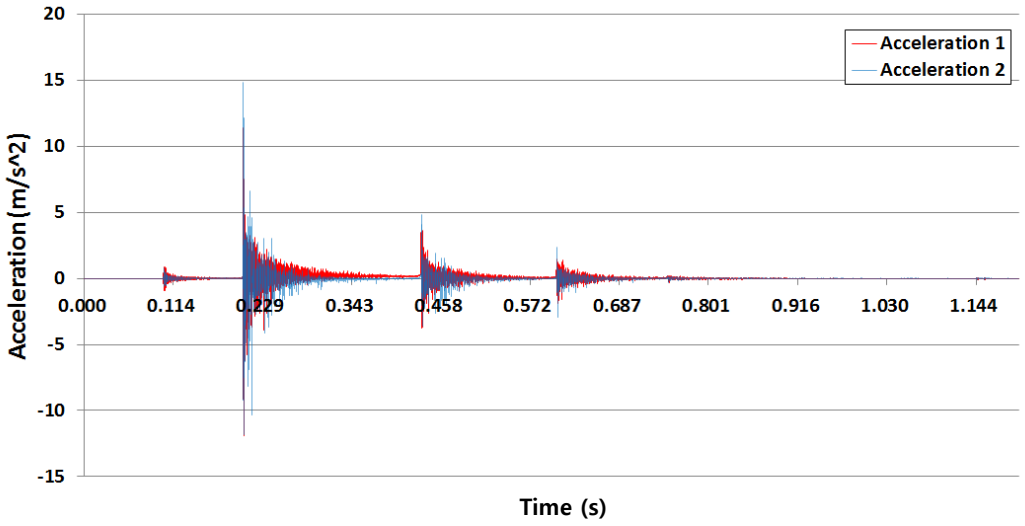

Figure 4.33 The results of structure acceleration.

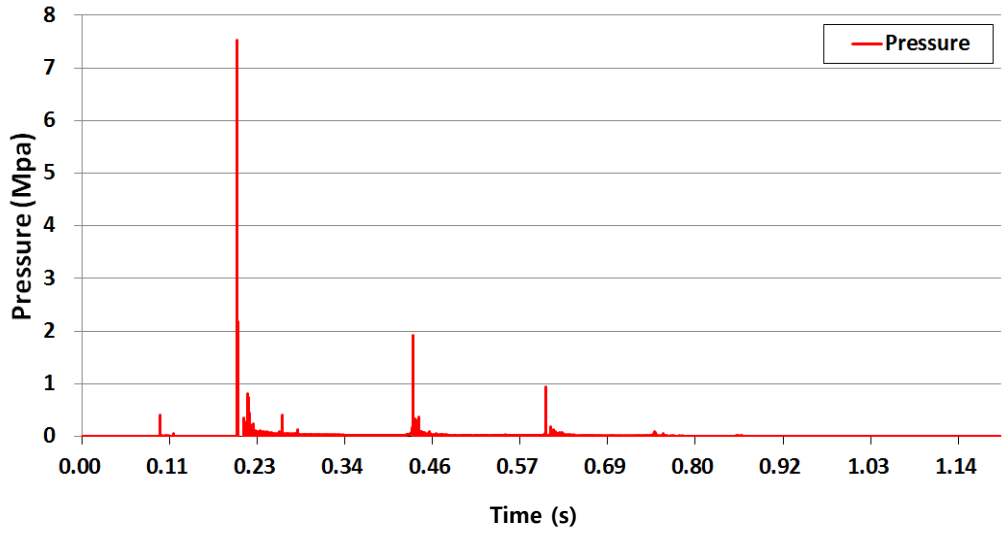

Figure 4.34 Input shock wave and bubble pulse pressure, max: 7.53 MPa (4.1 m).

All of the velocity sensors are overloaded because they are out of range. Thus, in this case, only the acceleration is measured. As shown in figure 4.29, the bubble pulse, which is bigger than that for 500 g of explosive, is measured by the acceleration sensors.

4.2.2.6 Response for structure subjected to underwater explosion test 6

Table 4.17 Summary of test 6.

No.	Explosive Weight (g)	Depth (m)	Number of channels	Relation of structure and explosive		
				Position	Distance (m)	Trim (°)
6	500	2	12	Right	4.7	0

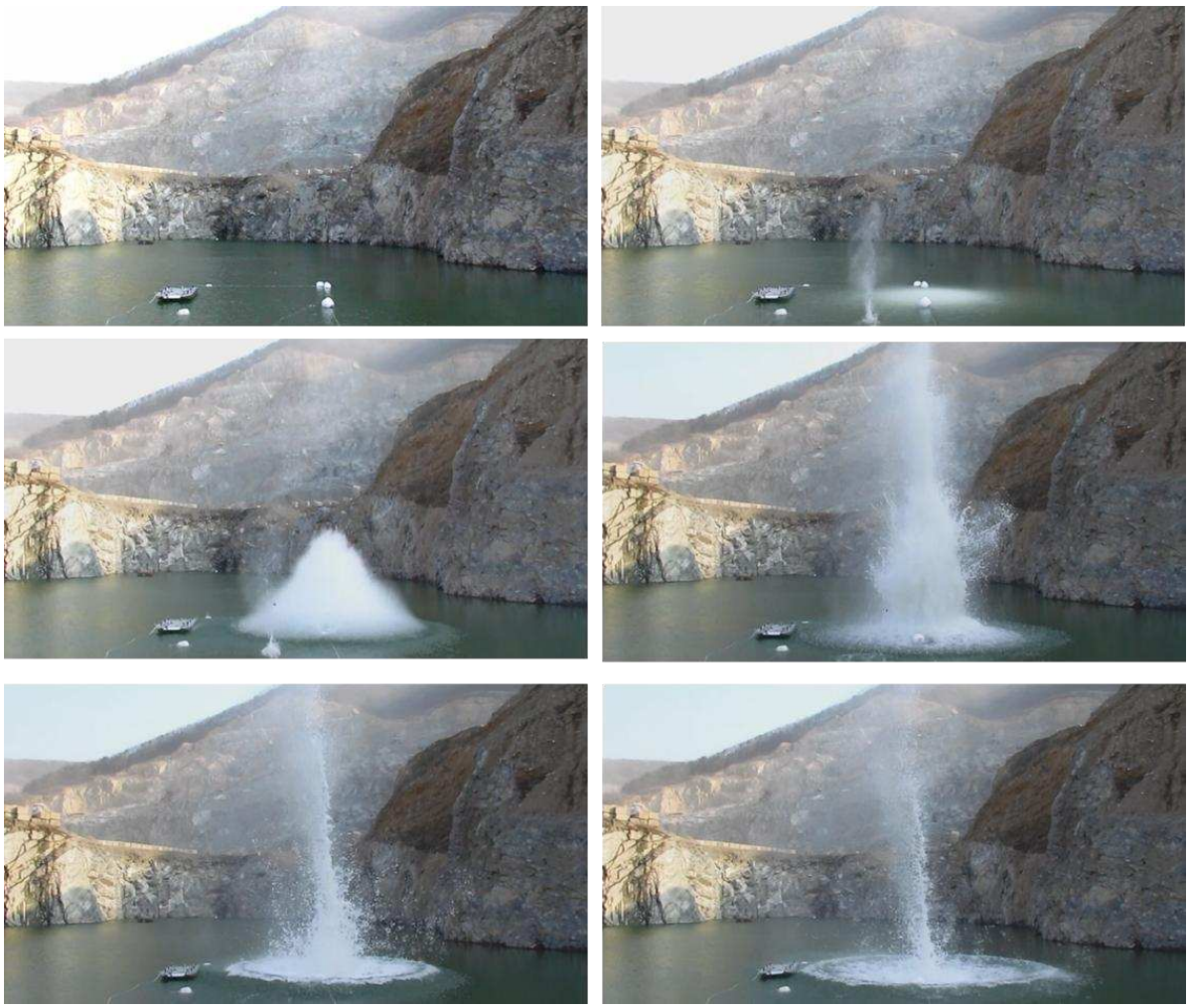

Figure 4.35 Response test for structure subjected to underwater explosion, test 6.

The basic procedure is also the same as in test 1. However, the distance from the explosive is 5 m because of the wind. A summary of test 6 is given in table 4.17, and the measured data are shown in figures 4.36 and 4.37.

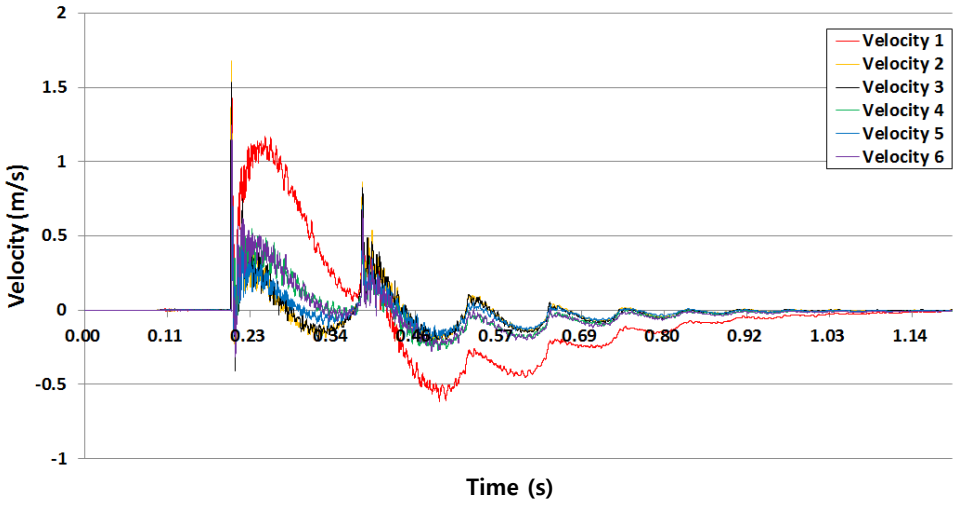

Figure 4.36 The results of structure velocity.

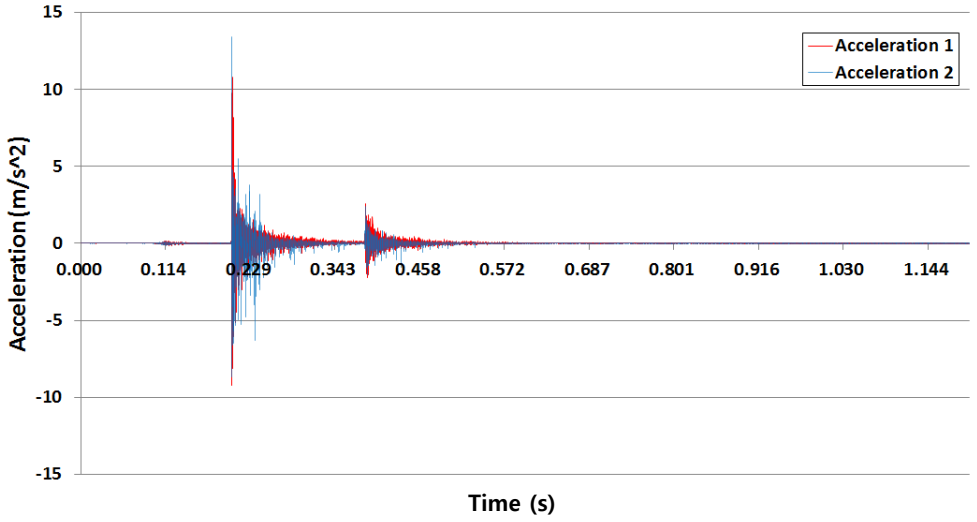

Figure 4.37 The results of structure acceleration.

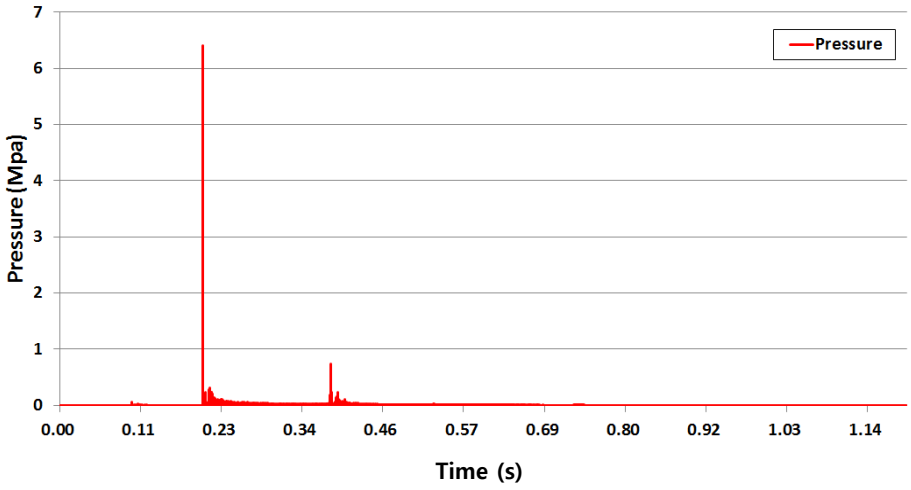

Figure 4.38 Input shock wave and bubble pulse pressure, max: 6.41 MPa (4.7 m).

4.2.2.7 Response for structure subjected to underwater explosion test 7

Table 4.18 Summary of test 7.

No.	Explosive Weight (g)	Depth (m)	Number of channels	Relation of structure and explosive		
				Position	Distance (m)	Trim (°)
7	500	2	12	Right	3.25	0

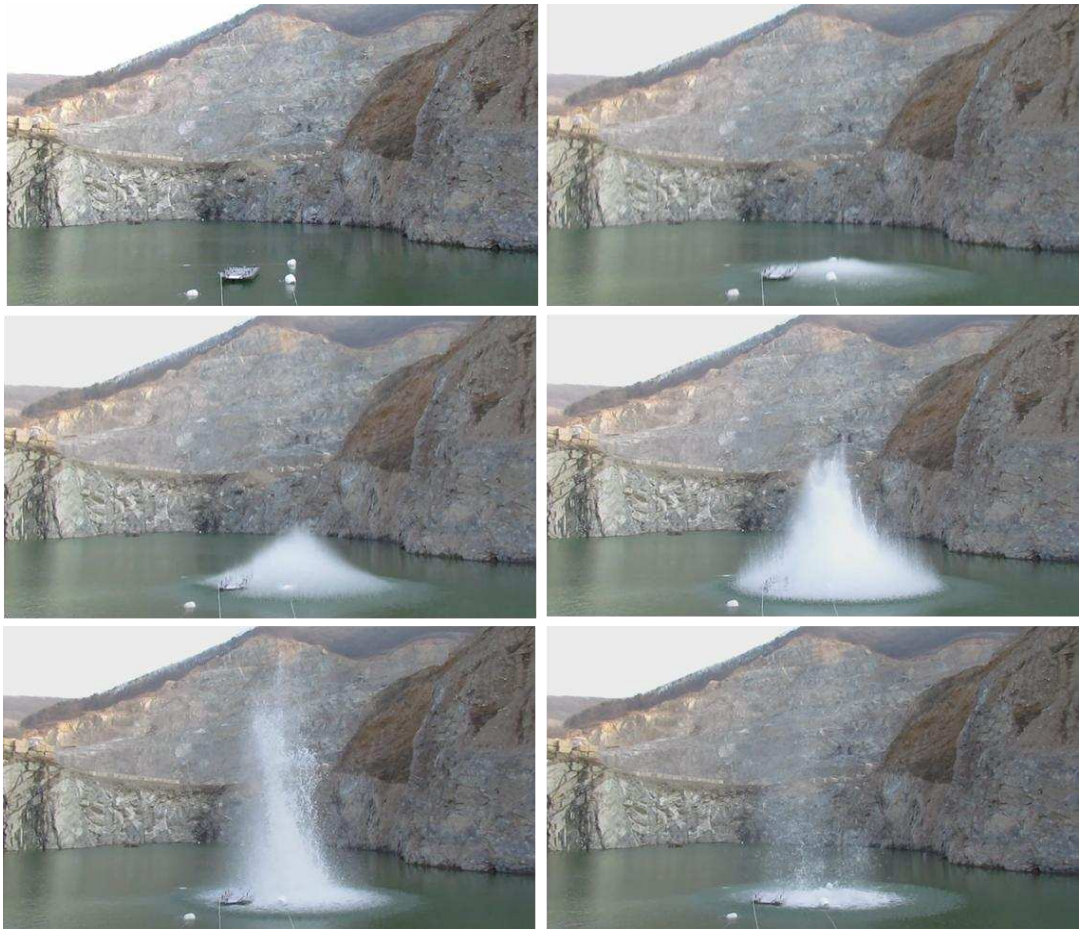

Figure 4.39 Response test for structure subjected to underwater explosion, test 7.

The basic procedure is also the same as in test 1. In this test, the original designed test distance is 2 m between the structure and explosive. However, the actual distance from the explosive becomes 1.5 m because of the difficulty of controlling the position of the structure as a result of the wind. This is too close to the explosion. Thus, the velocity data are not measured because the shock response of the structure exceeds the measurement range. The acceleration response results for the structure are shown in figure 4.40. Because of the proximity of the underwater explosion, the outer hull of the structure is deformed. A summary of test 7 is given in table 4.18.

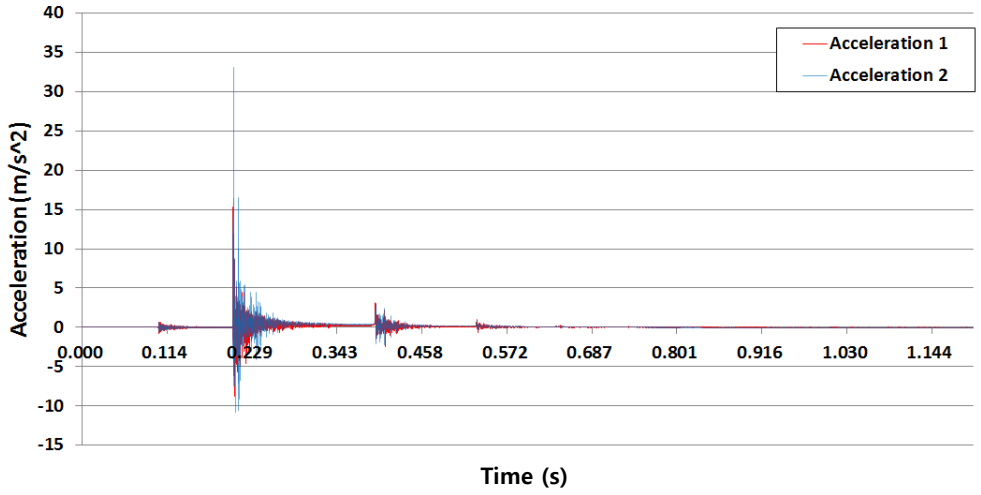

Figure 4.40 The results of structure acceleration.

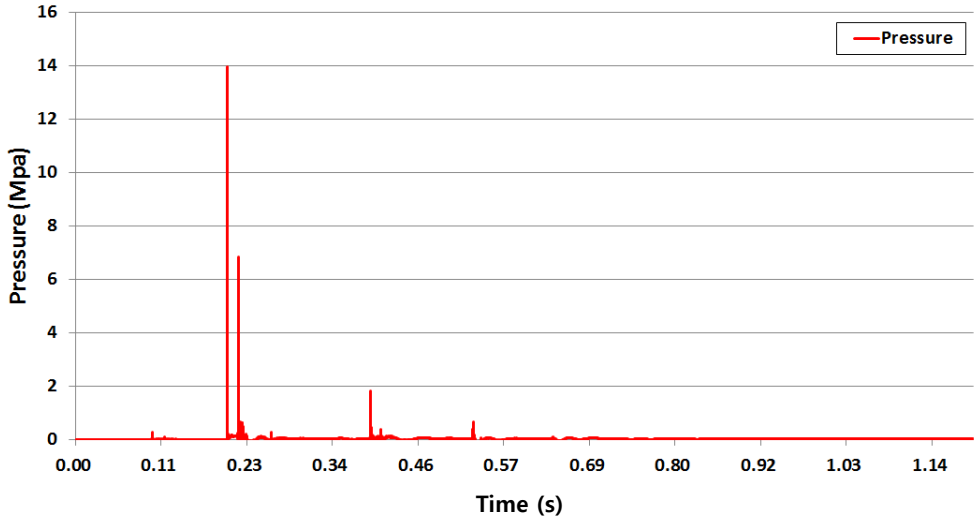

Figure 4.41 Input shock wave and bubble pulse pressure, max: 14.0 MPa (2.4 m).

All of the velocity sensors are overloaded because they are out of range. Thus, in this case, only the acceleration is measured. As shown in figure 4.40, the maximum acceleration is the largest for any of the tests. During this test, the outer hull of the structure is deformed by the strong shock wave pressure and bubble pulse impact.

4.2.2.8 Response for structure subjected to underwater explosion test 8

Table 4.19 Summary of test 8.

No.	Explosive Weight (g)	Depth (m)	Number of channels	Relation of structure and explosive		
				Position	Distance (m)	Trim (°)
8	500	2	12	Right	3.25	4

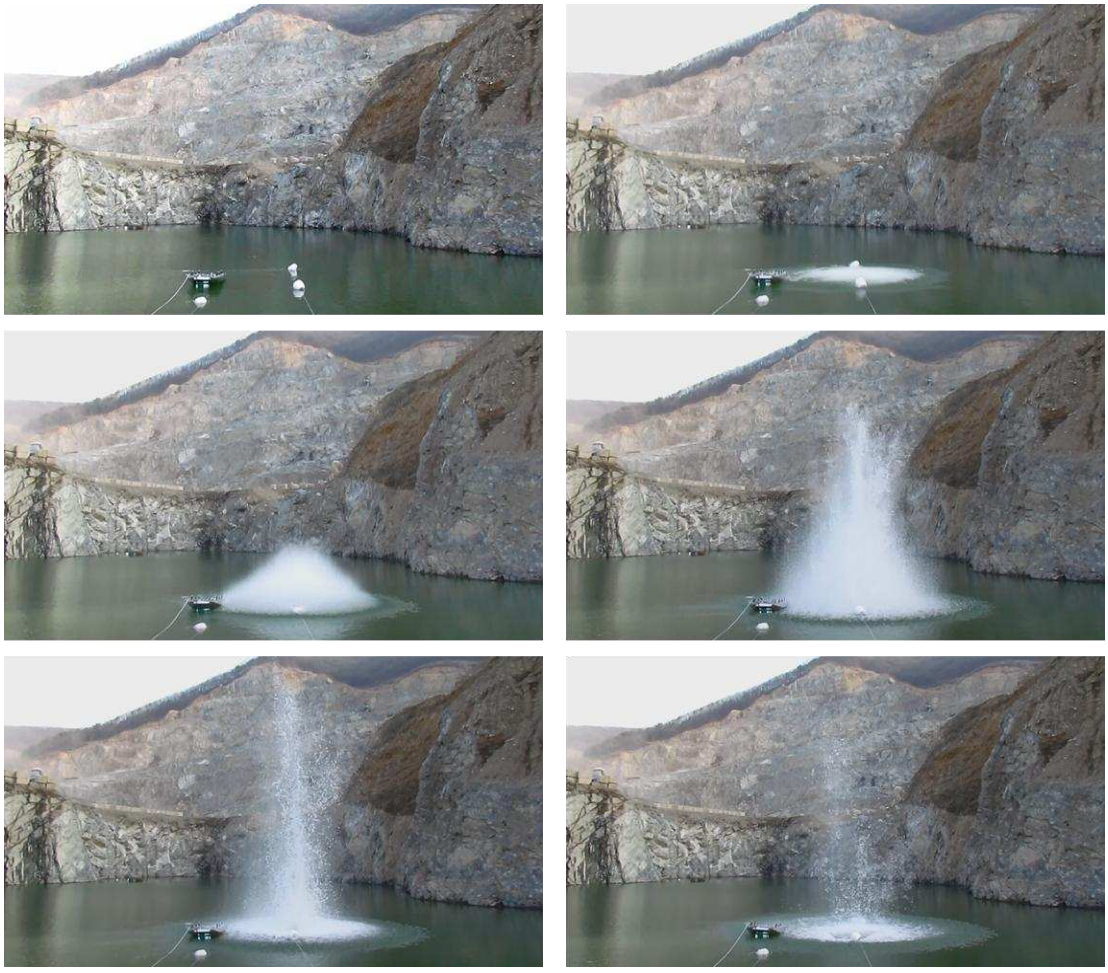

Figure 4.42 Response test for structure subjected to underwater explosion, test 8.

The basic procedure is also the same as in test 1. The test distance is 2 m between the structure and explosive. The ship-like structure has a 4° angle because it is assumed that it is moving at high speed, as in test 3. Test 8 is conducted for comparison with test 7 to verify the impact of the trim angle. However, in test 7, the distance between the explosive and structure is 1.5 m as a result of strong wind. A summary of test 8 is given in table 4.20, and the measured data are shown in figures 4.43 and 4.44.

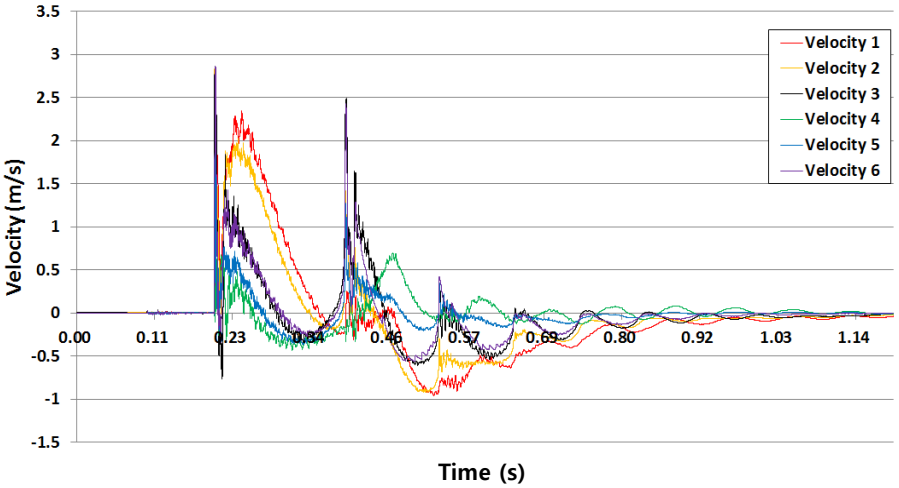

Figure 4.43 The results of structure velocity.

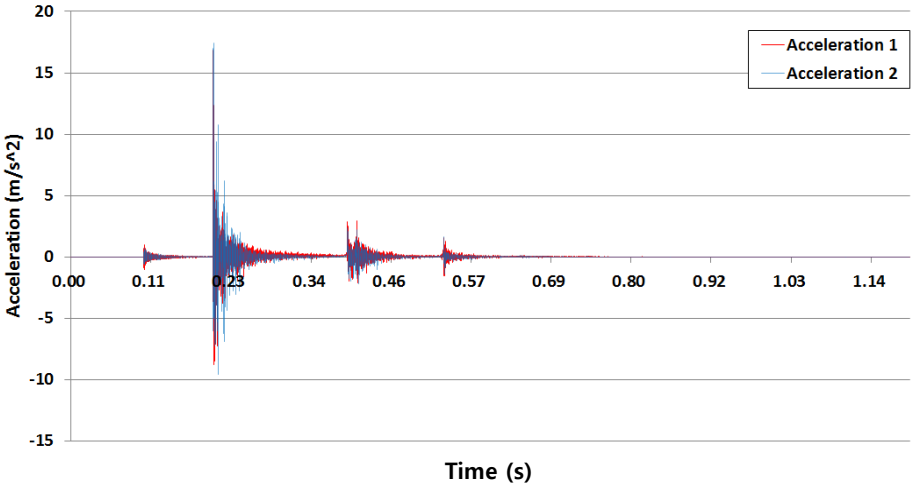

Figure 4.44 The results of structure acceleration.

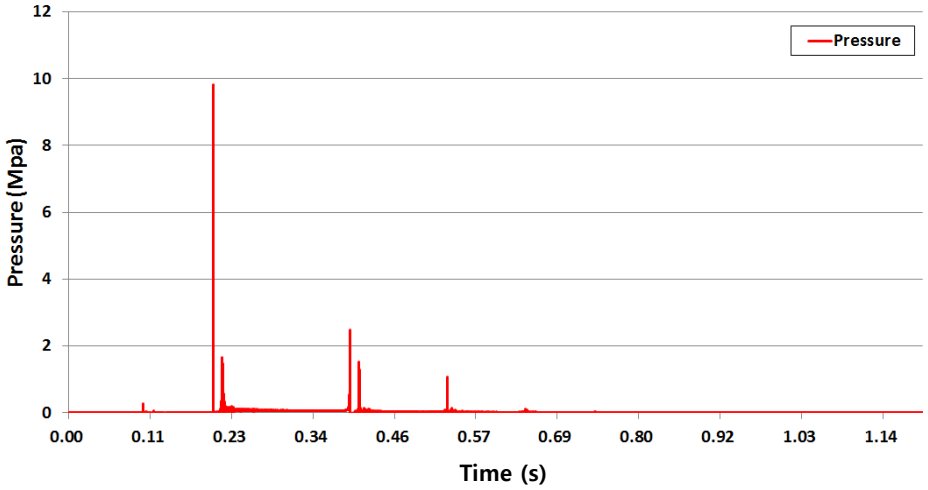

Figure 4.45 Input shock wave and bubble pulse pressure, max: 9.82 MPa (3.25 m).

As shown in figures 4.43 and 4.44, the results of test 8 are affected by the trim angle of the

structure. Velocities 1, 4, and 5 are only slightly affected by the trim angle. However, the wetted surface points (velocities 2, 3, and 6) are affected by the trim angle. As shown in figure 4.44, these points are affected by the second bubble pulse. Moreover, the bubble pulse is measured as shown in figure 4.44. Acceleration 2 is not measured, because the acceleration sensor is overloaded for unknown reasons, along with almost all of the velocity sensors. Thus, the velocity results cannot be trusted. However, the results are shown in this paper because all of the test results are worth studying.

4.2.2.9 Response for structure subjected to underwater explosion test 9

Table 4.20 Summary of test 9.

No.	Explosive Weight (g)	Depth (m)	Number of channels	Relation of structure and explosive		
				Position	Distance (m)	Trim (°)
9	500	2	12	Back	4.65	4

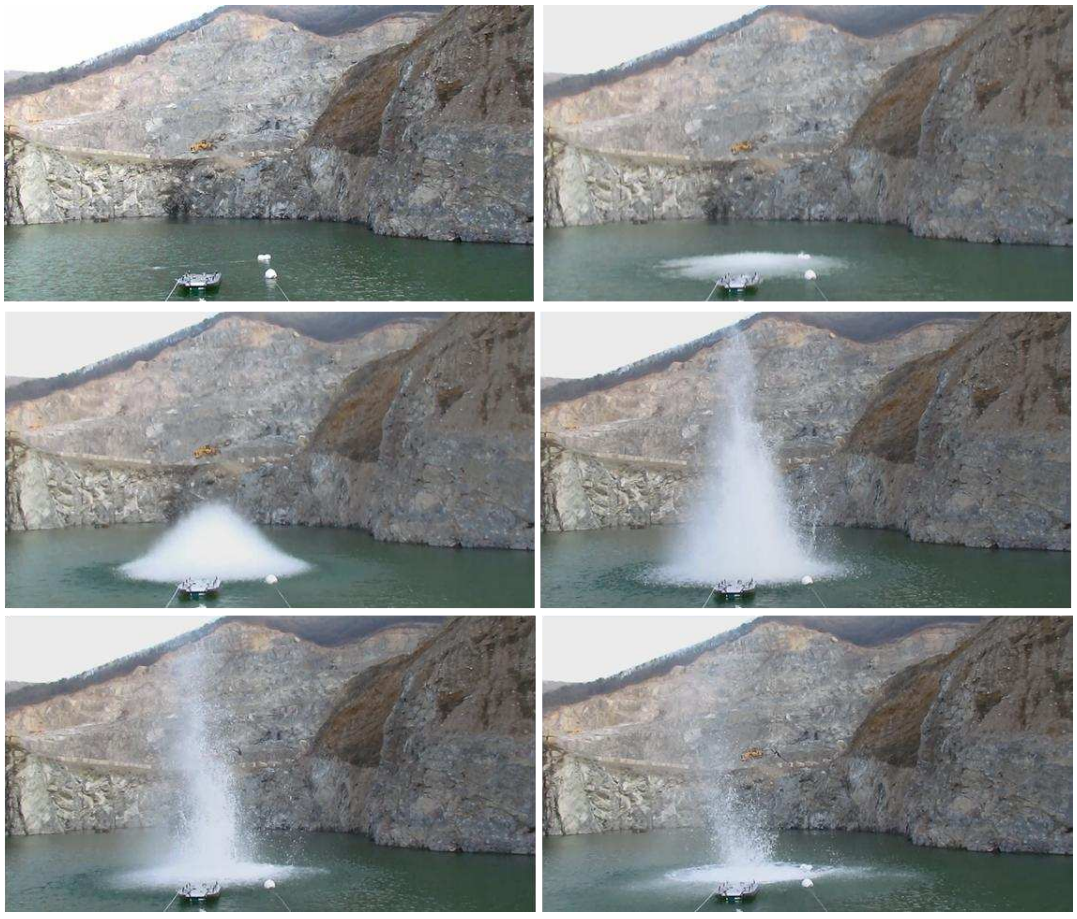

Figure 4.46 Response test for structure subjected to underwater explosion, test 9.

The basic procedure is the same as in test 3. However, the ship-like structure has a 4° angle. In the case of a high-speed ship, even if an explosive detonates precisely under the ship, the explosive's bubble is generated behind the ship because of the speed. Hence, this situation is assumed when conducting test 9. The test distance is 4.65 m between the structure and explosive. Test 9 is conducted for comparison with test 10 to verify the impact of the trim angle. A summary of test 9 is given in table 4.20.

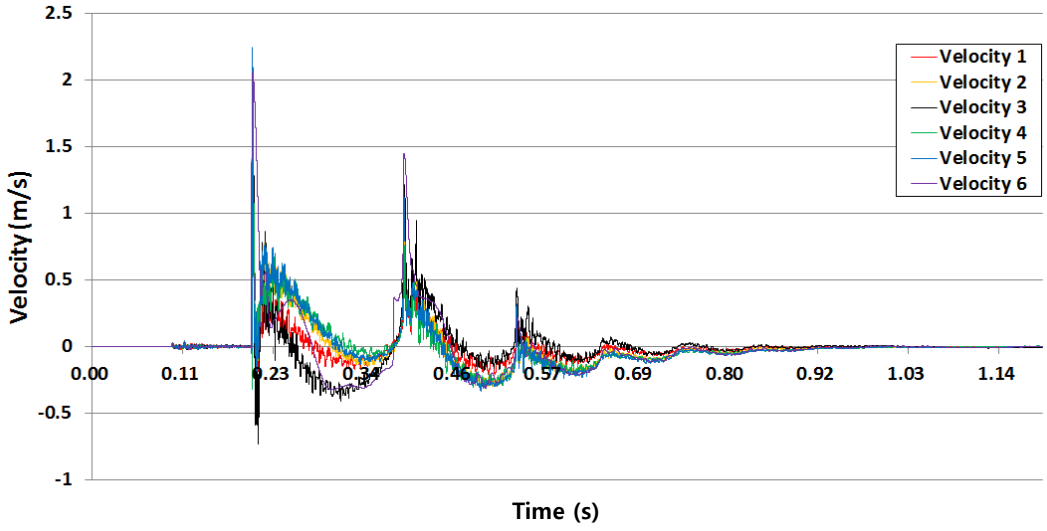

Figure 4.47 The results of structure velocity.

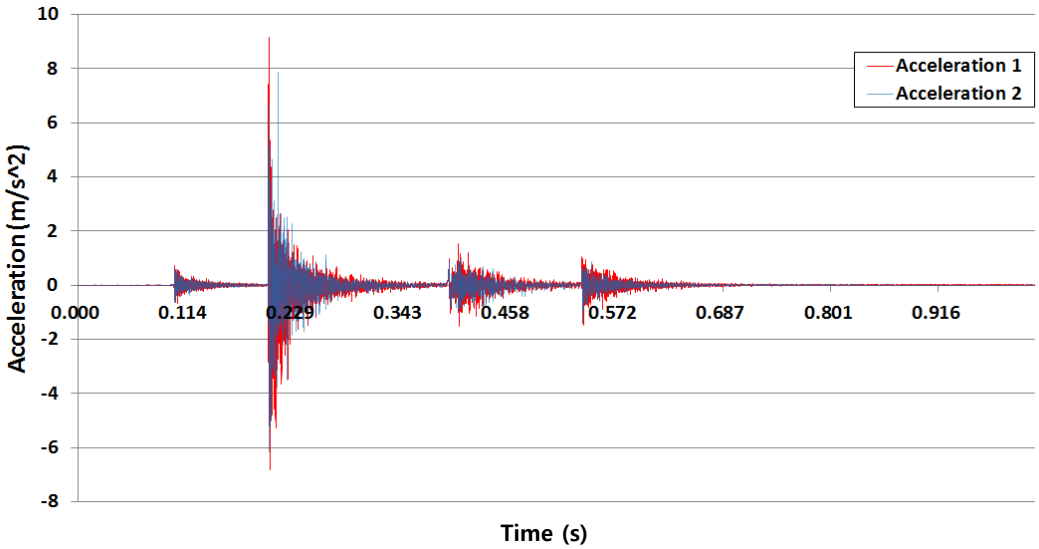

Figure 4.48 The results of structure acceleration.

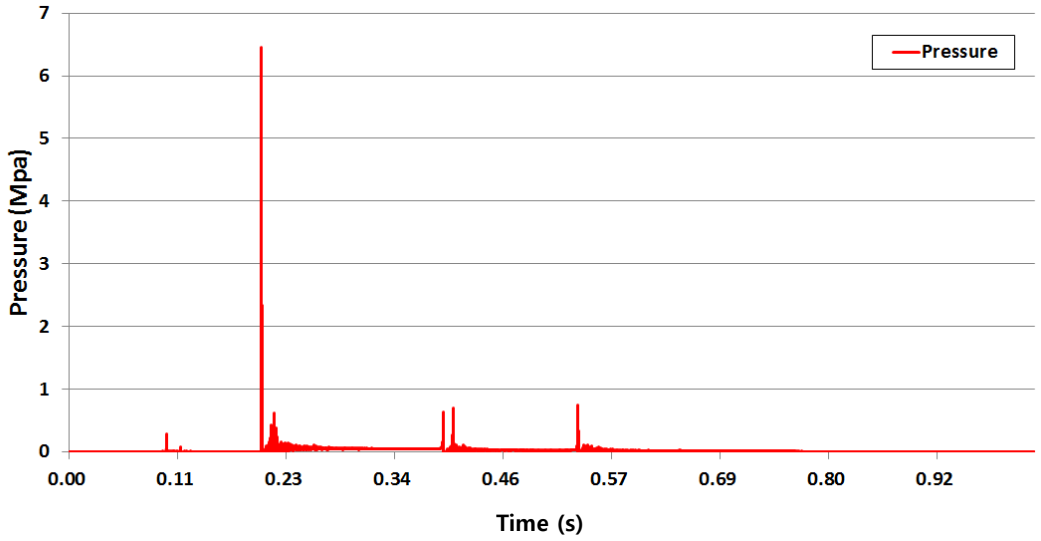

Figure 4.49 Input shock wave and bubble pulse pressure, max: 6.46 MPa (4.65 m).

When the explosive is detonated behind the structure, the trim angle effect does not occur. The results of test 9 are shown is figures 4.47 and 4.48.

4.2.2.10 Response for structure subjected to underwater explosion test 10

Table 4.21 Summary of test 10.

No.	Explosive Weight (g)	Depth (m)	Number of channels	Relation of structure and explosive		
				Position	Distance (m)	Trim (°)
10	500	2	12	Back	4.5	0

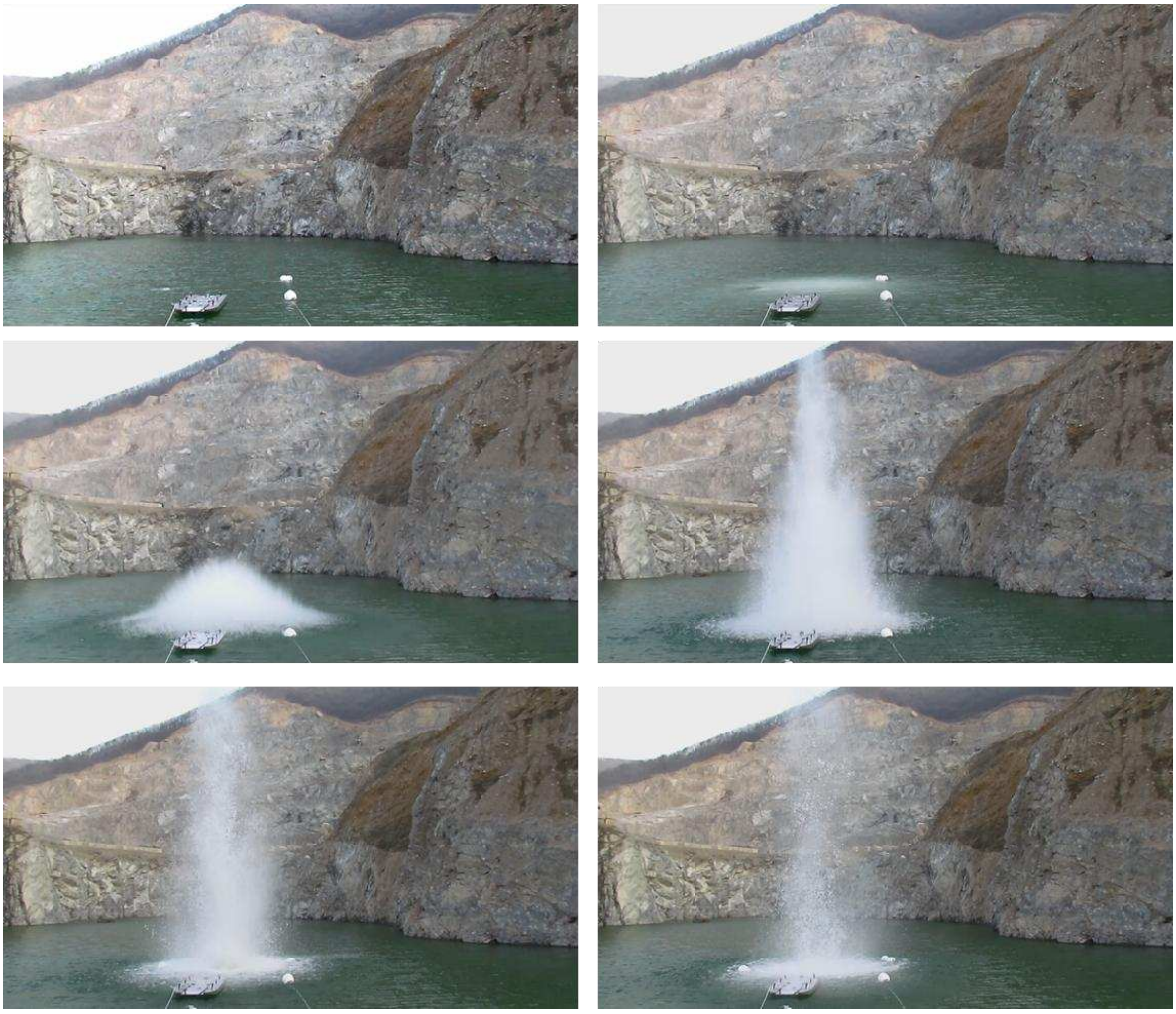

Figure 4.50 Response test for structure subjected to underwater explosion, test 10.

The basic procedure is the same as in test 1. Test 10 is conducted for comparison with test 9 to verify the impact of the trim angle. A summary of test 10 is given in table 4.23, and the measured data are shown in figures 4.42 and 4.43.

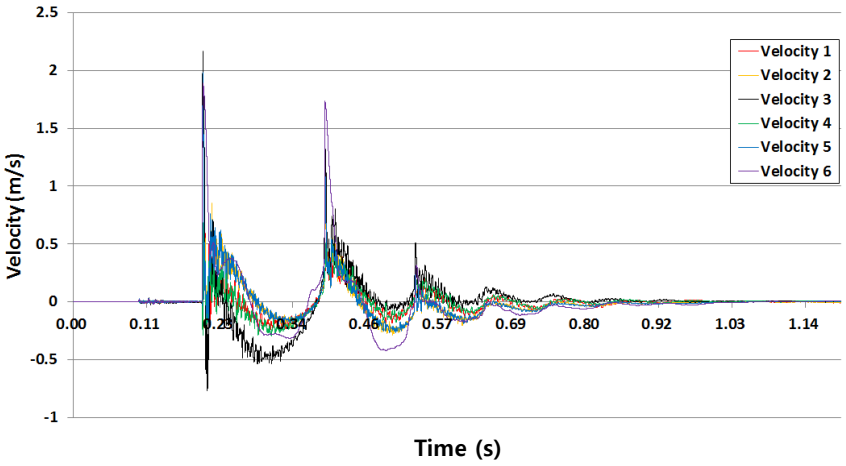

Figure 4.51 The results of structure velocity.

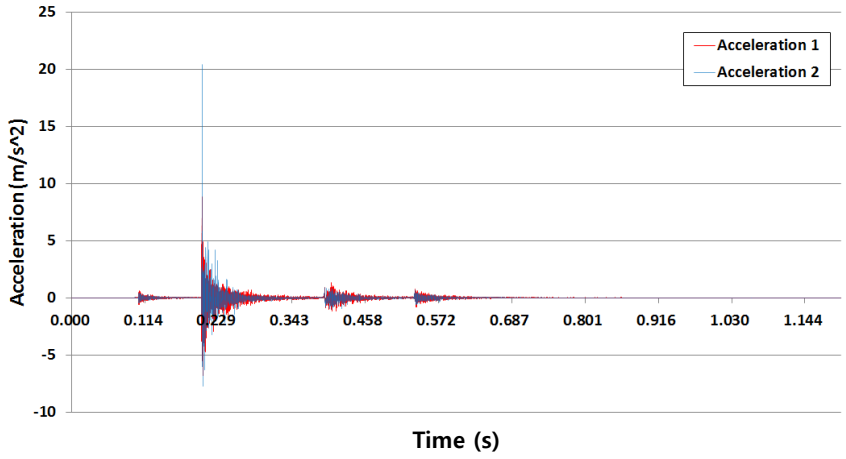

Figure 4.52 The results of structure acceleration.

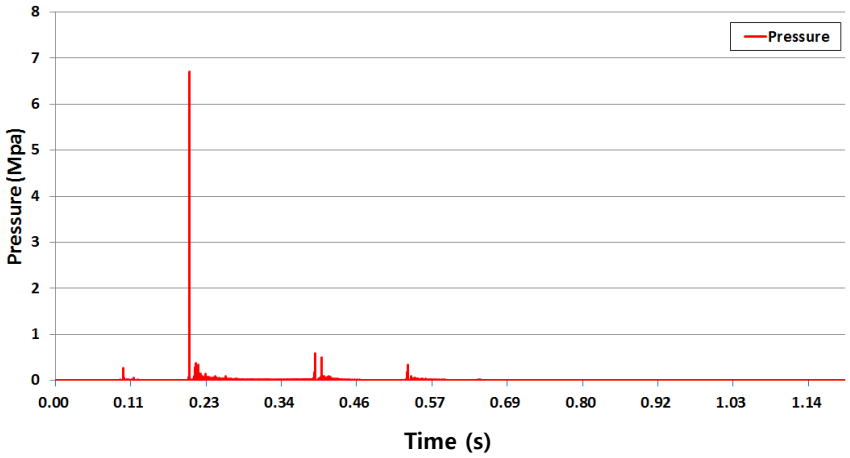

Figure 4.53 Input shock wave and bubble pulse pressure, max: 6.71 MPa (4.5 m).

When the explosive is detonated behind the structure, the trends for the results are almost the same as test 1. The results of test 10 are shown is figures 4.51 and 4.52.

4.2.3 Comparison of test data

4.2.3.1 Comparison of the tests

As described in chapters 4.2.3.1 and 4.2.3.2, these tests are conducted to verify the effect of the trim angle. The trim angle is set up when the assumption that the structure has a high speed is applied to the test. The results of this comparison are shown in figure 4.54.

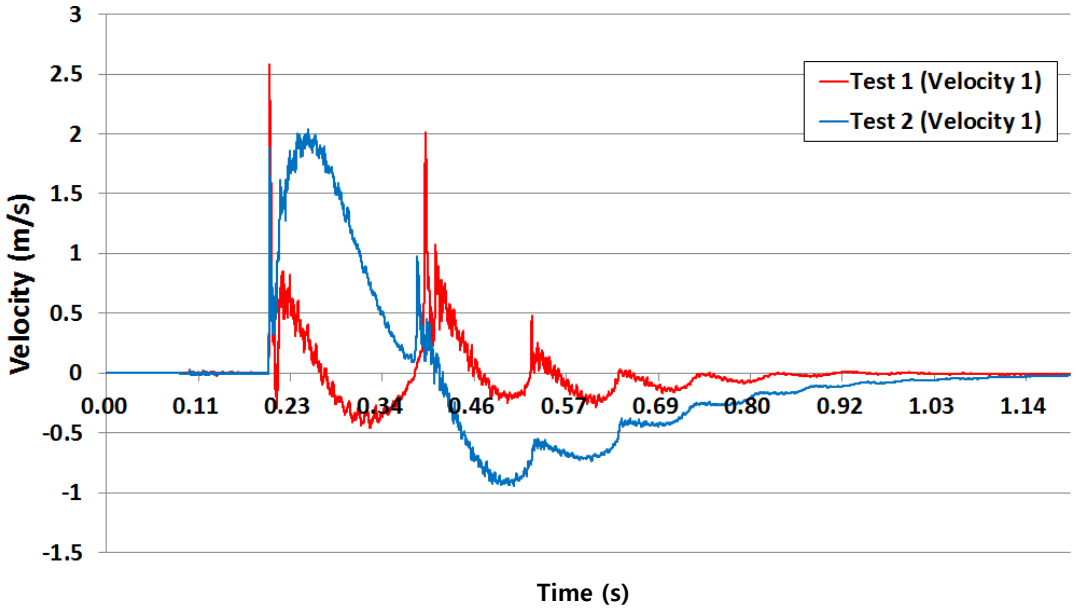

Figure 4.54 Comparison of results of test 1 and test 2.

First, the bubble pulse is not shown in test 2, and velocity responses of the incident shock wave and first bubble pulse are different. In this area, the velocity of test 1 is bigger than that of the first velocity caused by the incident shock wave.

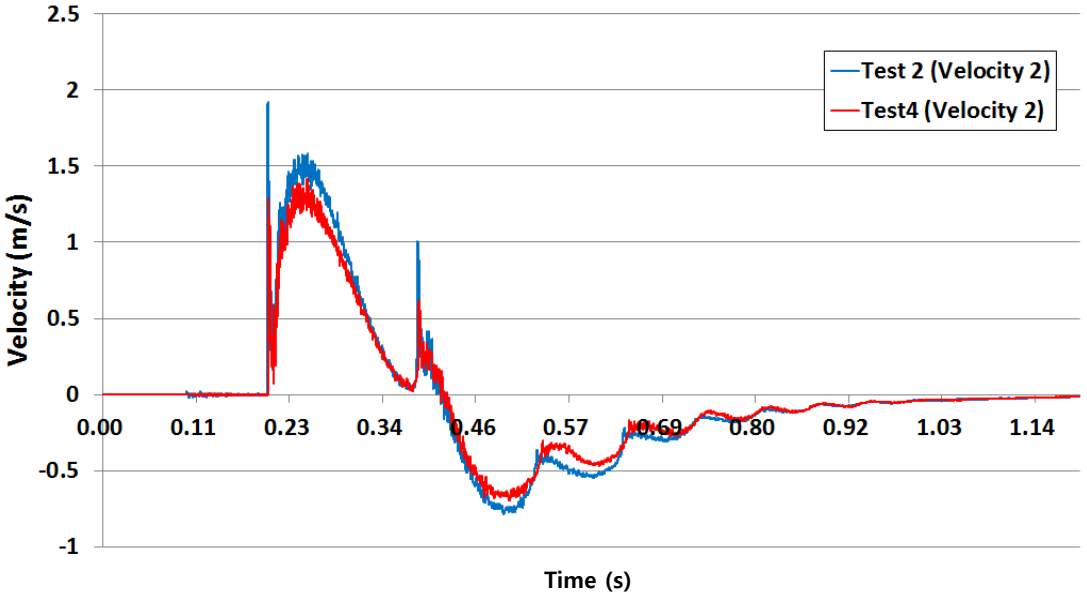

Figure 4.55 Comparison of results of test 2 and test 4.

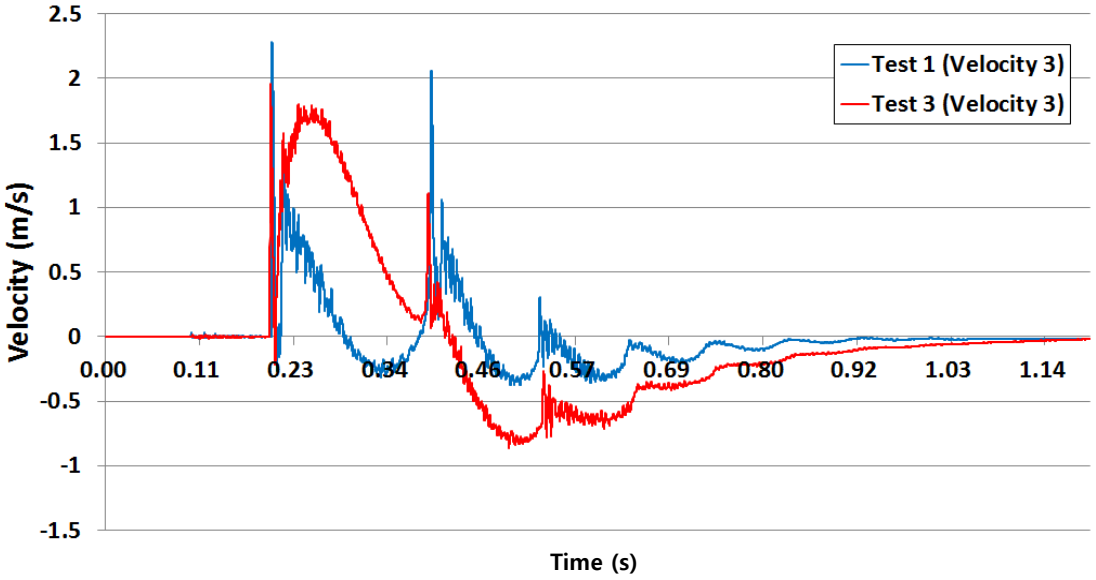

Figure 4.56 Comparison of results of test 1 and test 3.

As shown in figure 4.55, the dynamic response of test 2 caused by the vent out impact of the bubble is very similar to that of test 4. Test 4 shows the situation of the trim angle and vent out phenomena. As shown in figure 4.56, the trim angle effect is important for the dynamic response of the structure.

Chapter 5 Comparison of test and simulation results

5.1 Comparison of simulation and test

Figure 5.2 shows the phenomena of the underwater explosion. The relative positions of the structure and explosive are shown in figure 5.1. Figure 5.1 also shows that the characteristics of the test and simulation are similar.

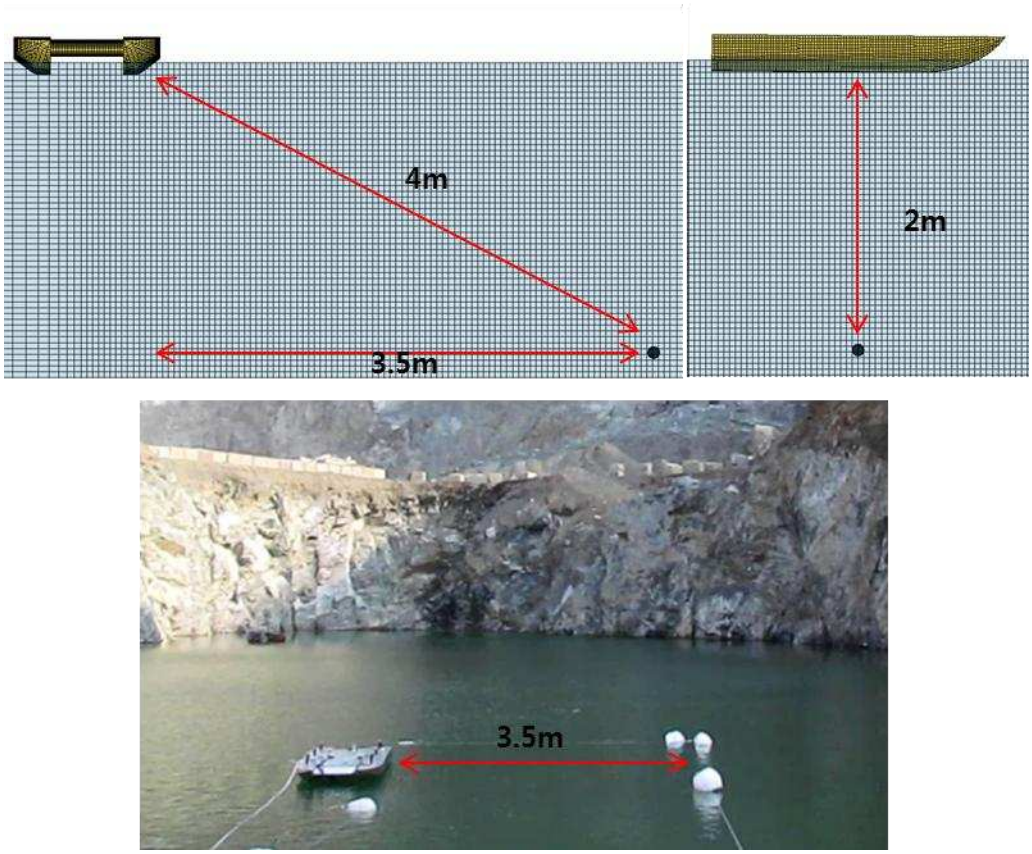

Figure 5.1 Relative positions of structure and explosive.

As shown in figure 5.2, at 0.1 s, the spray dome is observed on the free surface. After 1 s, the peaked flume is observed. Finally, the underwater explosion phenomenon is over at 2.2 s.

Because of the offsetting effect of the incident shock wave when using the ALE method, the measured dynamic response of the structure, including the velocity and acceleration, is smaller with the real explosion test for the same position of the explosive. The first column of figure 5.2 shows the

bubble caused by the underwater explosion with the flume and structure. The second column of figure 5.2 shows the ALE element of the water with the flume and structure. Finally, the third column of figure 5.2 shows a picture of the flume and structure in the test.

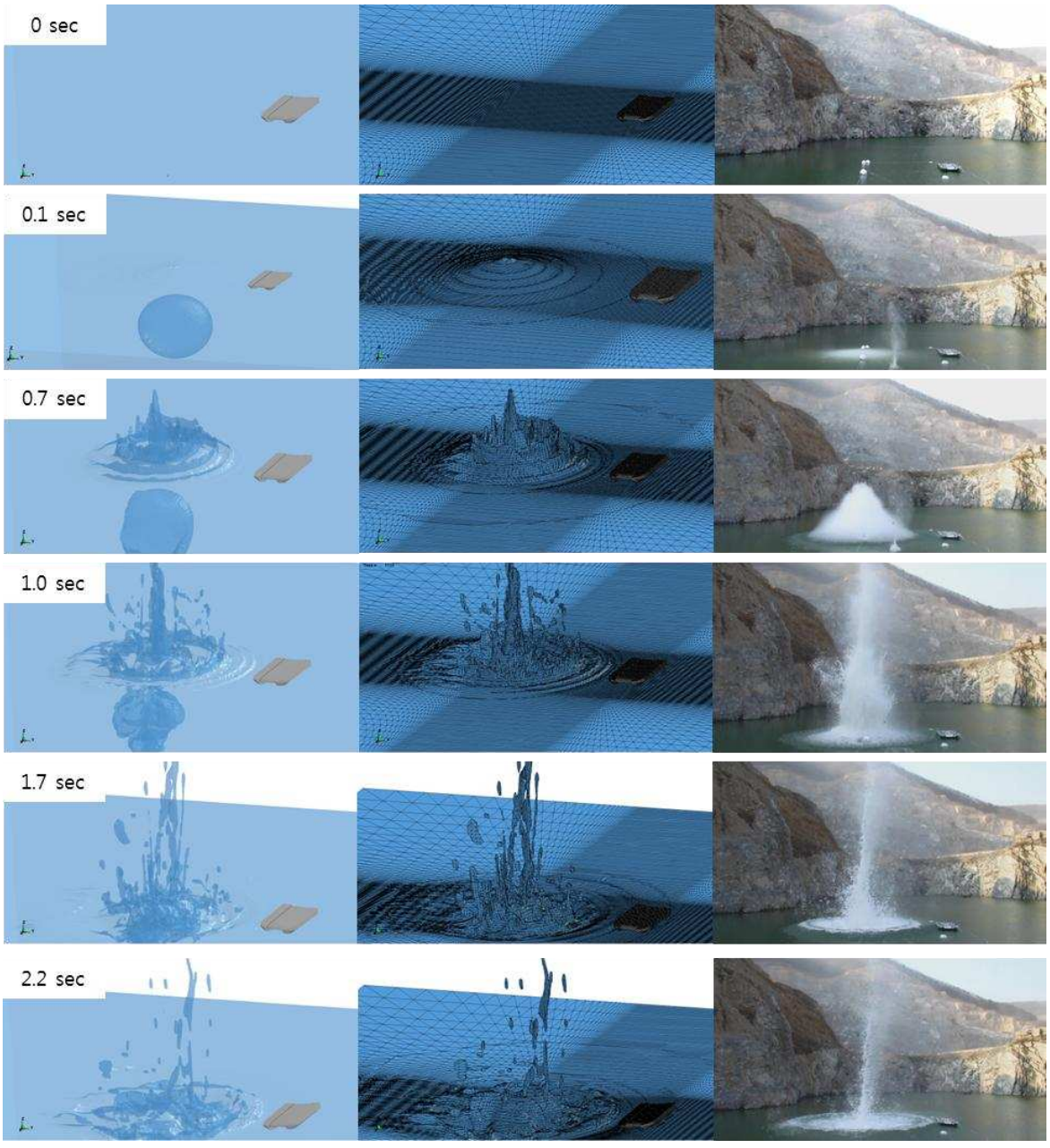

Figure 5.2 Comparison of simulation and test (4 m) results.

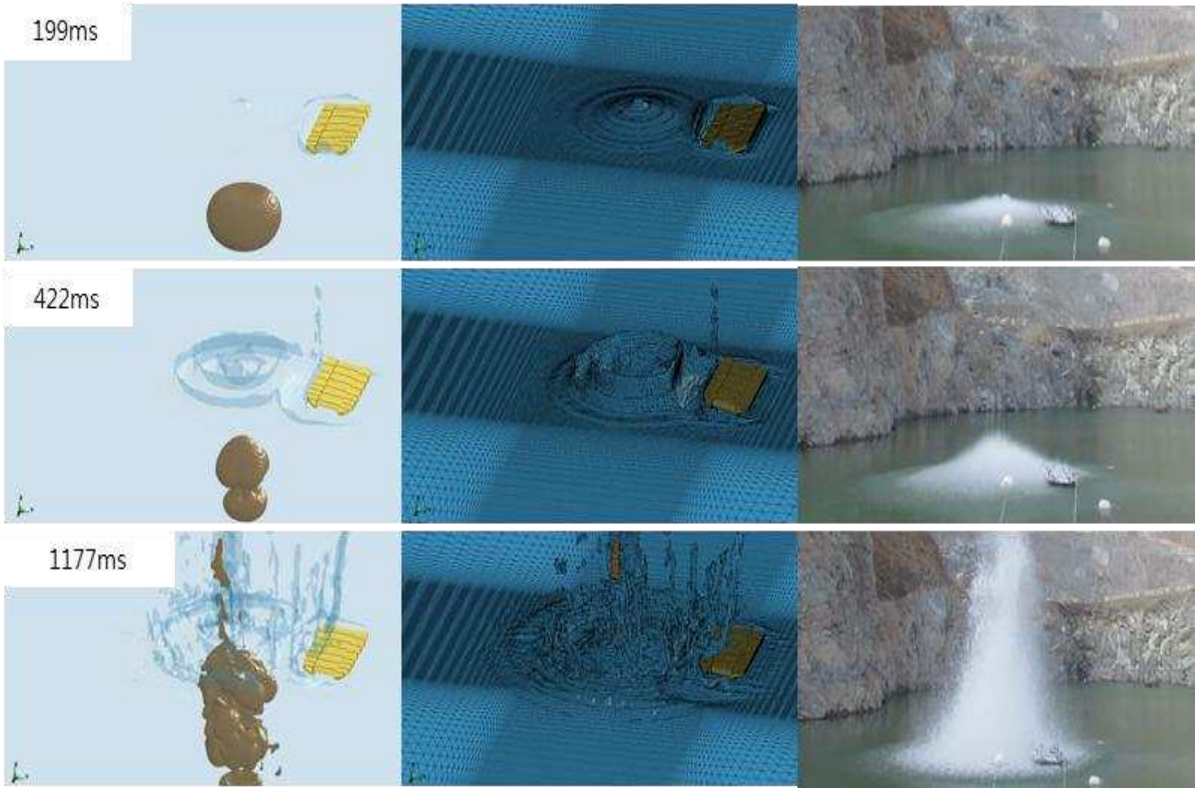

Figure 5.3 Comparison of simulation and test results for shape (1.5 m).

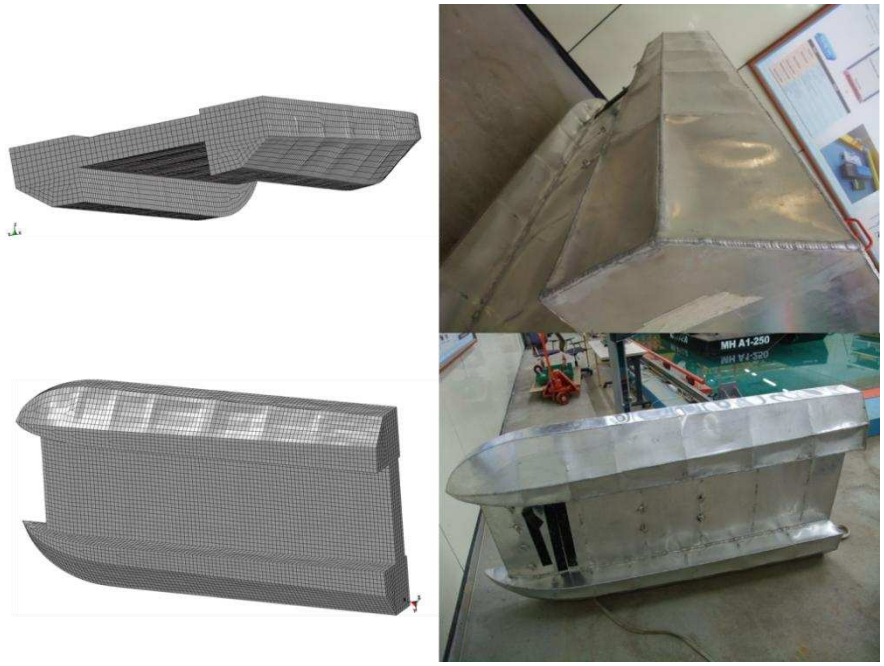

Figure 5.4 Comparison of deformations of structure in simulation and test.

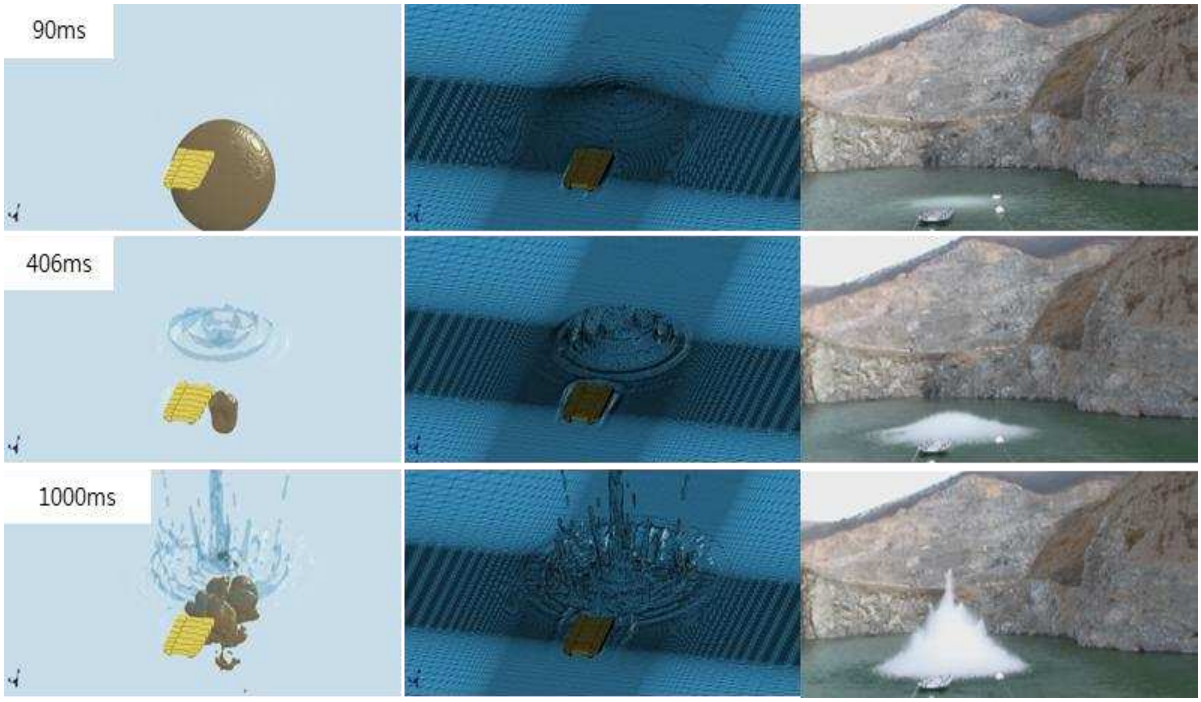

Figure 5.5 Comparison of simulation and test results for shape (behind 4 m).

In test 7, the stand-off distance is 2.2 m, and the appearance of the structure has been deformed by the shock wave pressure and bubble impact. The first column in figure 5.3 shows the simulated results. The second column shows the tested structure for test 7. The outer hull of the structure is deformed in a manner similar to the simulation result. When the stand-off distance is 2.2 m, the calculated shock wave pressure is 15 MPa. Figure 5.4 shows the similarity between the simulated deformation of the structure model and the tested deformation of the structure.

Figure 5.5 shows a comparison of test 10 and a similar simulation result.

5.2 Comparison of data (velocity and acceleration)

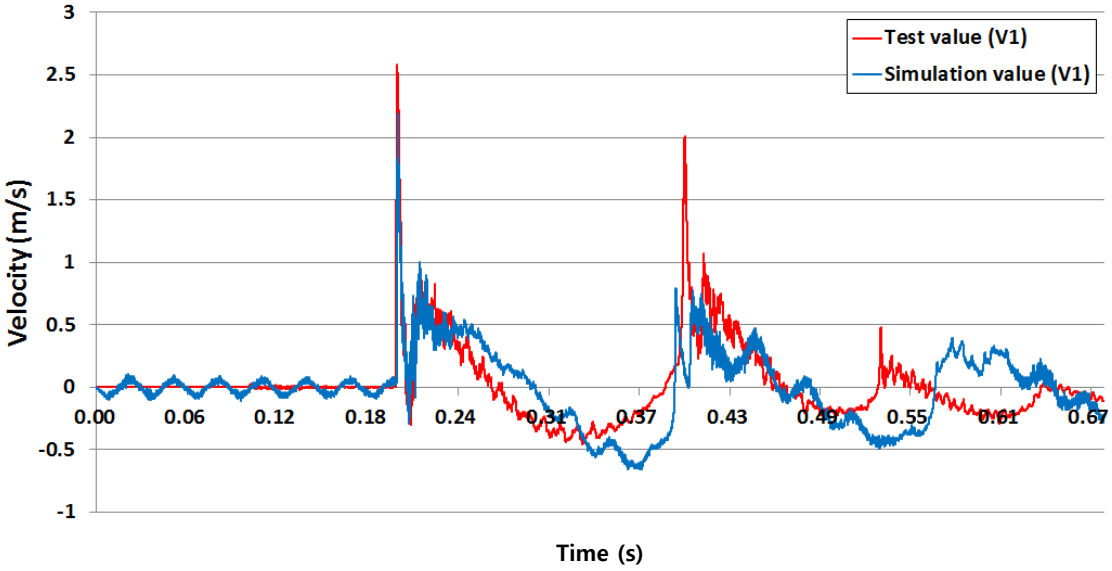

Figure 5.6 Comparison of simulation and test results (velocity).

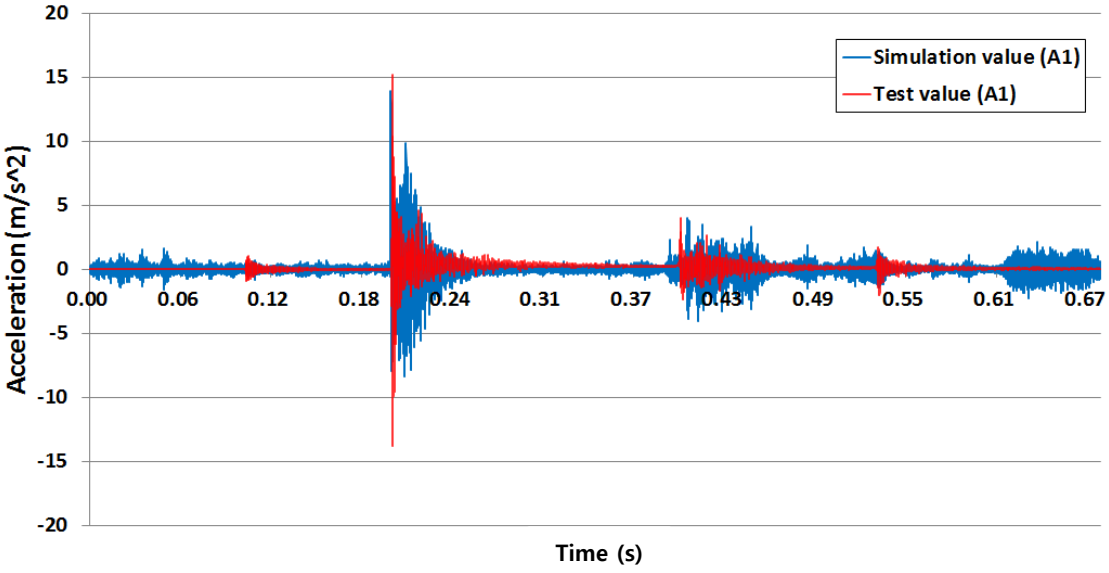

Figure 5.7 Comparison of simulation and test results (acceleration).

To compare the simulated and experimental results, the velocity and acceleration are compared in figure 5.5. The position of V1 is shown in figures 3.5 and 4.15.

The velocity caused by the incident shock wave (see figure 5.4) is smaller than the simulated

velocity of the shock response, because the incident shock wave pressure is reduced in the ALE elements.

Tests 2 and 4 are conducted to observe the vent out phenomenon of the bubble caused by the underwater explosion. Thus, the explosive is set at a depth of 1 m, although the bubble radius calculated by the empirical equation for TNT is 1.21 m. Therefore, when the first bubble oscillation occurs, the bubble is exposed to the air. Thus, the bubble is vented out to the air. Therefore, no further bubble oscillations occur. However, as shown in chapter 3, the vent out phenomenon does not occur precisely in the simulation by LS-DYNA. Figure 5.8 shows a comparison of test 10 and the simulation results. In this case, the position of the explosive is changed to match the test's input pressure. In the simulation, the trend is similar to the velocity response of the structure in test 10.

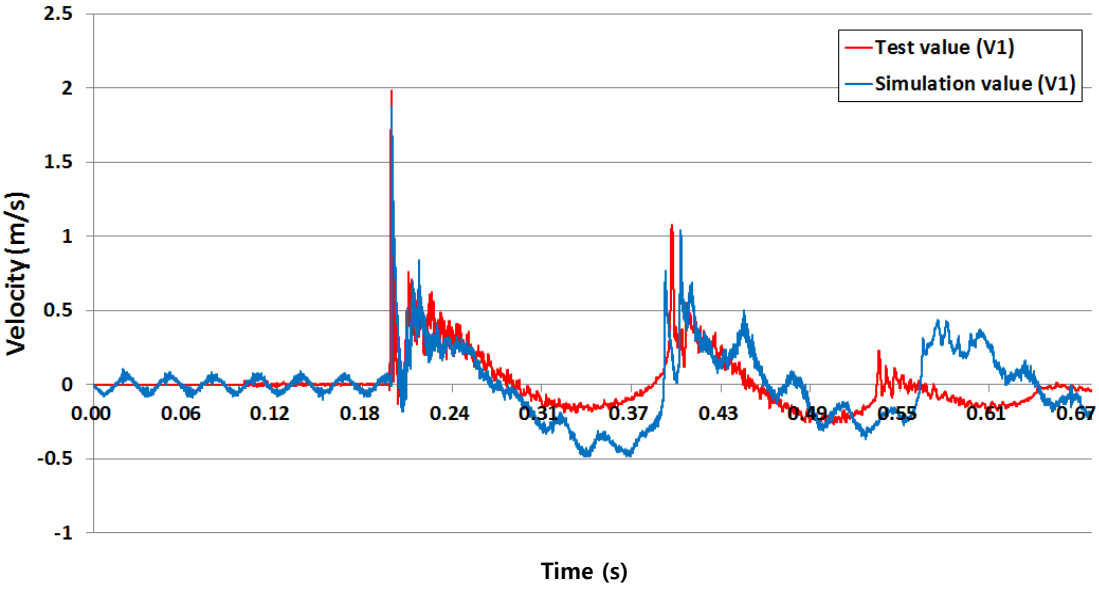

Figure 5.8 Comparison of simulation and test results (velocity).

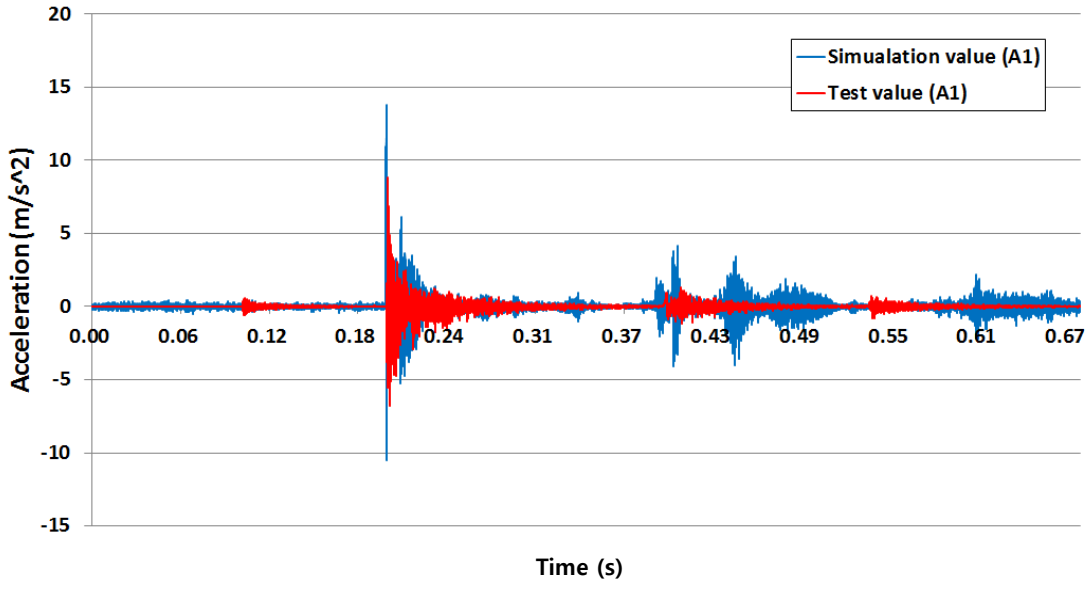

Figure 5.9 Comparison of simulation and test results (acceleration).

Chapter 6 Feasibility of scaling-down test

Figure 6.1 Large-scale ship shock test 2008 (USS, underwater explosion).

As shown in chapter 4, experiments using a small structure are relatively simple and less affected by space restrictions and environmental laws. Therefore, instead of using large-scale warships for hardening and survivability tests, scaled-down models could be used to reduce the cost and planning period for real explosion tests. Figure 6.1 shows a real-scale underwater explosion test conducted in the USA, off the Florida coast.

To conduct this kind of test, huge amounts of time and money are needed. Moreover, there are concerns about the side effects to the ocean environment. The advantages and disadvantages of real-scale explosion tests, scaling-down tests, and simulations are described in table 6.1. A scaled-down model test can extract much useful information quickly, efficiently, and economically.

Table 6.1 Features of alternatives.

Contents	Real-scale test	Scaling-down test	M&S
Cost	Relatively large	Relatively small	Small
Test range	Limited	Unlimited	Unlimited
Credibility	High	Low	Need to verify
Range of data acquisition	Limited	Limited	Unlimited
Mounted equipment	Existence	No	Option
Environment	Relatively large	Relatively small	No

The Hopkinson scaling law states that if the dimensions of a charge are scaled by a value λ, then at an equivalent distance λR from the charge, the peak pressure will remain unchanged but the impulse and pulse duration will both be scaled by λ. Hopkinson scaling applies only to the shock wave itself and does not extend to structural effects. To utilize the Hopkinson scaling law, it is desirable, if not necessary, that geometric similitude occurs, making the scaling between the model and prototype a relatively simple matter. The simple, linear relationships of Hopkinson scaling are presented in table 6.2 and illustrated in figure 6.2 [26].

Table 6.2 Hopkinson scaling relationships for shock wave [26].

Parameter	Prototype	Model
Geometrical Parameters (scaled by λ)		
Charge diameter	d	λ d
Stand-off distance	R	λ R
Characteristic length	L	λ L
Shock Wave Parameters		
Pulse duration	T	λ T
Impulse	I	λ I
Peak pressure	P_{max}	P_{max}

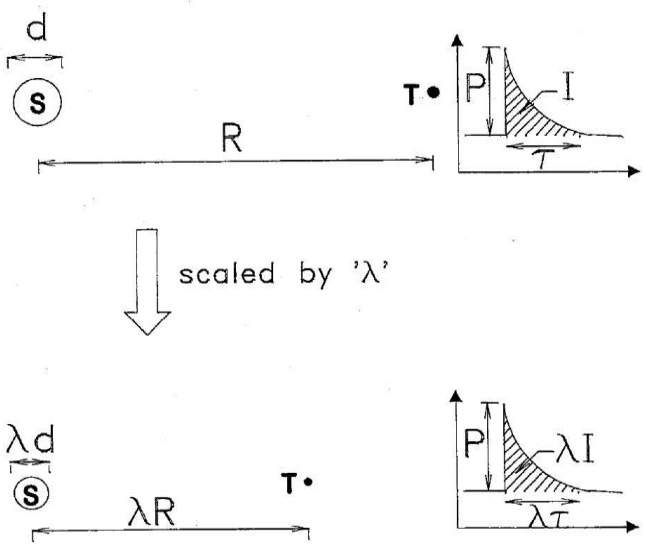

Figure 6.2 Hopkinson scaling applied to spherical underwater shock wave emanating from source S, impinging on target T. Parameters are scaled according to parameter λ [26].

6.1 Modeling of fluid and structure

In this study, the Hopkinson scaling law is verified for underwater explosion response phenomena. The scaled-down model test can be used to extract as much useful information as possible, as quickly and efficiently as possible, and at minimum cost. A deformable structure immersed in a fluid is subjected to shock wave loading imparted through the fluid. The experimental analysis method is used to construct small-scale models of the structure and perform shock response experiments on a smaller scale. To approach this problem, models are constructed of the same material as the prototype. The density and failure stress are kept invariant and the scaling is performed geometrically so that the length scales linearly. The gravity acceleration is the same for both the prototype and scaled-down model situations [8].

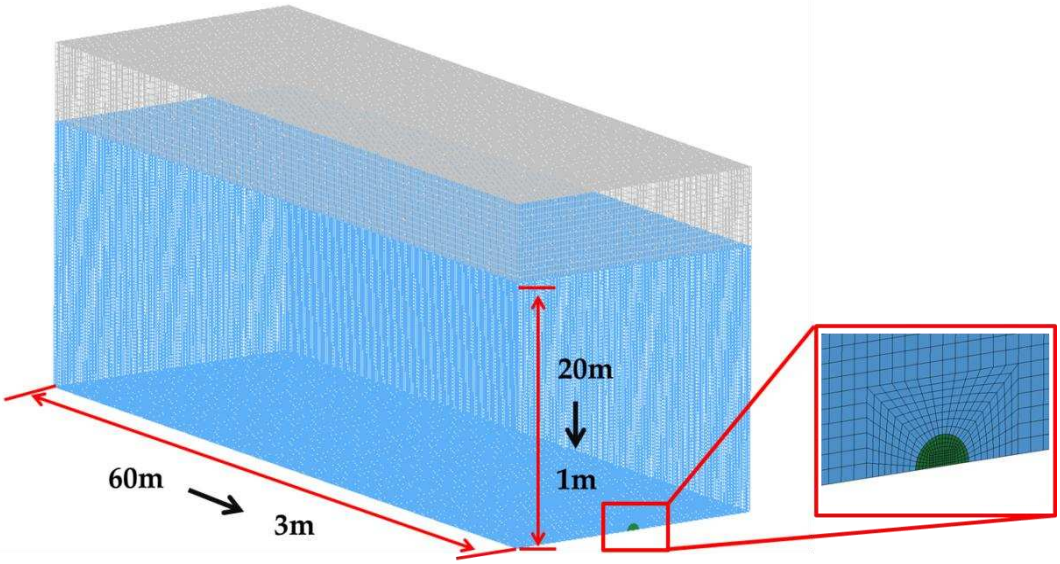

Figure 6.3 Fluid model for verification of Hopkinson scaling law.

As seen in table 6.2, if assumption λ is 20, the other scaled values are as shown in figures 6.3 and 6.4. The depth of the explosive is changed from 20 m to 1 m, and the explosive is changed from 1000 kg to 0.125 kg. The solid element size is proportionately increased because of the limitation for the number of elements.

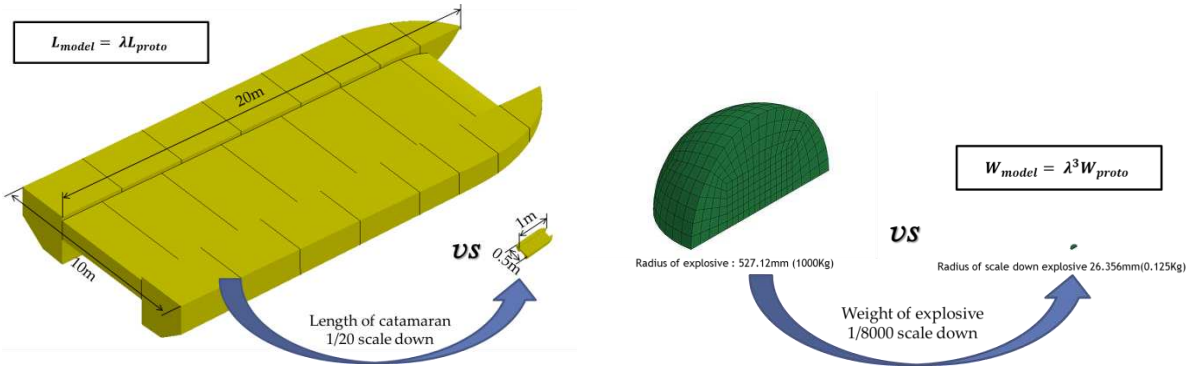

Figure 6.4 Structure model and explosive according to Hopkinson scaling law.

Because a far-field underwater explosion circumstance is assumed, a simulation is conducted for only the shock wave effect.

6.2 Simulation results

The measurement positions are shown in figure 6.5. Points 2, 5, and 8 are specified to verify the motion of the structure. Thus, these points are not affected by the elasticity of the material of the outer hull.

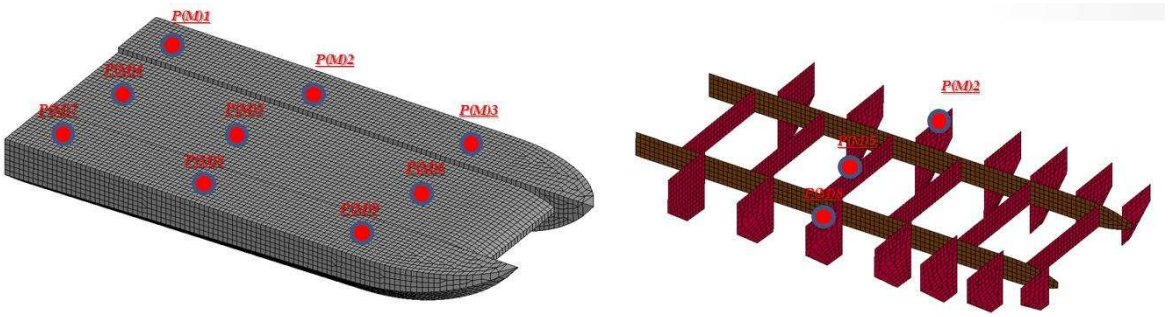

Figure 6.5 Positions for measurements.

Any energy dissipation mechanism such as viscous flow or structural damping will not scale according to Hopkinson scaling. This is because the stress gradient in a viscous flow is proportional to the velocity. A problem involving surface tension will not scale in this way. Thus, this simulation

must minimize the gravitational effects, energy dissipation, and surface tension

The prototype's maximum Z-displacement is 87.9 mm, and the scaled-down maximum Z-displacement is changed to 4.4 mm. The Z-velocity and stress of the scaled-down model are almost the same as the prototype. The cube of the Z-acceleration of the prototype is the Z-acceleration of the scaled-down model, and the energy is the cubic root.

The shock wave pressures are almost the same between the prototype and scaled-down model, as shown in table 2.3.

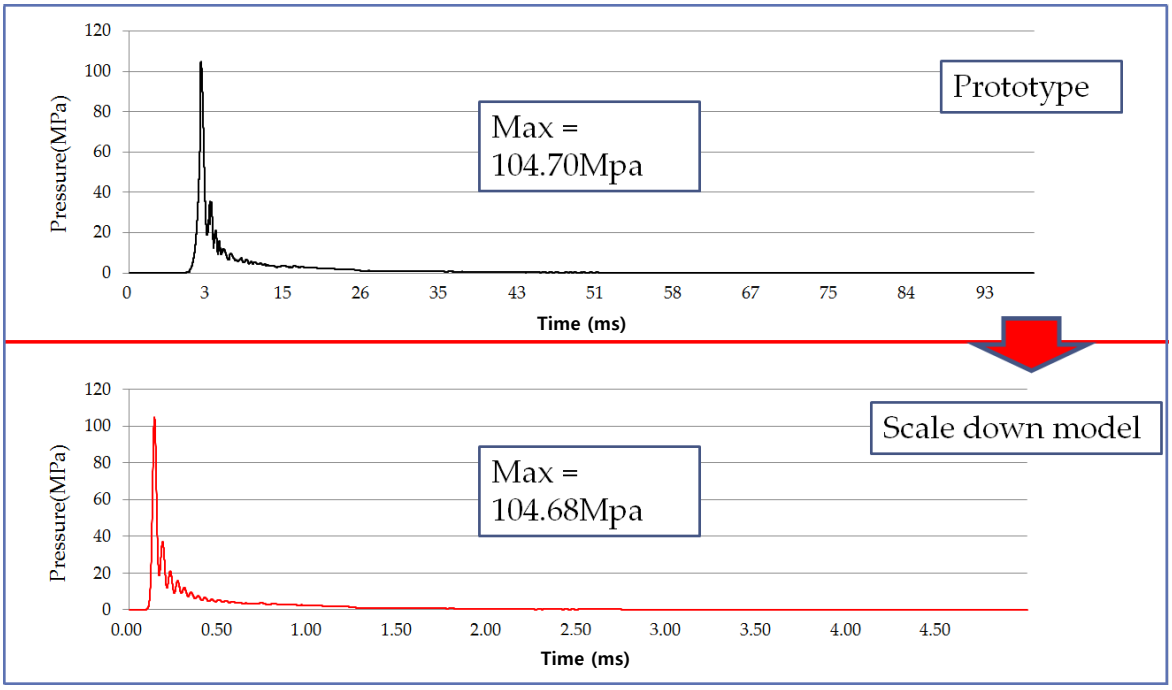

Figure 6.6 Results of shock wave scaling.

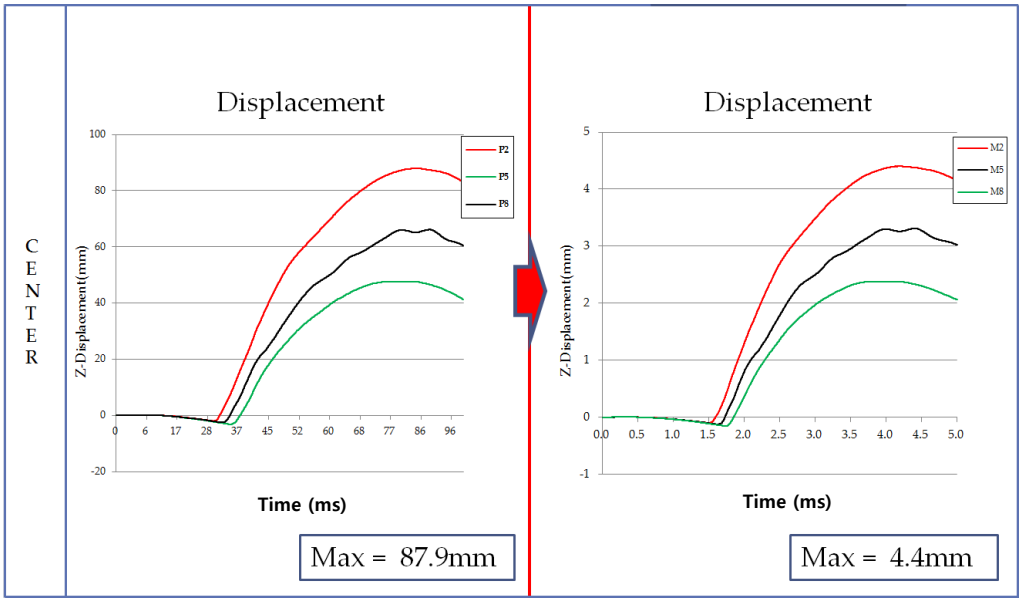

Figure 6.7 Results of displacement scaling.

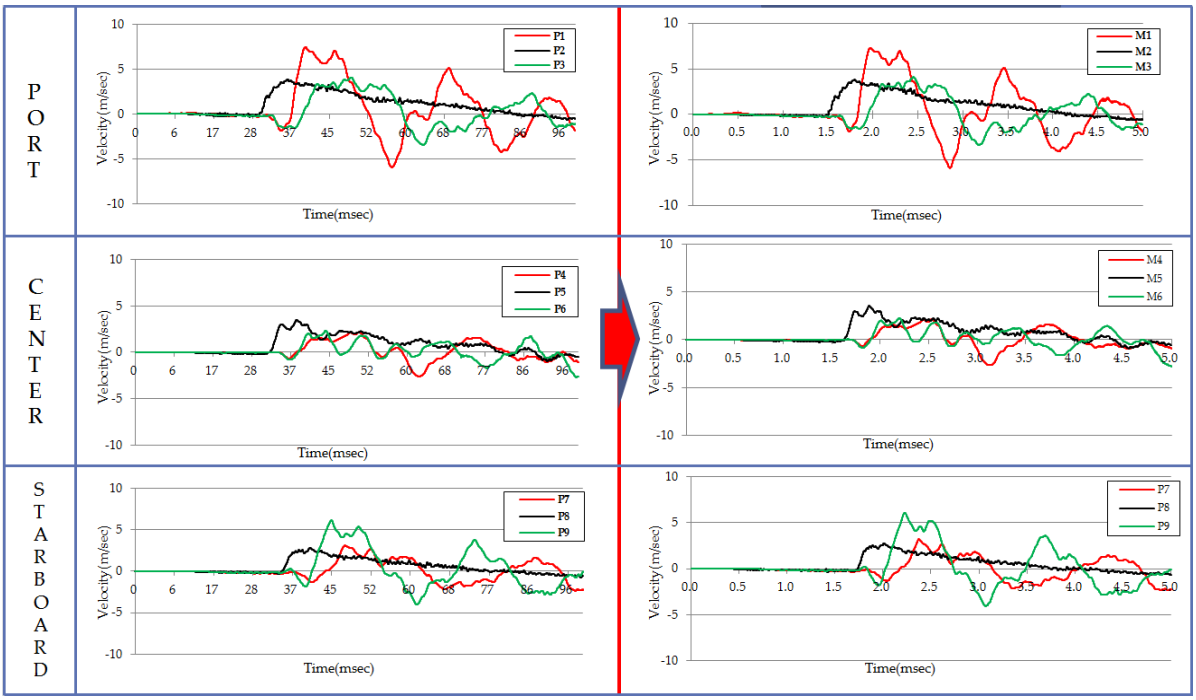

Figure 6.8 Results of velocity response scaling.

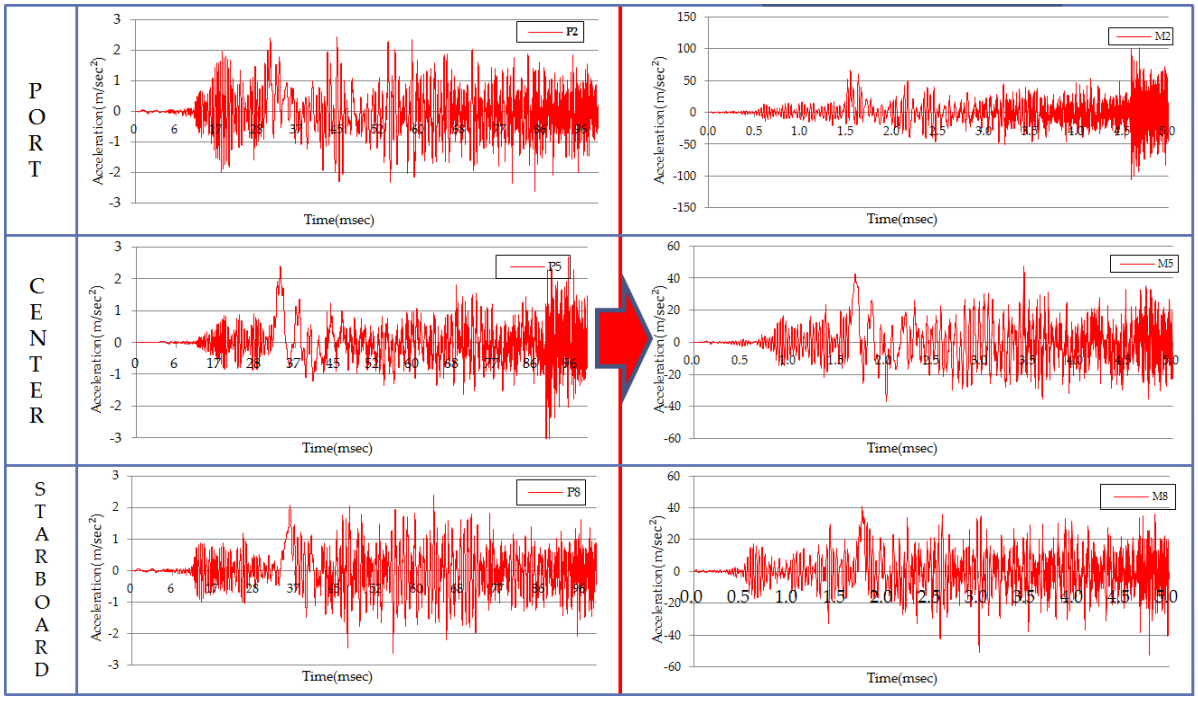

Figure 6.9 Results of acceleration scaling.

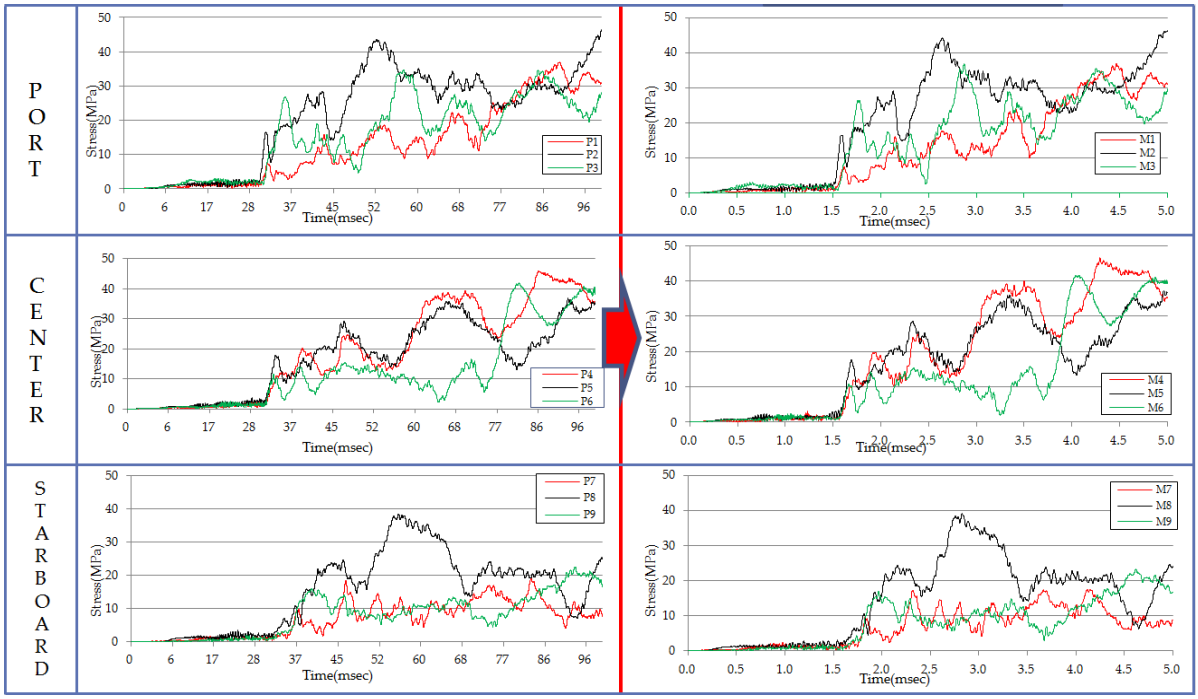

Figure 6.10 Results of stress scaling.

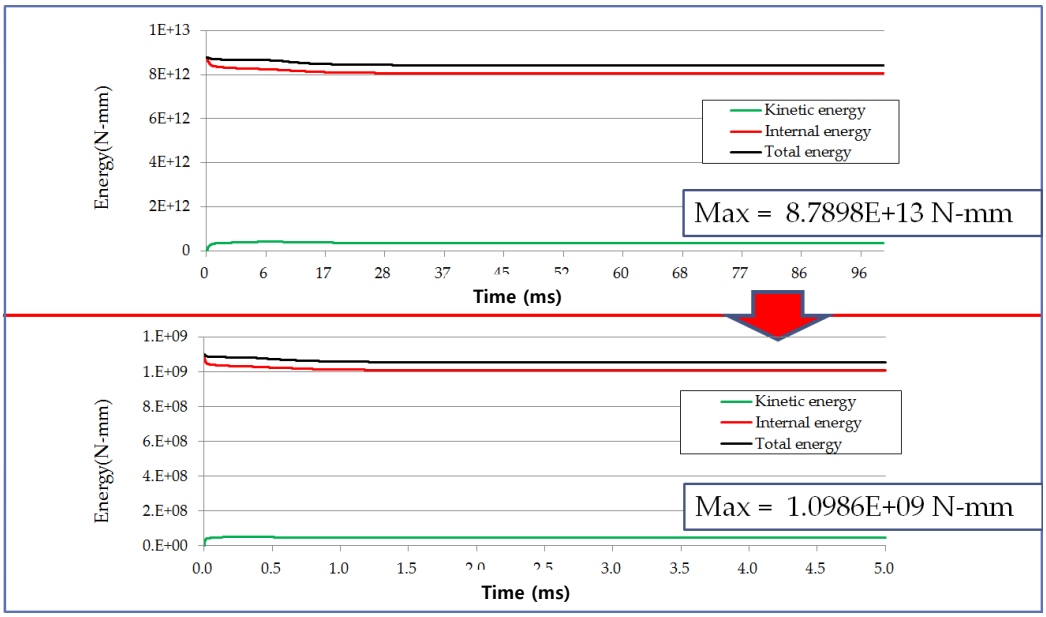

Figure 6.11 Results of energy scaling.

6.3 Results

The feasibility of the scaling law for the shock effect induced by the underwater explosion was confirmed by modeling and simulation. Now, we can test a scaled-down model ship instead of a real-scale ship, which can save cost, in order to enhance the shock resistance by changing the design. However, further scaling-down testing needs to be carried out together with a real-scale explosion test to increase the accuracy of the scaled-down model test and simulation.

Chapter 7 Conclusion

In this study, underwater explosion phenomena were researched. In particular, the dynamic responses of a structure caused by a shock wave and bubble pulse pressure were studied.

A real underwater explosion test for a structure is impossible in almost all cases because of environmental and cost problems. Hence, a computer simulation technique is an important alternative.

In this study, underwater explosion tests were conducted to compare the test values and simulation values. The results of this study confirmed the validity of simulations using the Arbitrary Lagrangian–Eulerian (ALE) technique. Moreover, the feasibility of using a scaling-down test technique, which is a relatively simple test, was verified through simulations.

In order to analyze the bubble pulse pressure, as well as the incident shock wave caused by an underwater explosion, the ALE method is good for simulation

Determining whether or not test and computer simulation results comparison is necessary before simulation results can be applied to design changes for a ship.

The size and number of elements are important parameters when conducting a simulation. These are based on an engineer's experience. Usually, increasing the size of the elements in proportion to the size of the explosives controls the number of elements.

1) The pressure caused by the underwater explosion was offset by the ALE elements by about 70% compared to the tested pressure. Hence, when simulating an underwater explosion using the ALE method, these offsetting effects should be considered.

2) The impact from the vent out of the bubble was verified by the tests. However, the simulation of the vent out phenomenon did not match the test results. In the simulation, the bubble bounced off the free surface. Hence, the results of the dynamic responses of the structure were different from the test results.

3) The trim angle of the ship-like structure that was utilized with the high speed craft assumption produced different trends in the dynamic response results compared to the results when no trim angle was used.

4) When comparison was made of the results of underwater explosions to the side and behind the structure, the dynamic responses of the structure showed almost similar trends. Hence, the position of the explosion does not affect the shock responses of the structure. However, if the explosion occurs directly below the ship, a whipping phenomenon occurs.

5) In this study, small-scale underwater explosion experiments were carried out. Therefore, the experiment procedures of this study can be applied to scaled-down ship shock tests. Hence, the feasibility of using the scaling-down method was investigated by a simulation technique. As shown by the results in chapter 6, the Hopkinson scaling law is good for underwater explosion scaling.

6) This was the first experiment of this kind performed for the purpose of research in Korea. Therefore, the data in this dissertation are important to develop codes for underwater explosion phenomena.

References

[1] Keith G. Webster. (2007). “Investigation of close proximity underwater explosion effects on a ship-like structure using the multi-material arbitrary lagrangian eulerian finite element method”

[2] Jin Qiankun. (2010). “Examined a finite element analysis of ship sections subjected to underwater explosion”

[3] J.H.Kim. (2003). “Researched a study of survivability improvement method for naval ship design(ll)-damage assesment method by ALE technique”

[4] Kengi Murata. (1999). “Suggested the precise measurements of underwater explosion phenomena by pressure sensor using fluoropolymer”

[5] Sang-Gab Lee. (2007). “Studied the intgrated structural dynamic response analysis considering the UNDEX shock wave and gas bubble pulse.”

[6] Lloyd Hammond. (1997) “The applicability of scaling laws to underwater shock tests”

[7] Cole RH. (1948). “Underwater explosions” Princeton University

[8] Shin, Y.S. (2011). "Naval Ship-Shock Design and Analysis", Course Notes for Underwater Shock Analysis, Korea Advanced Institute of Science and Technology, Daejeon, Republic of Korea.

[9] DeRuntz, Jr., J. A. (1996). “The Underwater Shock Analysis (USA) Manual” Unique Software Applications, Colorado Springs, Colorado

[10] Arons, A. B., et al. (1949) “"Long Range Shock Propagation in Underwater Explosion Phenomena II”", Underwater Explosion Compendium, Vol. 1

[11] DeRuntz, Jr., J.A. (1989) “"The Underwater Shock Analysis Code and Its Applications”", 60th Shock and Vibration Symposium, Vol. I, pp. 89-107

[12] Reid, W.D. (1996) “The Response of Surface Ships to Underwater Explosions”, Ship Structures and Materials Division, Aeronautical and Maritime Research Laboratory

[13] Cho-Chung Liang, Yuh-Shiou Tai. (2006). "Shock responses of a surface ship subjected to

noncontact underwater explosions", Ocean Engineering, 33, pp. 748-772.

[14] Costanzo, F. and Gordon, J. (1989) “A Procedure to Calculate the Axisymmetric Bulk Cavitation Boundaries and Closure Parameters.” David Taylor Research Center, Ship Structures and Protection Department, Underwater Explosions Research Division, Bethesda Maryland. Report SSPD-89-177-78

[15] Chisum, J.E. and Shin, Y.S., “Explosion Gas Bubble Near Simple Boundaries,” Shock and Vibration, 1997, Vol. 4, No. 1, pp. 11-25.

[16] Zukas, J.A., and others. (1992) “Impact Dynamics” Kreiger Publishing Company

[17] Souli, M. (2000) "LS-DYNA Advanced Course in ALE and Fluid/Structure Coupling", Course Notes for Arbitrary Lagrangian-Eulerian Formulation Technique, Livermore Software Technology Corporation, Livermore, CA

[18] Livermore Software Technology Corporation, (1999) “LS-DYNA Keyword User's Manual Nonlinear Dynamic Analysis of Structures” Livermore, CA.

[19] Livermore Software Technology Corporation, (1998) LS-DYNA Theoretical Manual, Livermore, CA.

[20] Mair, H.A. (1999) "Review: Hydrocodes for Structural Response to Underwater Explosions," Shock and Vibration 6/2, 81-96.

[21] Ian do, Jim Day, (2000), “Overview of ALE method in LS-DYNA”, LSTC

[22] Steven Hale, “Damping in ANSYS/LS-Dyna”, M.S.M.E Senior Engineering Manager

[23] Shin, Y. S. and Ham, I.,(2003) “Amping Modeling Strategy for Naval Ship System” Tech. Report NPS-ME-03-003, Naval Postgraduate School

[24] Dobratz, B.M. (1981) “LLNL Explosives Handbook, Properties of Chemicial Explosives and Explosive Simulants”, University of California, Lawrence Livermore National Laboratory, Rept. UCRL-52997.

[25] Baker, W.E, Westine, P.S (1991) "Similarity Methods in Engineering Dynamics : Theory and practice of scale modeling" Revised Edition, Elsevier, Amsterdam

[26] Lloyd Hammond and David Saunders (1997) "The applicability of scaling laws to underwater shock tests" Department of defence of Australia

[27] Lee, M. H. (2011). “Underwater shock response study of the planning trimaran applied to trim angle variation. Master’s thesis in ocean systems Eng. KAIST.

Summary

Underwater explosion testing of catamaran-like structure vs. simulation and feasibility of using scaling law

수중폭발시험의 대체수단인 시뮬레이션과 축소모형선시험의 타당성에 대한 연구이다. LS-DYNA를 이용하여 ALE기법을 이용한 시뮬레이션과 시험을 비교 분석하여 시뮬레이션의 타당성을 연구하였다. 또한 본 연구에 사용한 시험은 실사충격시험에 비해 작은 규모의 시험이었고, 그 간결함을 확인 하였기 때문에 그 절차를 축소모형선시험에 응용이 가능할 것이라고 판단하였다. 그렇기 때문에 수중폭발현상의 상사법칙의 적용가능성에 대한 연구를 수행하였다.

따라서 본 연구를 통하여 실사충격시험의 대체수단인 시뮬레이션과 모형선을 활용한 충격시험의 절차와 정확성을 확인할 수 있다.

감사의 글

본 연구는 한국연구재단을 통해 교육과학기술부의 세계수준의 연구중심대학육성 사업(WCU)으로부터 지원받아 수행 되었습니다. (R31-2008-000-10045-0)

먼저 석사과정을 무사히 수행할 수 있도록 이끌어 주시고, 학업으로 힘들어하는 제자에게 아버지처럼 격려해주시고 학문적으로 훌륭한 가르침과 삶의 지혜를 전수해주신 신영식교수님께 감사드립니다. 또한 바쁘신 와중에도 논문을 심사해주시고 조언을 주신 한순흥교수님, 정현교수님, 기계연구원의 정정훈 박사님께 감사 드리며, 갚진 수업으로 훌륭한 가르침을 주신 OSE 교수님들 께 감사 드립니다. 또한 실험에 많은 도움을 주신 KOTC의 김용욱 교수님, 김영수 연구원님께 깊은 감사의 말씀을 드립니다. 또한 좋은 추억과 도움을 주신 OSE 재학생들께 감사드립니다.

석사과정 동안 잊지 못할 추억 만들었던 UERL식구들에게 감사의 말을 드립니다. 잘생기셨지만 이제는 품절남 성은형님, 음악적 신세계를 보여주시고 많은 대화를 했던 태민형님, UERL에서 없으면 안 되는 존재 재호형님, 룸메이트자 UERL로 이끌어 주신 철홍형님, 순수하고 착한 동만이, 거침없는 명훈이, 홍일점 연옥이, 영원한 랩대표 천재소년 희규, 실험에 가장 많은 도움을 준 믿음직한 친구 용현이, 착한 프리랜서 경석이 모두 행복하고, 건강하기를 기원합니다. 또한 사고만치는 저를 가족처럼 잘 챙겨주는 3106호 식구들인 세상에서 제일 착한 영균이와 많은 이야기를 나누며 꿈을 키웠던 하정우 닮은 석인이에게 감사의 말을 전합니다.

마지막으로 부족한 아들이지만 항상 아낌없는 믿음과 사랑으로 응원해주시는 아버지, 어머니께 감사와 사랑을 전합니다. 무뚝뚝한 동생을 잘 챙겨주는 누나, 친형 같은 매형, 너무 귀여운 조카들 서린이, 효린이에게 또한 감사와 사랑을 전합니다.